

Chapter 1

Introduction

1.1 – Introduction

Proteins are the most diverse class of biomolecules, both structurally and functionally, and have evolved to accomplish many tasks in living systems. The variety of structures and sizes is quite remarkable. GroEL is a large, barrel shaped protein consisting of 14 subunits and an overall molecular weight of 840,000 that assists in protein refolding (1). Very small proteins, generally labeled antimicrobial peptides (AMPs), ranging from 15-50 amino acids function as part of the innate immunity in multicellular organisms (2). The features of proteins and peptides that contribute to their structure, stability and activity have been elucidated through an enormous body of experimental work that includes spectroscopic and kinetic measurements in response to changes in temperature, pH, and composition of solvents. Central to this endeavor have been protein engineering and design studies. Most recently, non-natural amino acids have provided a wider range of tools to expand the realm of protein engineering (3). Knowledge of the basic principles underlying protein folding, stability, and activity provide insight into the fundamental processes *in vivo* and offer the potential of designing protein/peptide based materials and therapeutic agents.

1.2 – Protein Structure

1.2.1 - Protein Structure and Folding

The twenty natural amino acid side chains include hydrophobic, hydrophilic, redox active and ionic functionalities. These basic properties allow the formation of precisely structured proteins and, in turn, have given Nature the ability to evolve proteins that interact specifically with other proteins, small molecules, and other biological components such as membranes and nucleic acids in addition to catalyzing reactions. To understand what drives the formation of protein structures one needs to understand how interactions between amino acid residues result in the formation of specific, repetitive secondary structures (Figure 1.1) and the energetic forces that drive protein folding.

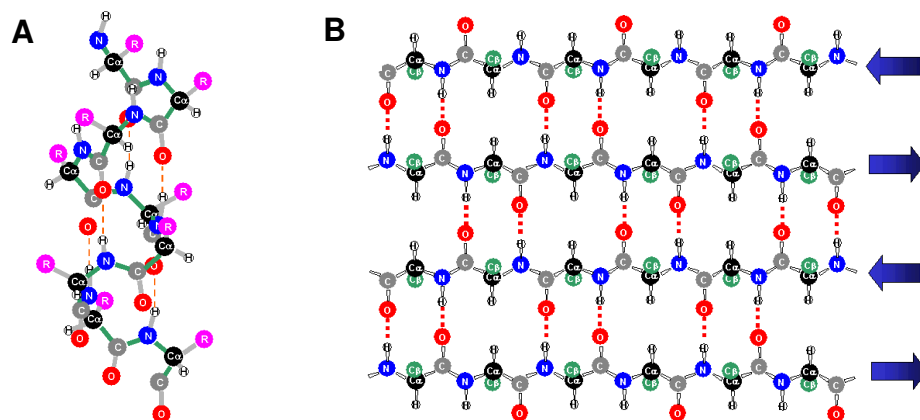


Figure 1.1. Diagrams depicting α -helix (panel A) and β -sheet (panel B) protein secondary structures and the backbone hydrogen bonding pattern (red dash).

1.2.2. – Protein Structure Prediction

An important goal in the field of protein folding has been to develop the ability to predict secondary structure based on amino acid sequence. Anfinsen found that the environment in which a polypeptide was placed did not dictate the structure of the folded protein. Instead, the properly folded protein structure was dictated by the polypeptide sequence (4). Our ability to predict helical structures based on experimentation with peptides/proteins (5-13) and molecular dynamics studies (14) is relatively good. For example, amino acids such as alanine, leucine, and glutamate are likely to stabilize α -helices (see Table 1.1). There have been more limited studies on the propensities of amino acids to be involved in the formation of β -sheet structures (15).

Table 1.1 Helix and sheet forming propensities of amino acids relative to alanine. Lower numbers indicate a higher propensity.

| Amino Acid | Relative Helix Propensity (13) | Relative Sheet Propensity (15) |
|------------|--------------------------------|--------------------------------|
| Gly | 1.00 | 1.00 |
| Ala | 0.00 | 0.00 |
| Val | 0.61 | -0.68 |
| Ile | 0.41 | -0.83 |
| Leu | 0.21 | -0.43 |
| Met | 0.24 | -0.60 |
| Phe | 0.54 | -0.72 |
| Tyr | 0.53 | -0.80 |
| Trp | 0.49 | -0.45 |
| Ser | 0.50 | -0.58 |
| Cys | 0.68 | -0.43 |
| Thr | 0.66 | -0.92 |
| Lys+ | 0.26 | -0.23 |
| Arg+ | 0.21 | -0.38 |
| Gln | 0.39 | -0.19 |
| Glu | 0.16 | |
| Glu- | 0.40 | -0.01 |
| Asn | 0.65 | 0.07 |
| Asp | 0.43 | |
| Asp- | 0.69 | 0.78 |
| His | 0.56 | 0.02 |
| His+ | 0.66 | |
| Pro | 3.01 | 2.50 |

The propensities of amino acid for various secondary structures can be rationalized based on the loss of entropy that results from restricting the torsion angles upon formation of secondary structure and a gain in enthalpy from the backbone hydrogen bonding and van der Waals interactions upon helix or sheet formation. For example, the entropy loss associated with placing glycine in α -helices and β -sheets is very great due to its ability to occupy many phi and psi

angles as illustrated in the Ramachandron plot (Figure 1.2). β -Branched residues experience entropy loss due to side chain conformational restrictions in the formation of helices; therefore, they have a lower propensity for helix formation. However, these amino acids have high propensity for sheet formation. Although amino acids may tend to prefer one structure over another, the local environment within a polypeptide chain alone is usually found to be insufficient information for accurate prediction of structure.

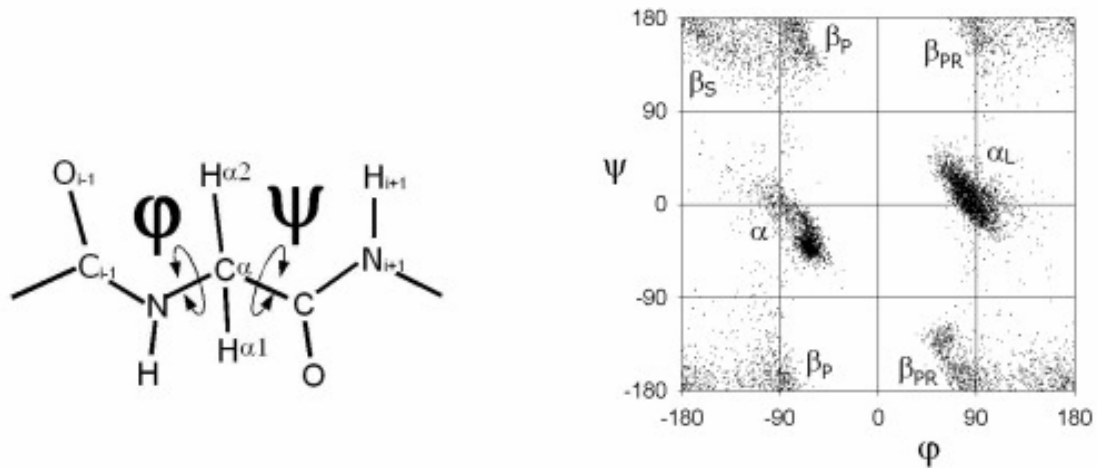


Figure 1.2 Ramachandran plot illustrating the torsion angles occupied by glycine based on 500 non-homologous, high resolution protein crystal structures in the PDB. Densely occupied areas labeled with the secondary structures formed (16).

Protein structure is known to be highly context dependant. This was shown by Peter Kim in a classic experiment with the protein GB1. In a mutagenesis experiment Kim replaced portions of the protein that were α -helical or β -sheet with the 11 residue chameleon sequence AWTVEKAFKTF. In doing so the protein maintained its native structure (17). Therefore, amino acid

sequence and the context of the sequence are both very important in predicting protein structure and in designing proteins of specific secondary structures.

1.2.3. – Molecular Interactions in Protein Folding

Protein folding and structural stability arise from basic physiochemical interactions including hydrogen bonding, ionic interactions, disulfide bonding, van der Waals forces, and cation/ π interactions. The energy contributions of these interactions, as determined by experimentation, are listed in Table 1.2. A combination of many energetically small interactions gives rise to complex folding pathways.

Classic and extensive studies with bovine pancreatic trypsin inhibitor by Kim and Creighton have shown that the pathways of protein folding follow a “rugged energy landscape” with many intermediates and local energy minima and maxima (18). The folding pathway of many proteins is reversible allowing the free energy of folding, $\Delta G_{\text{folding}}$, to be measured. This generally is in the range of 5-10 kcal/mol (18). The loss in entropy upon restricting torsion angles and amino acid side chain rotation is unfavorable, the loss of hydrogen bonding interactions of the protein with water molecules upon folding is energetically neutral, whereas the hydrophobic collapse is energetically favorable and is the driving force in folding.

Fersht has published extensive literature on the ‘Nucleation-Condensation’ mechanism observed in the initial folding events of such proteins as Cl2, barnase

and barster (19). In addition, Scheraga has contributed to the understanding of hydrophobic collapse as an initiation step of protein folding (20). Scheraga compiled evidence for the folding pathways of RNase A and apomyoglobin and observed folding of these proteins is initiated by collapse of hydrophobic regions.

Table 1.2 Energy contributions of various molecular interactions.

| Interaction | Energy contribution (kcal/mol) |
|----------------|------------------------------------|
| Van der Waals | 1.5-2.5 (per methylene) (19) |
| Ionic | 0.1-1.2 (21,22) |
| Cation/ π | 0.1-1.0 (23-26) |
| Hydrogen Bond | 0.5-2.0 (27) |
| Disulfide Bond | ~4 (28) |

The wealth of knowledge gained over the past 40 years has provided a basis for the understanding of protein structure, folding, stability, intermolecular and intramolecular interactions. Much of the information known about these basic principles was and continues to be based on protein design. Protein design allows for comparisons to be made between proteins differing by as little as a single amino residue and also gives us the ability to go beyond the limits of Nature by incorporating non-natural amino acids into proteins.

1.3 – Protein Design

1.3.1 - *de novo* Design

Two routes to the design of new proteins are often taken. The first route is *de novo* design. *De novo* design gives the scientist the opportunity to test his or her knowledge of the basic principles of protein structure, stability, and function. These principles include hydrophobic partitioning, satisfying H-bonding requirements, and charge complementarity. Generally the structural motifs of *de novo* designed proteins mimic those found in Nature, primarily α -helices and β -sheets. However the sequences are derived from first principles rather than evolution.

A large contribution has been made to the field of *de novo* designed α -helical based peptides by the laboratories of DeGrado, Kim, and Hodges among others. The coiled-coil motif has often been the target fold for *de novo* designed peptides (29). For example, two helix, antiparallel and parallel coiled-coil systems have been synthesized and characterized to test the understanding of how electrostatic interactions and hydrophobic packing direct the assembly of oligomerization of the peptides (30). Three helix bundles have been designed to bind metal ions for the purpose of creating simple model systems that mimic metalloprotein structure (31). Finally, a dimerizing 3 helix bundle design was shown to have domain swapping ability (Figure 1.3A) (32). As more information is gained the design targets have increased in complexity. More recently, there

has been success in designing catalytic and transmembrane proteins. For example, a four helix bundle was constructed that has catalytic oxidase activity due to incorporation of two diiron centers in the core of the helical bundle (Figure 1.3B) (33).

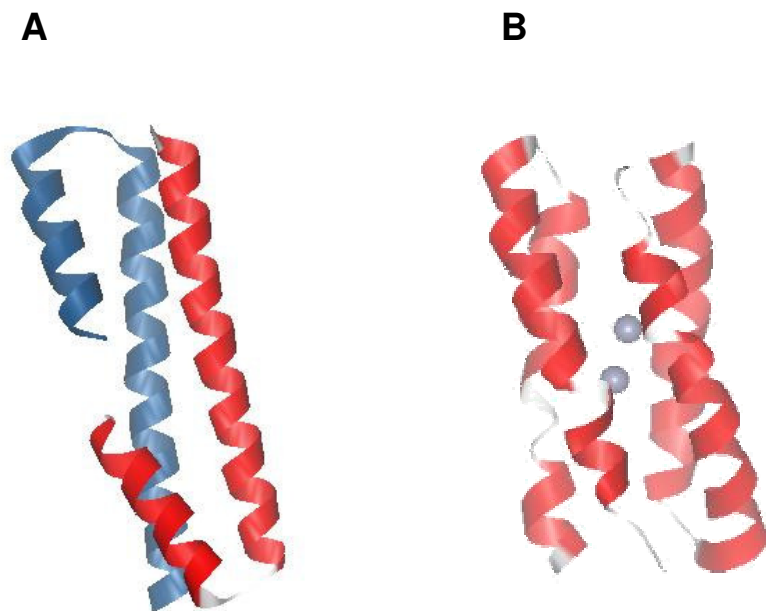


Figure 1.3. Structure of domain swapped dimer resulting in three helix bundle (PDB 1G6U) (A) and a four helix bundle with designed diiron center for oxidase activity shown with two zinc atoms bound (PDB 1U7J) (B).

Examples of *de novo* designed membrane spanning peptides have been reported (34-37). One such example is a peptide containing a string of 21 highly hydrophobic residues followed by a 6-lysine carboxy terminus. The peptide was found to be α -helical in the presence of SDS micelles and, upon association with micelles, dimerized (Figure 1.4) (37). These studies are important for gaining insight into natural membrane associated proteins that have been difficult to obtain and characterize. In addition to coiled-coils, *de novo* designed proteins

encompass folding motifs that include helical hairpins (38,39), β -hairpins (40-42), β -sheets (43, 44), loops (45), and even mixed α/β motifs (46).

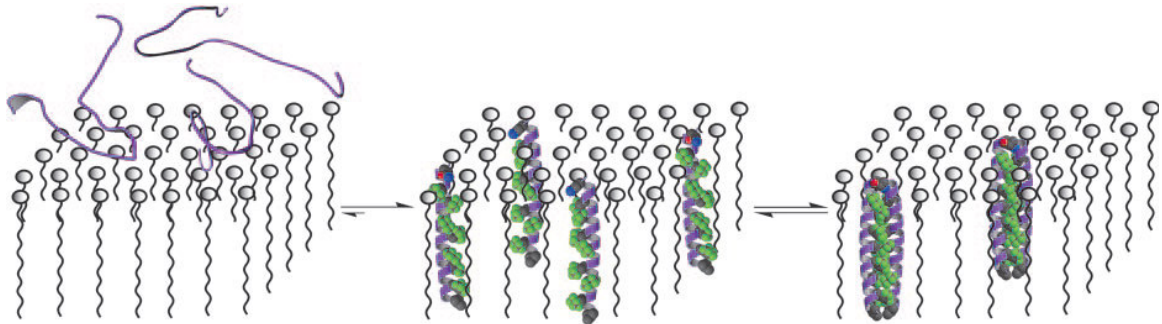


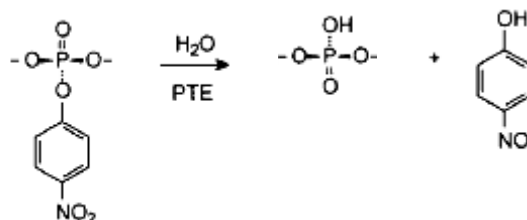
Figure 1.4 Assembly method of *de novo* designed membrane spanning peptides (34). Random coil peptides become helical in the presence of detergent molecules and associate into dimers upon insertion into the monolayer.

1.3.2 – Redesign of Natural Proteins

The second method used in protein design is to redesign natural proteins. This method of design also provides insight into the principles of protein folding. In addition, redesign allows a scientist to take natural proteins and make minimal changes to the sequences to extract knowledge pertaining to the activity, selectivity and specificity of proteins. We can use this knowledge to ‘fine tune’ protein properties or redesign proteins that are useful as biocatalysts or therapeutics. Protein redesign has become very accessible due to developments in the field of molecular biology. Site directed mutagenesis and cloning techniques allow simple changes to be made to recombinant protein systems quickly and easily.

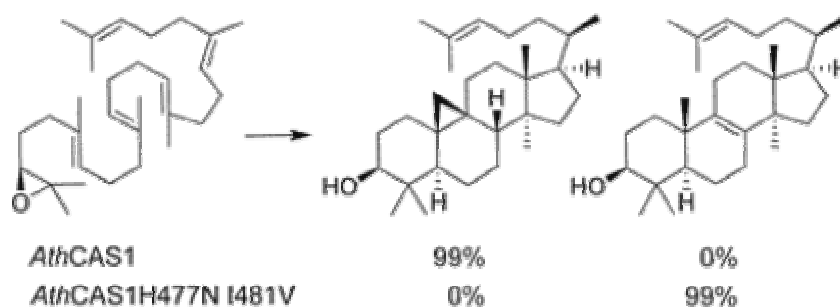
Of particular interest in the protein redesign field is the use of enzymes that have been optimized by redesign for chemical synthesis. This interest arises from the exquisite specificity and selectivity of enzymes. In addition, many enzymes, for example triose phosphate isomerase, have catalytic efficiencies of 10^8 - 10^9 $M^{-1}s^{-1}$ (47), indicating the reaction rates are diffusion controlled. To take advantage of Nature's remarkable catalysts research has been conducted to redesign enzymes to incorporate substrates that are synthetically valuable, to improve on the cost of biocatalyst production, and to increase the stability of enzymes for use in industrial environments.

The ability to redesign enzymes rationally is exemplified in the rational evolution of a bacterial phosphotriesterase to alter the enantioselectivity of the protein without compromising activity. The reaction catalyzed by the enzyme is the cleavage of P-O, P-F, or P-S bonds from insecticides and organo-phosphate nerve agents (Scheme 1.1). The wildtype enzyme has a high preference for the S_P -enantiomers of the chiral organo-phosphate substrates. Mutating three residues in the active site of the phosphotriesterase was sufficient to change the enantioselectivity of the protein from S to R by a factor of 400:1 (48).



Scheme 1.1 Reaction catalyzed by bacterial phosphotriesterase (PTE).

A second example of enzyme redesign is the conversion of cycloartenol synthase to lanosterol synthase (49). Here, two mutations result in an enzyme with altered substrate specificity (Scheme 1.2). These examples illustrate the ability to rationally redesign enzymes to change substrate selectivity. Use of enzymes from thermophilic bacteria and recombinant methods of enzyme production have resulted in cheaper and more stable enzymes for use in large scale synthesis in the presence of solvents.



Scheme 1.2 Reaction catalyzed by wild type cycloartenol synthase (*AthCAS1*) and the double mutant (*AthCAS1H477N I481V*) and their respective products (46).

Of particular interest here is the redesign of natural proteins for use as therapeutics. The list of protein/peptide therapeutics is continually growing and includes a variety of peptide based hormones such as insulin and calcitonin for treatment of diabetes and osteoporosis, respectively. An example of a designed therapeutic peptide is KL-4 surfactant. The peptide design is based on surfactant protein B and was developed for the treatment of pulmonary distress syndrome in preterm infants (50). The route for development of therapeutic peptides is first

to understand the mechanism of the natural peptide and then to modulate its activity by making systematic changes to the peptide. The advantage of peptides is that large libraries of peptides can be synthesized chemically and many variants screened relatively easily. In depth studies that look at the activity of peptides as a result of systematic changes to the peptide or protein sequence are very helpful for determination of the critical properties of the protein. Extensive studies have been conducted on many peptides including protegrin-1, an antimicrobial peptide from porcine leukocytes (51). Ostberg, et al. looked at the structure versus activity of >60 protegrin-1 based peptides to obtain information on the importance of such properties as hydrophobicity and globularity on activity.

1.4 – Non-natural Amino Acids

1.4.1 – New Tools for Protein Design

Incorporation of novel chemical functional groups or side chains of different shapes and sizes through the use of non-natural amino acids allows one to further exploit information gained from basic principle studies and expand the tools available for protein design studies and development. Hundreds of non-natural amino acids are available commercially from common vendors such as Fluka and Novabiochem. Many other non-natural amino acids can be synthesized based on published methods. A small sampling of non-natural

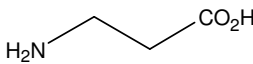
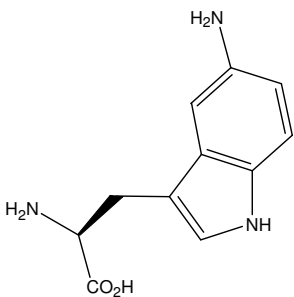
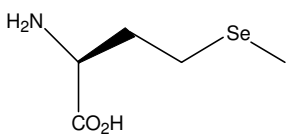
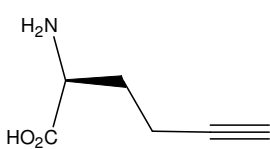
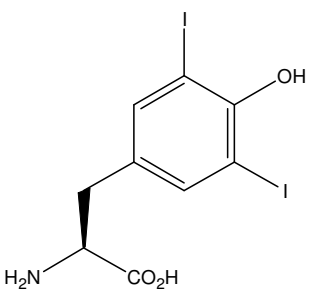
amino acids illustrating the different types of functionality that can be incorporated are presented in Table 1.3.

1.4.2 – β - and D-amino acids

β -Amino acids and D-amino acids have been used to produce peptides that are stable in the presence of proteases. β -Amino acid-containing peptides have been dubbed β -peptides (52). Since these peptides have an additional carbon atom in the peptide backbone, the β carbon, the amino acids are not subject to proteolysis and structural motifs of such peptides differ from those of α -amino acid containing peptides (52-55). The hydrogen bonding patterns also change significantly resulting in helices of wider radius and different connectivity than α -amino acid helices.

Merrifield and coworkers presented a study of antimicrobial peptides that disrupt bacterial membranes containing L and D-amino acids. The chirality of the L-peptides is opposite of that of the D-peptides but, since the pore forming peptides do not rely on chiral interactions this does not affect the antimicrobial activity of the peptides (56). D-amino acids are stable against proteolytic degradation due to the inability of proteases to recognize the non-natural enantiomer, therefore, increasing the potency of these antimicrobial peptides.

Table 1.3 Major classes of non-natural amino acids used in protein design with representative examples for each type of amino acid and the potential applications of the amino acids.

| Amino Acid Type | Example | Use |
|-----------------------|--|---|
| β -amino acids |  <p>β-alanine</p> | Proteolytic stability (52-55) |
| Fluorescent |  <p>5-Aminotryptophan</p> | Structural studies, Dynamics studies, Intramolecular interactions studies (57-61) |
| Heavy Atom containing |  <p>Selenomethionine</p> | Crystal structure determination (62-64) |
| Orthogonally reactive |  <p>Homopropargylglycine</p> | Derivatization, Selective reactivity (67) |
| Halogenated |  <p>3,5-Diiodotyrosine</p> | pK _a tuning, Hydrophobicity, Reactivity, Spectroscopic probes (68) |

1.4.3 – Fluorescent amino acids

UV-Visible and fluorescence spectroscopy methods are very convenient and fast techniques for the observation of proteins. Fluorophores are very sensitive to their local environment and, therefore, are very useful in monitoring protein folding events. In addition, FRET experiments that take advantage of energy transfer from one fluorophore to another result in spectral emissions at specific wavelengths that can be monitored in real time to study inter- and intramolecular interactions of biological molecules.

Amino acids that contain fluorescent side chains have been designed to provide signature spectroscopic signals for use as sensors for the study of protein structure, dynamics, and intramolecular interactions. Tryptophan analogs have been used extensively due to spectral changes upon pH adjustments (57) and to provide unique spectral and visual qualities in proteins (58, 59). Examples of non-natural fluorophores that have been incorporated into proteins include Aladan (60) and dansylalanine (61). Aladan is a 6-dimethylamino-2-acylnaphthalene (DAN) derivative of alanine (Ala). The amino acid has exquisite sensitivity to the electrostatic environment and is, therefore, ideal for probing the polarity and heterogeneity of the interior portions of proteins. Selective incorporation of Aladan in protein G at different sites allowed Cohen *et al.* (60) to determine that the protein is both hydrophobic and heterogeneous. Dansylalanine has been incorporated into superoxide dismutase as a probe for monitoring protein unfolding. The selective genetic incorporation of these and

other fluorescent amino acids should facilitate interesting studies on protein structure and function *in vivo*.

1.4.4. – Heavy Atom Containing Amino Acids

Non-natural analogs of methionine containing heavy atoms such as selenium and tellurium have been developed for incorporation into proteins. Importantly, these amino acid derivatives are recognized by the protein synthesis machinery and can, therefore, be incorporated *in vivo*. These heavy atoms allow crystallographers to more easily locate discrete positions in a protein due to the refractive patterns created by the large atoms.

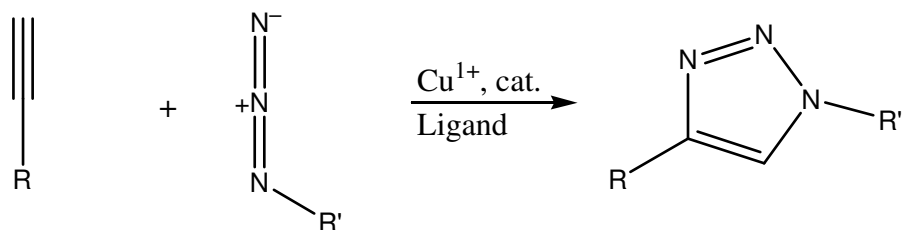
W. A. Hendrickson pioneered the important technique of employing selenomethionine for determination of protein crystal structures using multi-wavelength anomalous diffraction (MAD) crystallography (62, 63). The importance of this method is growing and researchers continue to determine ways to incorporate selenomethionine into proteins expressed in a variety of systems including insect cells (64).

1.4.5 – Orthogonally Reactive Amino Acids

Orthogonally reactive amino acids are used for selective derivatization of peptides and proteins. Natural amino acids such as lysine, cysteine, and glutamate are reactive and can be functionalized, however, these functional

groups are common in proteins and cellular systems. To take full advantage of labeling or derivatizing proteins it is important that the reactions are selective and able to be performed under physiological conditions. The most recent non-natural amino acid side chains to be used as reactive handles in proteins are azide and alkyne functional groups. These functional groups are not present in natural biological molecules and are stable under physiological conditions. They are small and reactive, only with each other under most 'biological' conditions. These characteristics make them ideal for incorporation into proteins with little disturbance to the protein structure and provide a selective, reactive "handle" for studying proteins in complex environments such as cells or tissues.

Commonly azides and alkynes are used in the Staudinger ligation reaction or, the very popular, 'click' reaction. Sharpless and Meldal's simultaneous publications on 'click' chemistry in 2002 kicked off a flurry of research employing the Cu^{1+} catalyzed Huisgen 1,3-cycloaddition reaction for many purposes (Scheme 1.3) (65, 66). Nearly 1000 papers have been published; the employment of click chemistry in protein derivatization is illustrated by one example from Tirrell *et al.* who demonstrated the use of homopropargylglycine in proteins for *in vivo* visualization of the proteins (67). The propargyl side chain is labeled by the membrane permeable dye 3-azido-7-hydroxycoumarin. The protein labeling event gives rise to fluorescent based images that reveal the location of the labeled protein within the cell.



Scheme 1.3 General reaction scheme of the Cu¹⁺ catalyzed, 1 + 3 Huisgen cycloaddition or 'click' reaction.

1.4.6 – Halogenated Amino Acids

The electronegativity of halogens result in shifts in the pK_a's of nearby ionizable groups. This atomic property allows halogenated amino acids to be employed to tune the pK_a's of amino acid side chains. The difference in electronegativity between fluorine, chlorine, bromine and iodine gives rise to the ability to fine tune pK_a's of hydroxyl groups in such amino acids as 3,5-diiodotyrosine.

An elegant example of this is the design and modulation of pH-sensitive pore-forming peptides by Haas and Murphy. The 30 residue peptide, GALA, is helical at acidic pH and inserts into lipid bilayers upon becoming structured (68). The transition to α -helix is shifted from pH 5.7 in GALA to pH 6.7 in YALA due to a 3,5-diiodotyrosine residue in the YALA analog.

1.5 – Fluorous Non-natural Amino Acids

1.5.1 – Fluorous Amino Acids

The use of fluorinated amino acids is very common among the halogenated non-natural amino acids. Fluorinated analogs of tyrosine have been used for tuning pKa's of the tyrosyl hydroxyl group, and fluorine provides a spectroscopic handle for ^{19}F NMR experimentation (69, 70). Highly fluorinated amino acids such as 5,5,5,5',5',5'-hexafluoroleucine are termed “fluorous”. The highly hydrophobic nature of fluorous materials has given rise to many protein design projects that involve the use of fluorous amino acids to produce hyperstable proteins through the repacking of the hydrophobic interior of proteins with highly fluorous amino acids. This topic is discussed in detail in Chapter 2.

1.5.2 – Characteristics of Fluorine

Fluorocarbon molecules have very distinct and desirable characteristics. These include chemical inertness, high thermal stability and self-segregation from non-fluorous compounds. These characteristics are evident in the use of perfluorinated compounds as surface coatings for high temperature environments such as frying pans and for treatment of fabrics to prevent stains. Fluorous compounds continue to be useful in industrial settings and more recently have found use in the design and improvement of biological molecules.

Fluorine has high electronegativity, low polarizability and a small size, with a van der Waals radius of 1.35 Å, similar to the radius of hydrogen at 1.20 Å (71). These atomic properties give rise to the significant differences between the physical properties of hydrocarbons and perfluorocarbons, but also make fluorine a reasonable replacement for hydrogen in terms of size. The large dipole moments and very low polarizability of C-F bonds result in the polar, hydrophobic properties of fluorinated compounds (72). A comparison of C-H versus C-F bonds, including the size and strength of these bonds, is illustrated in Table 1.4. The high C-F bond strength results in perfluorocarbon compounds having an inert quality.

Table 1.4 Bond lengths and dissociation energies of fluoromethanes (73).

| | CH ₄ | CH ₃ F | CH ₂ F ₂ | CF ₃ H | CF ₄ |
|--|-----------------|-------------------|--------------------------------|-------------------|-----------------|
| C–F bond length/Å | 1.09 (C-H) | 1.39 | 1.36 | 1.33 | 1.32 |
| C–F bond energy/kcal mol ⁻¹ | 98.8 (C-H) | 107 | 109.6 | 114.6 | 116 |

The increased hydrophobicity, thermal stability and chemical inertness of fluorinated compounds have spurred interest in investigating the effect of incorporating fluorinated amino acids into proteins. The importance of hydrophobic collapse in the initiation of protein folding events and the stability of protein structure make fluorinated amino acids an ideal tool in protein design. In addition to the hydrophobicity of fluorinated compounds, the self-segregating properties of highly fluorinated molecules hold out the intriguing possibility that fluorinated protein

interactions could be designed that would be orthogonal to natural, non-fluorous proteins in a living system. The focus here is on fluorous analogs of natural amino acids in protein design as exemplified in Table 1.5. Other fluorous amino acids, particularly C α -fluoroalkyl amino acids, have also been studied (74).

1.5.3 – Fluorous Aliphatic Amino Acids

Fluorous versions of aliphatic amino acids, including those in Table 1.5, have been employed to stabilize small proteins by repacking the hydrophobic core with fluorous analogs of hydrophobic residues. The increased hydrophobicity of the highly fluorinated amino acid compared with the non-fluorinated amino acids results in proteins with increased thermal and chemical stability.

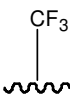
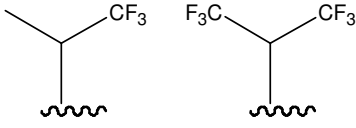
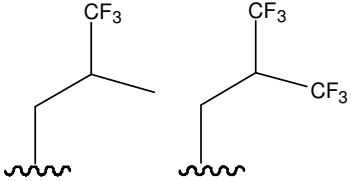
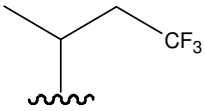
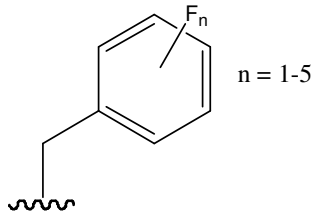
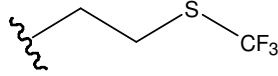
Trifluorovaline and trifluoroisoleucine have been incorporated into GCN4-like coiled-coil peptides (75). Replacing leucine residues in the (*d*) position of a four heptad peptide with trifluorovaline resulted in a 0.5-1.2 kcal/mol increase in free energy of folding and a 13°C increase in melting temperature at 30 μ M peptide concentrations. The fluorous analog of GCN4 retained a similar DNA-binding activity, affinity and specificity to that of the wildtype protein.

A second set of GCN4-like peptides was studied that contained trifluorovaline or trifluoroisoleucine in the (*a*) position of the heptad (76). Thermal unfolding and chemical denaturation studies showed both fluorinated peptides had increased stability over the non-fluorinated peptide, moreover, the

trifluoroisoleucine variant was significantly more stable than the trifluorovaline variant.

Hexafluoroleucine (hFLeu) has also been employed to stabilize proteins through fluorine interactions. A series of progressively more fluorinated four helix bundle proteins studied by Marsh and coworkers revealed that repacking of the hydrophobic core with hexafluoroleucine results in an increase in the free energy of folding by an average of 0.3 kcal/mol/residue (77). This model system will be discussed in further detail in Chapter 2. In addition, other groups have employed hexafluoroleucine to study the self-segregating properties of highly fluorinated peptides, and in designs of transmembrane helical peptides (37, 78). These studies suggest that the highly hydrophobic nature of hexafluoroleucine results in self-segregation of fluorinated peptides from non-fluorinated analogs and promotes higher order oligomerization of transmembrane helices in micelles.

Table 1.5. Fluorinated analogs of hydrophobic amino acid side chains.

| Amino acid | Structure |
|---------------|--|
| Alanine |  |
| Valine |  |
| Leucine |  |
| Isoleucine |  |
| Phenylalanine |  |
| Methionine |  |

1.5.4 – Fluorous Aromatic Amino Acids

Hydrophobic, aromatic amino acids containing fluorine have also been studied in peptides and proteins. In particular, the fluorous analog of phenylalanine, pentafluorophenylalanine (pFPhe), is interesting due to its cationic quadrupole moment. This results in, not only increased hydrophobicity, but also a change from a negative to a positive quadrupolar moment. The ability of pFPhe to affect the stability of proteins was examined by Woll *et al.* using the protein chicken villin headpiece subdomain (cVHP) as a model. Analogs containing pFPhe residues in different combinations at positions 6, 10, and 17 were synthesized (79). Of the peptides studied only one, a single pFPhe in position 10, had increased stability over the non-fluorous peptide. These results indicate a possible destabilization effect due to sterics or destabilizing conformational rearrangements for optimization of side-chain interactions.

1.6 – Goals

The extensive research on protein design and incorporation of non-natural amino acids into peptides and proteins forms the basis for the research described in the proceeding chapters. A *de novo* designed peptide is used to study the increased stability and potential self-segregating properties imparted by use of the highly fluorinated amino acid, hFLeu. Also, a series of antimicrobial peptides have been studied to deduce the affects of fluorination on the stability

and antimicrobial activity of α -helical and β -hairpin peptides. Finally, an α -helical peptide has been investigated for its use in mediating higher order assembly of the highly symmetric cholera toxin B protein. The long term objectives of this research is to contribute to our basic knowledge of protein design principles and apply this to the development of protein/peptide based therapeutics and biomaterials.

1.7 – References

1. Sigler, P. B., Xu, Z., Rye, H. S., Burston, S. G., Fenton, W. A., Horwich, A. L., *Annu. Rev. Biochem.*, **67**, 581-608, (1998).
2. Oppenheim, J. J., Biragyn, A., Kwak, L. W., Yang, D., *Ann. Rheum. Dis.*, **62**, 17-21 (2003).
3. Hendrickson, T. L., Crecy-Lagard, V., Schimmel, P., *Annu. Rev. Biochem.*, **73**, 147-176 (2004).
4. Anfinsen, C. B., *Science*, **181**, 223-230 (1973).
5. Scheraga, H. A. *Pure appl. Chem.* **50**, 315-324, (1978).
6. Padmanabhan, S., Marqusee, S., Ridgeway, T., Laue, T. M., Baldwin, R. L., *Nature* **344**, 268-270 (1990).
7. O'Neil, K. T., and DeGrado, W. F., *Science* **250**, 646-651 (1990).
8. Lyu, P. C., Liff, M. I., Marky, L. A., Kallenbach, N. R., *Science* **250**, 669-673 (1990).
9. Horovitz, A., Matthews, J. M., Fersht, A. R., *J. Mol. Bio.* **227**, 560-568 (1992).
10. Blaber, M., Zhang, X., Matthews, B. W., *Science* **260**, 1637-1640 (1993).
11. Munoz, V., and Serrano, L. *J. Mol. Bio.*, **245**, 275-296 (1995).
12. Luque, I., Mayora, O. L., and Freire, E., *Biochemistry*, **35**, 13681-13688 (1996).
13. Pace, N. C., and Scholtz, J. M., *Biophys. J.*, **75**, 422-427 (1998).
14. Bysroff, C., and Garde, S., *Proteins*, **50**, 552-562 (2003).
15. Minor Jr., D. L., and Kim, P. S., *Nature*, **367**, 660-663 (1994).
16. Ho, B. K. and Brasseur, R., *BMC Struct. Bio.*, **5**, 14-25 (2005).
17. Minor, D. L. and Kim, P. S., *Nature*, **380**, 730-734 (1996).
18. Creighton, T. E., 1993. Proteins: Structures and Molecular Properties, 2nd Ed., pp. 419-429. Freeman, New York.
19. Fersht, A. 1998. Structure and Mechanism in Protein Science, p. 533-596. Freeman. New York.
20. Dyson, H. J., Wright, P. E., Scheraga, H. A., *Proc. Natl. Acad. Sci.*, **103**, 13057-13061 (2006).
21. Loewenthal, R., Sancho, J., Reinikainen, T., Fersht, A. R., *J. Mol. Bio.*, **232** 574-583 (1993).
22. Horovitz, A., Serrano, L., Avron, B., Bycroft, M., Fersht, A., *J. Mol. Bio.*, **216**, 1031-1044 (1990).
23. Fernandez-Recio, J., Vazquez, A., Civer, C., Sevilla, P., Sancho, J., *J. Mol. Bio.*, **267**, 184-197 (1997).
24. Tsou, L., Tatko, C. D., Waters, M. L., *J Am. Chem. Soc.*, **124**, 14917-14921 (2002).
25. Tatko, C. D., Waters, M. L., *J. Am. Chem. Soc.*, **126**, 2028-2034 (2004).
26. Anderson, M. A., Ogbay, B., Arinoto, R., Sha, W., Kisselev, O. G., Cistola, D. P., Marshall, G. R., *J. Am. Chem. Soc.*, **128**, 7531-7541 (2006).
27. Fersht, A. R. and Serrano, L., *Curr. Opin. Struct. Biol.*, **3**, 75-83 (1993).

28. Pace, C. N., Grimsley, G. R., Thomson, J. A., Barnett, B. J., *J. Biol. Chem.* **263**, 11820-11825 (1988).
29. Bryson, J. W., Betz, S. F., Lu, H. S., Siuch, D. J., Zhou, H. X., O'Neil, K. T., DeGrado, W. F., *Science*, **270**, 935-941 (1995).
30. Oakley, M. G. and Hollenbeck, J. J., *Curr. Opin. Struct. Bio.*, **22**, 450-457 (2001).
31. Dieckmann, G. R., McRorie, D. K., Tierney, D. L., Utschig, L. M., Singer, C. P., O'Halloran, T. V., Penner-Hahn, J. E., DeGrado, W. F., Pecoraro, V. L., *J. Am. Chem. Soc.*, **119**, 6195-6196 (1997).
32. Ogihara, N. L., Ghirlanda, G., Bryson, J. W., Bindery, M., DeGrado, W. F., Eisenberg, D., *Proc. Natl. Acad. Sci.*, **98**, 1404-1409 (2001).
33. Kaplan, J. And DeGrado, W. F., *Proc. Natl. Acad. Sci.*, **101**, 11566-11570 (2004).
34. Whitley, P., Nilsson, I. M., Heijne, G. *Nat. Struct. Bio.*, **1**, 858 - 862 (1994)
35. Choma, C., Gratkowski, H., Lear, J. D. & DeGrado, W. F., *Nat. Struct. Biol.* **7**, 161-166 (2000).
36. Hofmann, M. W., Weise, K., Ollesch, J., Agrawal, P., Stalz, H., Stelzer, W., Hulsbergen, F., Groot, H., Gerwert, K., Reed, J., Langosch, D., *Proc. Natl. Acad. Sci.*, **101**, 14776-14781 (2004).
37. Bilgicer, B., Kumar, K., *Proc. Natl. Acad. Sci.*, **101**, 15324-15329 (2004).
38. Fezoui, Y., Weaver, D. L., Osterhout, J. J., *Proc. Natl. Acad. Sci.*, **91**, 3675-3679 (1994).
39. Fezoui, Y., Hartley, D. M., Walsh, D. M., Selkoe, D. J., Osterhout, J. J., Teplov, D. B., *Nat. Struct. Bio.*, **7**, 1095-1099 (2000).
40. Gunasekaran, K., Ramakrishnan, C., Balaram, P., *Protein Engineering*, **10**, 1131-1141 (1997).
41. Dhanasekaran, M., Prakash, O., Gong, Y. X., Baures, P. W., *Org. Biomol. Chem.*, **2**, 2071-2082 (2004).
42. Hughes, R. M. and Waters, M. L., *Curr. Opin. Struct. Bio.*, **16**, 514-524 (2006).
43. Hecht, M. H., *Proc. Natl. Acad. Sci.*, **91**, 8729-8730 (1994).
44. Quinn, T. P., Tweedy, N. B., Williams, R. W., Richardson, J. S., Richardson, D. C., *Proc. Natl. Acad. Sci.*, **91**, 8747-8751 (1994).
45. Hu, X., Wang, H., Ke, H., Kuhlman, B., *Proc. Natl. Acad. Sci.*, **104**, 17668-17673 (2007).
46. Struthers, M. D., Cheng, R. P., Imperiali, B., *Science*, **271**, 342-345 (1996).
47. Blacklow, S. C., Raines, R. T., Lin, W. A., Zamore, P. D., Knowles, J. R., *Biochemistry*, **27**, 1158-1167 (1988).
48. Chen-Goodspeed, M., Sorgorb, M. A., Wu, F., Raushel, F. M., *Biochemistry*, **40**, 1332-1339 (2001).
49. Lodeiro, S., Schulz-Gasch, T., Matsuda, S. P. T., *J. Amer. Chem. Soc.*, **127**, 14132- 14133 (2005).
50. Cochrane, C. G., Revak, S. D., Merritt, T. A., Heldt, G. P., Hallman, M., Cunningham, M. D., Easa, D., Pramanik, A., Edwards, D. K., Alberts, M. S., *Am. J. Respir. Crit. Care Med.*, **153**, 404-410 (1996).
51. Ostberg, N. and Kaznessis, Y, *Peptides*, **26**, 197-206 (2005).

52. Appella, D. H.; Christianson, L. A.; Karle, I. L.; Powell, D. R.; Gellman, S. H., *J. Am. Chem. Soc.*, **118** 13071-13072 (1996).
53. DeGrado, W. F., Schneider, J. P., Hamuro, Y., *J. Peptide Res.*, **54**, 206-217 (1999).
54. Daniels D. S., Petersson E. J., Qiu J. X., Schepartz A., *J. Am. Chem. Soc.* **129**, 1532–153 (2007).
55. rackenpohl, J., Arvidsson, P. I., Schreiber, J. V., Seebach, D., *ChemBioChem*, **2**, 445-455 (2001).
56. Wade, D., Bowman, A., Wahlin, B., Drain, C. M., Andreu, D., Boman, H. G., Merrifield, R. B., *Proc. Natl. Acad. Sci.*, **87**, 4761-4765 (1990).
57. Budisa, N., Rubini, M., Bae, J. H., Weyher, E., Wenger, W., Golbik, R., Huber, R., Moroder, L., *Angew. Chem. Int. Edit. Engl.*, **41**, 4066-4069 (2002).
58. Rae, J. H., Rubini, M., Jung, G., Wiegand, G., Seifert, M. H. J., Azim, M. K., Kim, J. S., Zumbusch, A., Holak, T. A., Moroder, L., Huber, R., Budisa, N., *J. Mol. Bio.*, **328**, 1071-1081 (2003).
59. Ross, J. B. A., Senear, D. F., Waxman, E., Kombo, B. B., Rusinova, E., Huang, Y. T., Laws, W. R., Hasselbacher, C. A., *Proc. Natl. Acad. Sci.*, **89**, 12023-12027 (1992).
60. Cohen, B. E., McAnaney, T. B., Park, E. S., Jan, Y. N., Boxer, S. G., Jan, L. Y., *Science*, **296**, 1700-1703 (2002).
61. Summerer, D., Chen, S., Wu, N., Deiters, A., Chin, J. W., Schultz, P. G., *Proc. Natl. Acad. Sci.*, **103**, 9785-9789 (2006).
62. Yang W. , Hendrickson W. A., Crouch R. J. , Satow Y., *Science*, **249**, 1398-1405 (1990).
63. Leahy D. J. , Hendrickson W. A., Aukhil I. , Erickson H. P., *Science*, **258**, 987-991 (1992).
64. Cronin, C. N., Lim, K. B., Rogers, J., *Protein Sci.* **16**, 2023-2029 (2007).
65. Rostovtsev, V. V., Green, L. G., Fokin, V. V., Sharpless, K. B., *Angew. Chem. Int. Ed.*, **41**, 2596-2599 (2002).
66. Tornoe, C. W., Christensen, C., Meldal, M., *J. Org. Chem.* **67**, 3057-3064 (2002).
67. Beatty, K. E., Liu, J. C., Xie, F., Dieterich, D. C., Schuman, E. M., Wang, Q, Tirrell, D. A., *Angew. Chem. Int. Ed.*, **45**, 7364-7367 (2006).
68. Haas, D. H. and Murphy, R. M., *J. Peptide Res.*, **63**, 9-16 (2004).
69. Gerig, J. T., *Prog. NMR Spectrosc.*, **26**, 293-370 (1994).
70. Chambers, S. E., Lau, E. Y., Gerig, J. T., *J. Amer. Chem. Soc.*, **116**, 3603-3604 (1994).
71. Smart, B. E., *J. Fluorine Chem.*, **109**, 3-11 (2001).
72. Biffinger, J. C., Kim, H. W., DiMagno, S. G., *ChemBioChem*, **5**, 622-627 (2004).
73. O'Hagan, D., *Chem. Soc. Rev.*, **37**, 308-319 (2008).
74. Smits, R. and Koksche, B., *Curr. Top. Med. Chem.*, **6**, 1483-1498 (2006).
75. Tang, Y., Ghirlanda, G., Vaidehi, N., Kua, J., Mainz, D. T., Goddard, W. A., DeGrado, W. F., Tirrell, D. A., *Biochemistry*, **40**, 2790-2796 (2001).

76. Son, S., Tanrikulu, I. C., Tirrell, D. A., *ChemBioChem*, **7**, 1251-1257 (2006).
77. Lee, H-Y., Lee, K-H., Al-Hashimi, H. M., Marsh, E. N. G., *J. Amer. Chem. Soc.*, **128**, 337-343 (2006).
78. Bilgiçer, B., Xing, X., Kumar, K., *J. Amer. Chem. Soc.*, **123**, 11815-11816 (2001).
79. Woll, M G., Hadley, E. B., Mecozzi, S., Gellman, S. H., *J. Amer. Chem. Soc.*, **128**, 15932-15933 (2006).

Chapter 2

Fluorinated Coiled-coils: A Model System

2.1 – Introduction

2.1.1 – Coiled-coils

The coiled-coil is a commonly observed motif in protein structures. A coiled-coil is composed of two or more α -helices wrapped around one another to form a supercoiled tertiary structure. The supercoiling of the helices results in a structure that is composed of helices with 3.5 residues per turn as opposed to 3.7 residues per turn in an undistorted α -helix. Therefore, two turns of the helix form a heptad repeat and the residues within each heptad occupy spatially unique positions that are labeled *a-g* (see Figure 2.1). The positioning of the amino acid side chains in a heptad is very significant. The side chains in the *a* and *d* positions are primarily hydrophobic and form a hydrophobic core upon oligomerization of the helices to form the coiled-coil. Side chains in the *b*, *c*, *e*, and *g* positions are often ionic and provide intramolecular salt bridge and/or H-bonding interactions that may promote either parallel or antiparallel assembly of the helices in the tertiary structure. Amino acids that are located at the *f* position

are generally hydrophilic in simple coiled-coil proteins. This exposed hydrophilic surface promotes solubility in aqueous solutions.

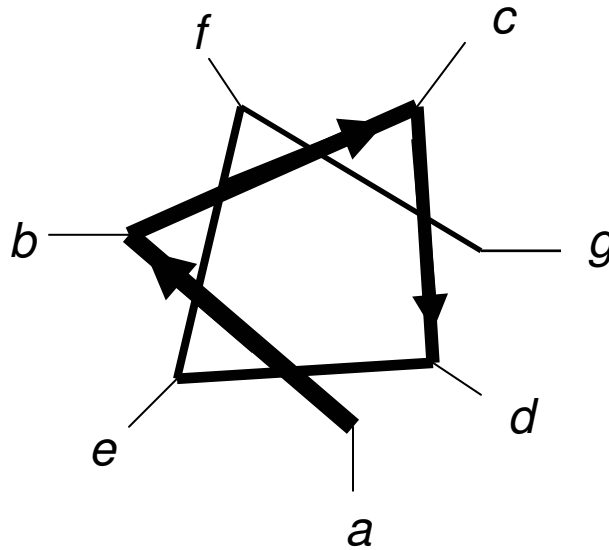


Figure 2.1. Helical wheel diagram denoting the amino acid side chain positions as *a-g* to signify a heptad repeat.

2.1.2 – ROP; a Naturally Occurring Coiled-coil.

A simple and important example of a coiled-coil in Nature is the Repressor of Primer protein (ROP) from *E. coli* (see Figure 2.2). The protein is a negative regulator of plasmid replication and functions by increasing the association of the RNAII primer to RNAI. Therefore, the RNAII primer is unable to bind the plasmid to form the DNA-RNA hybrid primer needed for initiation of plasmid replication (1). ROP is an antiparallel homodimer composed of two helix-turn-helix subunits. The resulting structure is a 4- α -helix bundle. These structures are of particular

interest in *de novo* protein design due to their prominent occurrence in natural proteins and their robust structures.

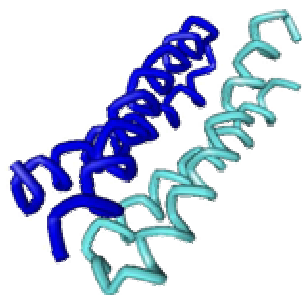


Figure 2.2. ROP backbone structure viewed in solid-ribbon (PDB 1ROP).

2.1.3 – Design of a 4- α -Helix Bundle

In connection with our interests on the effects of fluorinated amino acids on protein structure and stability we have designed an α -helical peptide that forms an antiparallel homotetramer and is denoted α_4H . The sequence and heptad notation of the amino acids is seen in Figure 2.3. The helical wheel diagram of the designed peptide is shown in Figure 2.4. The hydrophobic core of the tetramer is packed with leucine residues at positions *a* and *d* of the heptad. Complementary ionic interactions between positions *c* and *g*, and positions *b* and *e* dictate the antiparallel orientation of the tetramer. The 3 heptad design results in 6 layers within the hydrophobic core packed with leucine residues and allows for systematic replacement of leucine with 5,5,5',5',5'-hexafluoroleucine

(hFLeu) to investigate changes in the properties of the peptide upon incorporation of increasing amounts of fluorine in the hydrophobic core.

fg abcdefg abcdefg abcdefg abcd
 GN ADE**LY**KE **LE**D**LQ**ER **LR**K**LR**KK **LR**SG

Figure 2.3. α_4 H sequence (capital letters) and heptad notation (lower case letters). Leucine residues depicted in bold are hFLeu in the α_4 F₆ peptide.

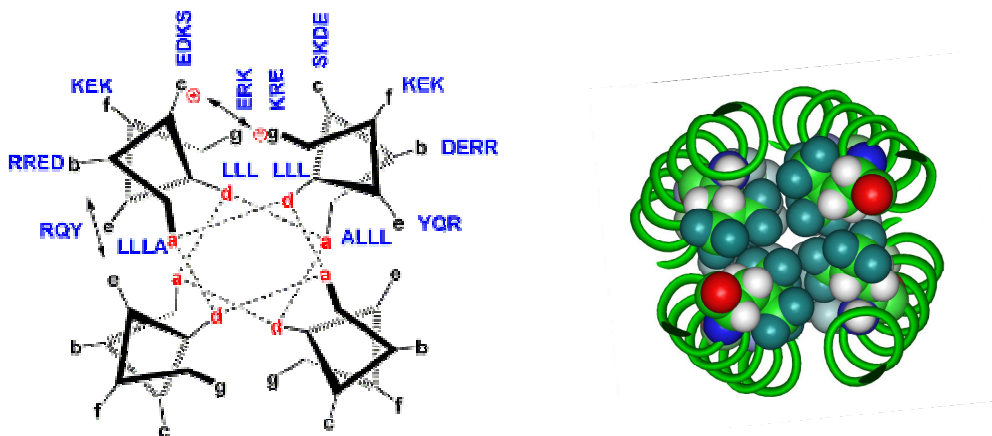


Figure 2.4. Helical wheel diagram (A) and computer generated model (B) of the α_4 peptide design. The computer model depicts the protein backbone as ribbon and a layer of the hydrophobic hFLeu packed core in CPK.

The systematic replacement of leucine in the α_4 H peptide results in a series of peptides with 0, 2, 4 or 6 hFLeu residues per peptide in the hydrophobic core. The parent peptide containing only leucine in the hydrophobic core is named α_4 H, replacing 2 leucines in the central layers of the hydrophobic core

results in α_4F_2 , replacing 4 leucines in the central 4 layers of the hydrophobic core results in α_4F_4 , and replacing all 6 leucines with hFLeu results in the fully fluorinated α_4F_6 (see Figure 2.5).

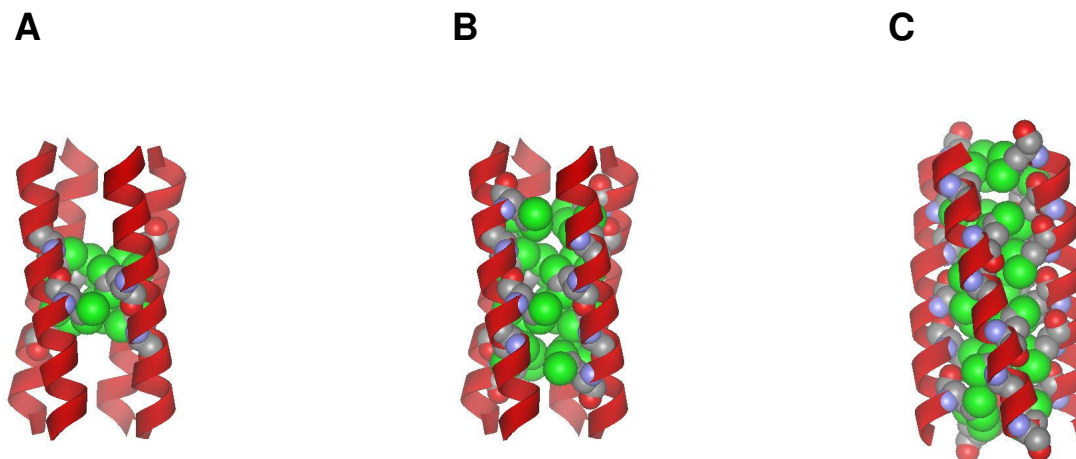


Figure 2.5. Computer generated models of (A) α_4F_2 , (B) α_4F_4 and (C) α_4F_6 . hFLeu residues are shown in CPK with fluorine atoms in green.

2.1.4 – Properties of α_4H , α_4F_2 , α_4F_4 , and α_4F_6

Previous experiments with the α_4 peptide series revealed that the design is structurally robust in that replacement of 2, 4, or 6 leucine residues with hFLeu in the hydrophobic core does not result in gross changes in the structure of the protein. The oligomerization state remains tetrameric and the peptides remain highly structured as determined by gel filtration analysis, sedimentation equilibrium, ANS binding, and NMR (2,3). The ^{19}F NMR spectrum of α_4F_6 exhibits a high degree of dispersity and appears more complex than can be

accounted for simply by the signals from 12 CF₃- groups in which the three fluorine atoms are chemically equivalent, suggesting that the fluorine atoms are in an anisotropic environment (3) and the protein is highly structured. The helical secondary structure of the peptides was also retained upon addition of fluorine to the hydrophobic core as determined by Circular Dichroism (C.D.) spectroscopy. Most interestingly, the peptide stability was increased, almost linearly, with increasing hFLeu residues within the peptides. The average per-residue stabilization affected by substituting hFLeu for Leu was determined to be $\Delta\Delta G \sim -0.3$ kcal/mol/residue (3).

2.1.5 – Solvent Stability, Protease Stability, Self-segregation

The predicted thermal stability and stability towards denaturation by chaotropic agents of fluorinated coiled-coils has been established for the α_4 peptide series, as well as other coiled-coil peptides discussed in Chapter 1. Based on the characteristics of simple fluorocarbons, such proteins are predicted to have increased biological stability, increased chemical stability, and self-segregating properties. Few studies have been conducted to test the validity of these later properties; however, those that have support the predicted properties (4,5). To better understand the effects of fluorination on the properties of peptides and proteins, α_4H and α_4F_6 have been compared to determine the biological and chemical stability, and self-segregation properties imparted by fluorine.

2.2 - Experimental Procedures

2.2.1 – Materials

L-5,5,5,5',5',5'-hexafluoroleucine (hFLeu) was synthesized as described previously (6) and converted to fmoc- or t-Boc- protected derivatives by standard procedures. The sequences of the peptides α_4F_6 and α_4H used in this study are shown in Figure 2.3. These were synthesized by automated fmoc procedures (α_4H) or manual boc procedures (α_4F_6) as described previously (2, 3). Trypsin and chymotrypsin from bovine pancreas were purchased from Boehringer Mannheim. Methanol, ethanol, isopropanol, trifluoroethanol (TFE), and hexafluoroisopropanol (HFIP) were purchased from Fisher Chemical Co and were of HPLC grade.

2.2.2 – Proteolysis Experiments

Stock solutions of peptides at a concentration of 1 mM in Milli-Q grade water were prepared and stored at -20°C. A 0.5 mg/mL solution of tryptophan was prepared and stored at 4°C. Solutions of chymotrypsin and trypsin were prepared at a concentration of 1 mg/mL in 1 mM HCl just prior to use. Proteolytic digestions were performed at 25°C by mixing together 10 μ L of peptide stock solution, 10 μ L of 200 mM Tris/Cl buffer, pH 7.8, containing 20 mM $CaCl_2$, and 0.5 μ L tryptophan solution (as an internal standard). Digestion reactions were

initiated by the addition of protease, 0.5 μL , to give a ratio of 80 : 1 (w/w) peptide to protease. At various times 5 μL of the reaction mixture was removed and quenched using an equal volume of 1 M HCl. Samples were stored at -20°C until analysis by HPLC. All digests were repeated 3 times. Control reactions containing all reagents except protease were performed and no degradation of the parent peptide was observed.

The products of proteolytic digestion were analyzed by reverse phase HPLC using a C_{18} column. Samples were diluted to $\sim 40 \mu\text{L}$ with 5 % acetonitrile, 0.15 % acetic acid for injection onto the column and eluted with a linear gradient of 5 to 90 % acetonitrile, containing 0.15 % acetic acid. The relative amount of peptide remaining undigested at a given time was determined from the peak area relative to that of the internal standard tryptophan peak.

2.2.3 - Solvent-induced Unfolding of Peptides

Circular dichroism (C.D.) spectra of peptides (20 μM or 200 μM) were recorded with an Aviv 62DS spectropolarimeter at 25°C . Mean residue ellipticities, Θ_{M} , were calculated using equation 1.

$$\Theta_{\text{M}} = \Theta_{\text{obs}}/10lcn \quad (1)$$

where Θ_{obs} is the ellipticity measured in millidegrees, c is the molar concentration, l is the cell path length in centimeters, and n is the number of residues in the

protein. The hydrophobicity of the solvent water mixtures (LogP_{mix}) were calculated assuming that the hydrophobicity varied as a linear function of solvent composition according to equation 2.

$$\log P_{\text{mix}} = X_{\text{solvent}} \log P_{\text{solvent}} + (1 - X_{\text{solvent}}) \log P_{\text{water}} \quad (2)$$

where X is the mole fraction of each solvent and logP values were obtained from previously reported values (7, 8).

2.2.4 - Analytical Ultracentrifugation

Sedimentation equilibrium experiments were performed using a Beckman XLA analytical ultracentrifugation equipped with scanning u.v.-visible optics (29). Initial peptide concentration was 200 μM in 10 mM potassium phosphate buffer, pH 7.0, containing various mole fractions of ethanol or TFE. The temperature was 293 K. The samples were centrifuged at 30,000, 35,000, 37,500, 40,000, 42,500 and 45,000 rpms and were judged to have obtained equilibrium when successive radial scans were indistinguishable. The data were fitted to either a monomer – tetramer equilibrium, assuming a monomer molecular weight of 3300 for $\alpha_4\text{H}$ and 3947 for $\alpha_4\text{F}_6$, or to a single species using the Ultrascan software package (B. Demeler, University of Texas Health Science Center at San Antonio; www.ultrascan.uthscsa.edu). Partial specific volumes were calculated using the method of Cohn and Edsall (10): the partial specific volume of $\alpha_4\text{H}$ was

calculated as $0.74 \text{ cm}^3\text{g}^{-1}$; the partial specific volume $\alpha_4\text{F}_6$ was calculated as $0.66 \text{ cm}^3\text{g}^{-1}$.

2.2.5 - ^{19}F NMR Spectroscopy

^{19}F NMR spectra were recorded using a Varian 400 MHz NMR spectrometer equipped with a ^{19}F probe. Peptide samples (0.5 – 2.0 mM) were prepared in 10% D_2O in a final volume of 0.5 mL and adjusted to pH 7.0 with NaOH unless otherwise noted. Spectra were recorded at 25°C and were referenced to trifluoroacetate ion = 0 ppm.

2.3 – Results

2.3.1 – Biological Stability of $\alpha_4\text{H}$ vs. $\alpha_4\text{F}_6$

Peptides composed entirely of natural amino acids are often subject to poor metabolic stability hindering their use in many therapeutic applications. This is a result of being either unstructured or having highly dynamic structures which make them highly susceptible to proteolytic degradation. The protective effects of non-natural amino acids such as β -amino acids and D-amino acids have been well established, however, the ability of other non-natural amino acids, such as hFLeu to protect against proteolysis, remains to be determined. A report in the literature on fluorinated antimicrobial peptides suggests that a single hFLeu

residue can reduce the rate of proteolytic degradation, however, these results only include data on trypsin, a protease that targets lysine and arginine residues, and the results are contradictory to results to be discussed in Chapter 3 (5).

We examined the stability of $\alpha_4\text{H}$ and $\alpha_4\text{F}_6$ towards digestion by trypsin and chymotrypsin because both peptides contain a number of potential cut sites for each protease. Proteolytic digestions were set up at 25 °C using an 80 : 1 ratio (w/w) of peptide to protease and the time course of the disappearance of the parent peptide was monitored by HPLC. $\alpha_4\text{H}$ was much more susceptible to proteolysis by trypsin (Figure 2.6) and chymotrypsin (Figure 2.7) than $\alpha_4\text{F}_6$. Whereas $\alpha_4\text{H}$ was almost completely digested by trypsin after 15 min, less than 50 % of $\alpha_4\text{F}_6$ had been digested after 110 min. Similarly, whereas over 90 % of the $\alpha_4\text{H}$ peptide was degraded by chymotrypsin after 110 min, $\alpha_4\text{F}_6$ is essentially impervious to digestion by chymotrypsin under the same conditions.

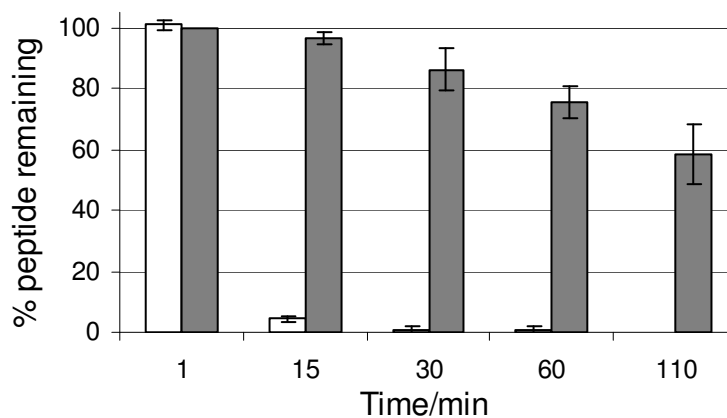


Figure 2.6. Trypsin digests of $\alpha_4\text{H}$ (white) and $\alpha_4\text{F}_6$ (gray).

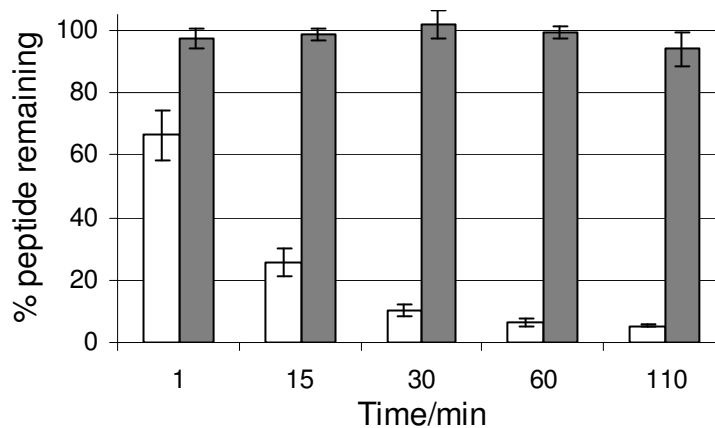


Figure 2.7. Chymotrypsin digests of $\alpha_4\text{H}$ (white) and $\alpha_4\text{F}_6$ (gray).

2.3.2 – Solvent Stability of $\alpha_4\text{H}$ vs. $\alpha_4\text{F}_6$; Secondary Structure

One of the more unusual properties of fluorocarbon solvents is their tendency to self segregate into separate phases due to their low solubility in hydrocarbon solvents; for example hexane and perfluorohexane are immiscible. This has been generally ascribed to “fluorophilic” interactions between fluorocarbon molecules, based on the principle of like dissolving like. As discussed previously (11), this property predicts that, by comparison with natural proteins, fluorous proteins should be resistant to denaturation by organic solvents. The rationale for this prediction is that fluorous amino acid side-chains should be less soluble than hydrocarbon side-chains in hydrocarbon solvent molecules. On the other hand, a fluorous protein should be more prone to denaturation by fluorinated solvents as the fluorous side-chains would be expected to partition into the fluorinated solvent molecules. .

To test this hypothesis the solvent-induced unfolding of α_4F_6 and α_4H by water-miscible fluorocarbon and hydrocarbon organic solvents that vary in their hydrophobicity was examined. First, the unfolding of both peptides was investigated in response to increasing concentrations of methanol, ethanol and 2-propanol, which form a series of chemically similar but increasingly more hydrophobic water-miscible solvents. Peptide unfolding was monitored by following the increase in ellipticity at 222 nm due to the loss of α -helical structure in buffered solutions containing 20 μ M peptide and increasing mole fractions of organic solvent. The results are shown in Figure 2.8 in which relative ellipticity of the each peptide is plotted against both mole fraction of alcohol and $\log P$ calculated for the solvent mixture.

The unfolding of α_4H follows a trend in which methanol, ethanol and 2-propanol are increasingly effective denaturants. Methanol has little effect on the helicity of the peptide, whereas, increasing concentrations of ethanol initially result in a slight increase in helicity before the peptide begins to unfold. 2-propanol is the most effective denaturant, with the peptide becoming almost completely unfolded at high 2-propanol concentrations. In marked contrast, none of the alcohols were able to effectively unfold α_4F_6 and the peptide retained ~ 80 % or greater helicity, as judged by ellipticity at 222 nm, under all solvent conditions. Indeed, at high concentrations of ethanol or 2-propanol the helicity of the peptide begins to increase slightly.

The fluororous effect predicts that the peptides should demonstrate the opposite behavior in fluorinated solvents and therefore, the effect of

trifluoroethanol (TFE) and hexafluoroisopropanol (HFIP) were examined, as shown in Figure 2.8 D and E. As expected, TFE and HFIP did not denature α_4 H. Instead there is an initial sharp increase in helicity with increasing mol fraction of solvent, which levels off after about $X_{\text{TFE}} = 0.15$. This is in accord with the well known property of fluorinated alcohols to increase the helical content of partially structured peptides (12-14). However, contrary to predictions, TFE does not appear to denature α_4 F₆, as judged by C.D. spectroscopy (Figure 2.8D); instead it promotes an increase in helicity similar to that observed for α_4 H. HFIP induces little change in the secondary structure of either peptide until $X_{\text{HFIP}} > 0.6$. At a mol fraction above 0.6 of HFIP α_4 H appears to have a slight increase in helicity while α_4 F₆ begins to decrease in helicity.

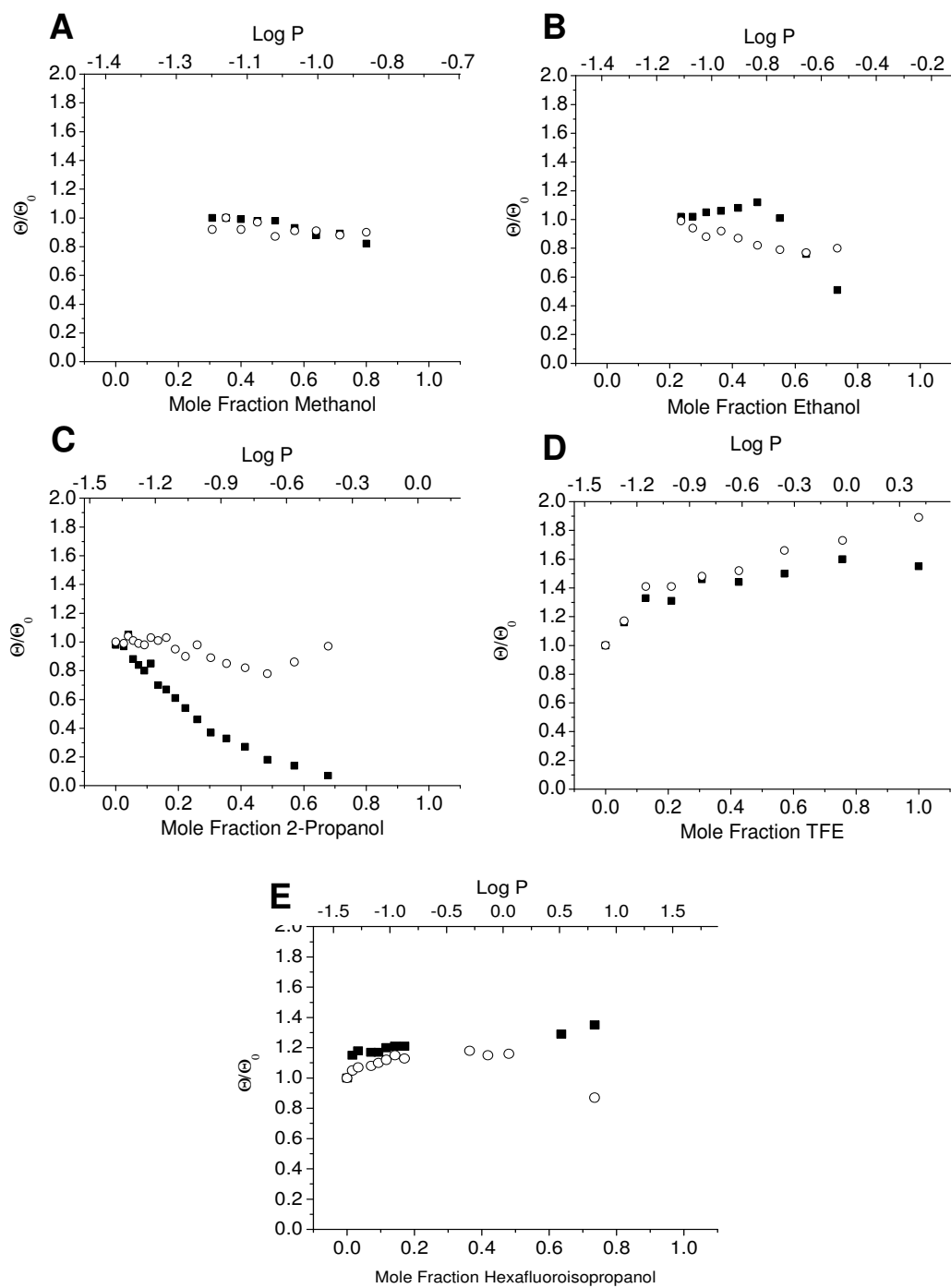


Figure 2.8. Helicity of α_4H and α_4F_6 in different alcohol-water mixtures. The relative helicity of α_4H (■) and α_4F_6 (○), defined as $\Theta_X/\Theta_{\text{water}}$, is plotted as a function of mole fraction of alcohol (lower scale) and $\log P$ for the alcohol-water mixture (upper scale). **A:** Water-methanol mixtures; **B:** Water-ethanol mixtures; **C:** Water-2-propanol mixtures; **D:** Water-TFE mixtures; **E:** Water-HFIP mixtures.

2.4.3 – Solvent Stability of $\alpha_4\text{H}$ vs. $\alpha_4\text{F}_6$; Effect on Tertiary Structure

C.D. spectroscopy is primarily sensitive to changes in secondary structure, but it is possible that the solvents may disrupt the tertiary structure of the 4-helix bundle while maintaining the helical conformation of the individual peptides. To investigate this possibility, sedimentation equilibrium analytical ultracentrifugation was used to examine the effect of these solvents on the apparent molecular weight of the proteins. It has been shown previously that in the absence of organic solvents both $\alpha_4\text{H}$ and $\alpha_4\text{F}_6$ form well-structured tetramers (3).

The sedimentation of the peptides was investigated in the presence of various concentrations of either ethanol or TFE (Table 2.1). In 25 % (v/v) ethanol, ($X_{\text{ethanol}} = 0.13$) the average apparent molecular weights of $\alpha_4\text{H}$ ($M_{r \text{ app}} = 11000 \pm 1000$) and $\alpha_4\text{F}_6$ ($M_{r \text{ app}} = 14000 \pm 1000$) are consistent with both peptides remaining predominantly tetrameric. However, at 50 % (v/v) ethanol ($X_{\text{ethanol}} = 0.31$) the molecular weight of $\alpha_4\text{H}$ ($M_{r \text{ app}} = 4500 \pm 500$) indicates that it is nearly completely dissociated into monomers, although from the C.D. spectrum it still appears to be helical. In contrast, the $\alpha_4\text{F}_6$ peptide remains predominantly tetrameric in 50 % ethanol ($M_{r \text{ app}} = 12,400 \pm 1000$), consistent with the prediction that hydrocarbon alcohols would not be effective denaturants of the fluorocarbon core of $\alpha_4\text{F}_6$.

Table 2.1 Apparent molecular weights in the presence of ethanol or TFE as determined by sedimentation equilibrium.

| % ethanol | Mole Fraction ethanol | $\alpha_4\text{H}$ MW | $\alpha_4\text{F}_6$ MW |
|-----------|-----------------------|-----------------------|-------------------------|
| 25 | .13 | 11000 \pm 1000 | 14000 \pm 1000 |
| 50 | .31 | 4500 \pm 500 | 12400 \pm 1000 |
| % TFE | Mole Fraction TFE | $\alpha_4\text{H}$ MW | $\alpha_4\text{F}_6$ MW |
| 20 | .10 | 15800 \pm 1000 | 15000 \pm 1000 |
| 25 | .13 | 11400 \pm 1000 | 8200 \pm 600 |
| 30 | .16 | 6800 \pm 700 | 5800 \pm 500 |
| 40 | .23 | 4300 \pm 500 | 4600 \pm 500 |

Initial centrifugation experiments in the presence of TFE showed a progressive decrease in the apparent molecular weight of both peptides with increasing mole fraction of TFE, suggesting that TFE was promoting dissociation of the peptides (Table 2.1). Therefore, a more extensive series of sedimentation measurements were conducted at various concentrations of TFE ranging from 5 - 40 % (v/v), ($X_{\text{TFE}} = 0.03 - 0.23$). Association constants were calculated from fits to the sedimentation traces obtained at multiple speeds assuming the sedimenting species were involved in a monomer-tetramer equilibrium. The association constants are plotted as a function of X_{TFE} in Figure 2.9. The data shows a clear trend in which $\log K_a$ decreases as a function of increasing TFE concentration. $\log K_a$ is significantly larger for $\alpha_4\text{F}_6$ at low concentrations of TFE, consistent with the peptide forming a more stable 4-helix bundle in water. However, as the TFE concentration increases, $\log K_a$ for both peptides converge, such that the transition from predominantly tetrameric to predominantly monomeric species occurs for both peptides at $X_{\text{TFE}} = \sim 0.15$. There is no evidence that TFE

preferentially dissociates α_4F_6 , as would be predicted if preferential “fluorous” interactions between hFLeu and TFE were occurring.

Interestingly, the break in the plot of TFE concentration versus relative helicity of the peptides, shown in Figure 2.8D, occurs at the same concentration of TFE as the monomer-tetramer transition observed by ultracentrifugation. This suggests that the initial steep increase in Θ_{222} observed by C.D. results from the transition of the peptides from a 4-helix bundle structure, in which the α -helices are distorted by superhelical coiling, to monomeric α -helices which are free to adopt an undistorted structure.

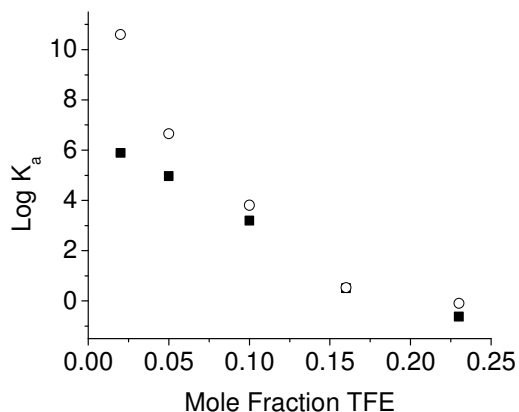


Figure 2.9. Plots of $\log K_a$ for α_4H (■) and α_4F_6 (○) as a function of mole fraction of TFE. K_a was determined from analytical ultracentrifugation experiments as described in the text, assuming an equilibrium between monomeric and tetrameric peptide species.

2.3.4 – Self-segregating Properties of $\alpha_4\text{H}$ and $\alpha_4\text{F}_6$

The self-segregating properties of small fluorinated molecules (15, 16) lead to the interesting prediction that it should be possible to design specific protein-protein interactions based on fluororous interactions between fluorinated amino acid residues. If this is the case, one would predict that $\alpha_4\text{F}_6$ and $\alpha_4\text{H}$ should not form mixed hetero-tetramers because fluorocarbon-fluorocarbon interactions between hFLeu residues in the hydrophobic core of $\alpha_4\text{F}_6$ should be energetically preferred over the corresponding hydrocarbon-fluorocarbon interactions of Leu and hFLeu residues comprising the core of a $\alpha_4\text{F}_6$ - $\alpha_4\text{H}$ heterotetramer. ^{19}F -NMR spectroscopy was used to probe for interactions between the $\alpha_4\text{F}_6$ and $\alpha_4\text{H}$ peptides because the ^{19}F chemical shift is extremely sensitive to changes in chemical environment (17, 18) that would occur if the peptides are interacting with each other.

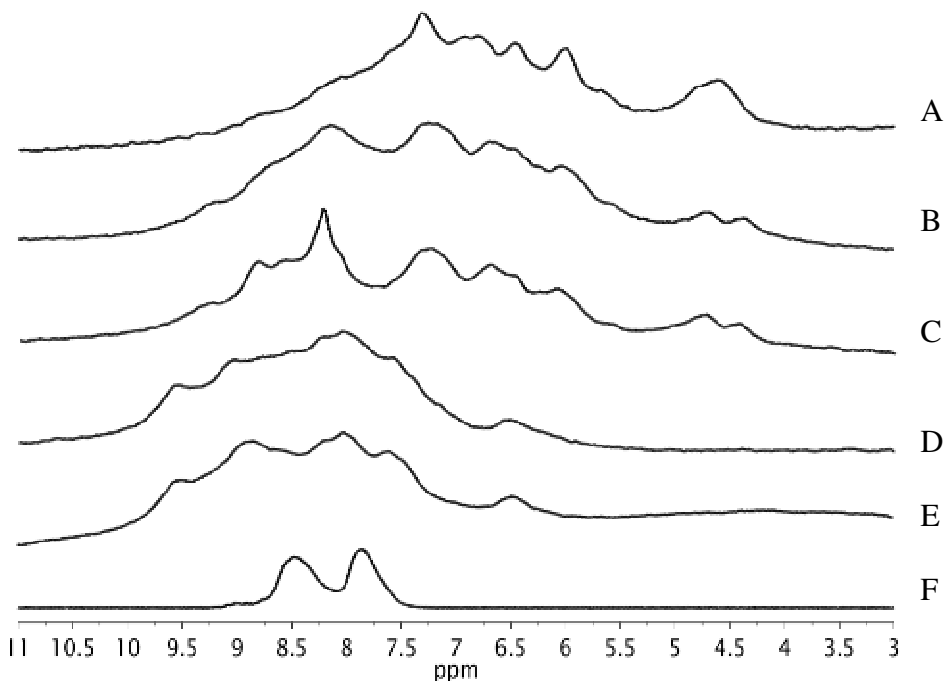


Figure 2.10 ^{19}F NMR spectra of $\alpha_4\text{F}_6$ in the presence of increasing concentrations of $\alpha_4\text{H}$. The spectra are: A: 2 mM $\alpha_4\text{F}_6$; B: 2 mM $\alpha_4\text{F}_6$ and 0.67 mM $\alpha_4\text{H}$; C: 2 mM $\alpha_4\text{F}_6$ and 2 mM $\alpha_4\text{H}$; D: 2 mM $\alpha_4\text{F}_6$ and 6 mM $\alpha_4\text{H}$; E: 1 mM $\alpha_4\text{F}_6$ and 6 mM $\alpha_4\text{H}$; F: 0.5 mM $\alpha_4\text{F}_6$, in 8 M urea, pH 2.0, where the peptide is fully denatured. All the spectra (except F) were recorded at 25 °C and neutral pH, and are referenced to trifluoroacetate = 0 ppm.

The 1-D- ^{19}F NMR spectrum of the folded $\alpha_4\text{F}_6$ is shown in Figure 2.10 (spectrum A); for comparison, the spectrum of the peptide unfolded in 8 M GuHCl at pH 2 is also shown (spectrum F) in which the two peaks correspond to the two chemical inequivalent trifluoromethyl groups of hFLeu. As has been discussed previously, the folded spectrum (A) exhibits a high degree of dispersity and appears more complex than can be accounted for simply by the signals from 12 CF_3 - groups in which the three fluorine atoms are chemically equivalent, suggesting that the fluorine atoms are in an anisotropic or chemically

heterogeneous environment (3). As shown in Figure 2.10, titration of the α_4F_6 peptide with increasing concentrations of α_4H peptide results in a progressive change to the ^{19}F NMR spectrum of α_4F_6 . As the concentration of α_4H increases, the spectrum of α_4F_6 shifts progressively further down field. There also appears to be fewer peaks indicative of more chemically equivalent fluorines in the hydrophobic core, potentially due to the protein becoming more dynamic and the chemical shifts of the fluorine atoms averaging on the NMR time scale. This suggests that the fluorine atoms are experiencing a less hydrophobic and possibly more dynamic environment, consistent with the α_4F_6 peptide forming helical bundles with the less hydrophobic α_4H peptide.

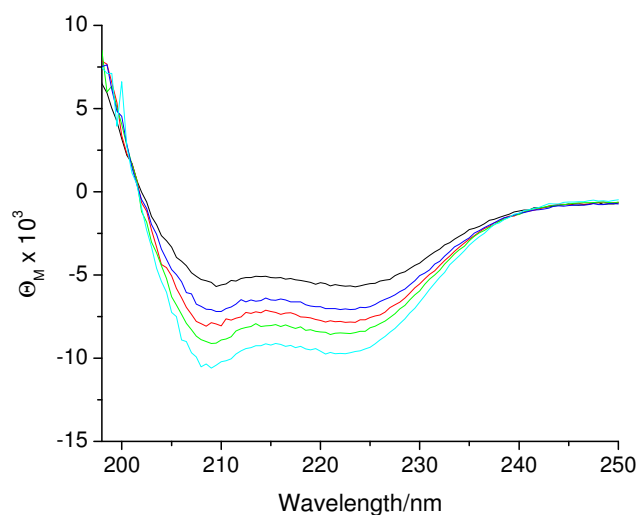


Figure 2.11 C. D. spectra of peptide mixtures; α_4H at 200 μM (cyan); α_4H at 150 μM and α_4F_6 at 50 μM (green); α_4H at 100 μM and α_4F_6 at 100 μM (red); α_4H at 50 μM and α_4F_6 at 150 μM (blue); and α_4F_6 at 200 μM (black).

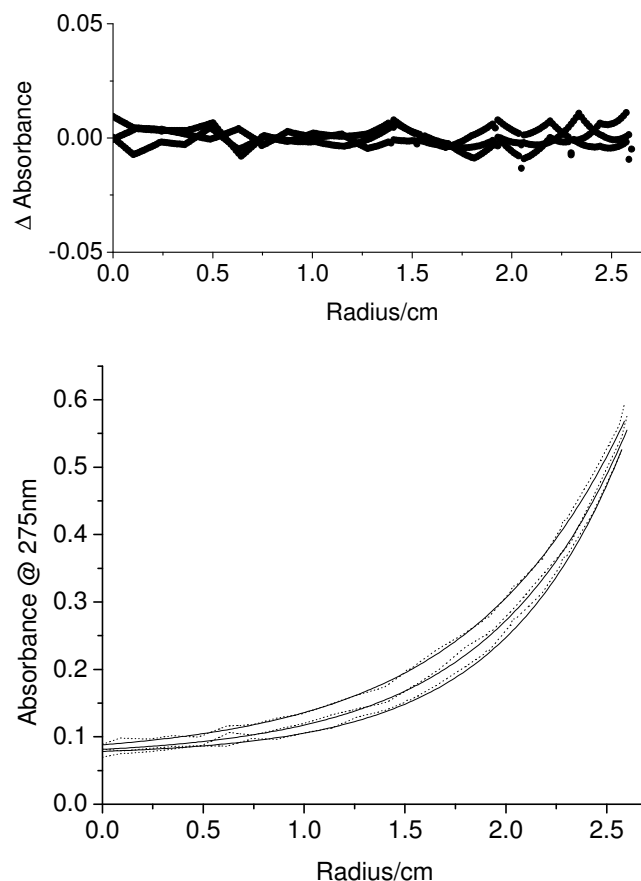


Figure 2.12 Sedimentation equilibrium scans (lower panel, dotted lines) of 1:1 mixture of $\alpha_4\text{H}$ and $\alpha_4\text{F}_6$ at a total peptide concentration of 200 μM . The fit to a single component sedimenting species (lower panel, solid line) results in an apparent molecular weight of 15700 ± 1000 Da (theoretical Mr of 14494 for $\alpha_2\text{H}/\alpha_2\text{F}_6$ tetramer). Scans from speeds of 30K, 35K, 37.5K, and 40K RPM's were included for fitting. Residuals are shown in top panel.

Clearly, if the peptides exhibited true self-segregating behavior, the addition of $\alpha_4\text{H}$ should have no effect on the spectrum of $\alpha_4\text{F}_6$. The C.D. spectra of the peptides did not change appreciably upon mixing the peptides (Figure 2.11), indicating that the peptides remain highly helical. In addition, sedimentation equilibrium experiments indicate that the peptide mixtures have average apparent molecular weights indicative of tetramers, therefore, the oligomerization state is unchanged upon mixing $\alpha_4\text{H}$ and $\alpha_4\text{F}_6$ (Figure 2.12). From these observations

we conclude that the peptides do *not* exhibit the self-segregating behavior predicted by the fluorous effect.

2.4 – Discussion

These experiments have demonstrated that incorporation of extensively fluorinated side-chains, such as hFleu, into a protein can significantly stabilize the protein against proteolysis and unfolding by “conventional” organic solvents. These properties can be attributed to the greater thermodynamic stability of α_4F_6 compared to α_4H , which, as we have discussed previously (2, 3), can be explained by the increase in hydrophobicity of the hFleu side-chains that comprise the hydrophobic core of the protein. Notably, however, these experiments have failed to find any evidence for the “fluorous” behavior predicted for α_4F_6 , i.e. preferential interactions between fluorocarbon groups, either within the protein or between protein and solvent molecules.

It was found that α_4H becomes increasingly more unfolded by methanol, ethanol and 2-propanol respectively. This trend is qualitatively described by the increasingly hydrophobic nature (as measured by logP) of these alcohols. This is consistent with the idea that the more hydrophobic solvents are better able to solvate the hydrophobic leucine residues that pack the protein core. That these alcohols do not effectively unfold α_4F_6 is not surprising, given that fluorocarbon core of this protein is intrinsically more hydrophobic.

The slight increase in helicity seen for $\alpha_4\text{H}$ at intermediate concentrations of ethanol and for $\alpha_4\text{F}_6$ at the highest concentrations of 2-propanol, and for both peptides in TFE, is a phenomenon that has also been observed for other proteins in high concentrations of alcohols (19). The structuring effect is generally thought to be due to interactions between the alcohols and the protein that displace solvating water molecules (12, 14). This, in turn, decreases the local dielectric constant resulting in back-bone hydrogen bonds of the α -helix becoming stronger and stabilizing the helix.

Contrary to the initial hypothesis, TFE did not unfold the $\alpha_4\text{F}_6$ peptide in a manner analogous to the unfolding of $\alpha_4\text{H}$ by ethanol and 2-propanol. One might have expected, based on the behavior of $\alpha_4\text{H}$ in ethanol and isopropanol, that TFE would at least partially unfold $\alpha_4\text{F}_6$. Instead, the peptide remains highly helical, although it is dissociated into monomers. Similar results were also obtained with the more highly fluorinated alcohol HFIP (Figure 2.8E).

Although it is unclear why TFE and HFIP do not unfold $\alpha_4\text{F}_6$, it should be noted that the helix-inducing properties of fluorinated alcohols such as TFE and HFIP are well known, and that the interactions of these solvents with proteins in aqueous media are complicated by the fact that they form nano-scale aggregates in water (12, 13). Indeed, although the unfolding of proteins in water-organic solvent mixtures is often simply ascribed to hydrophobic effects, the situation is actually more complex (19). A variety of physical parameters, such as logP, polarity index, dielectric constant and E_T (9), have been examined for their ability to describe the effectiveness of solvents to unfold or inactivate proteins, but such

measures do not appear to have general predictive value (20, 21). Other empirically derived measures of solvent-induced unfolding such as denaturation capacity (22) have met with more success, but the behavior of fluorinated solvents remains poorly understood.

In a previous study (4), self-segregating behavior was observed in peptides designed to form a parallel coiled-coil dimer; in one peptide, **H**, 6 leucines were incorporated at the 'a' and 'd' positions, while in the other peptide, **F**, hFLeu was substituted at these positions. The preference for the peptides to form **HH** and **FF** homodimers over **HF** heterodimers was estimated to be about 26:1, as assessed by disulfide crosslinking. Based on their result, it is surprising that we did not observe self-segregation of $\alpha_4\text{H}$ and $\alpha_4\text{F}_6$ because these peptides are of a similar size and contain the same number of hFLeu residues. Even substoichiometric concentrations of $\alpha_4\text{H}$ peptide perturbed the ^{19}F -NMR spectrum of $\alpha_4\text{F}_6$, arguing that there is little, if any, preference for the peptides to segregate; indeed, mixed peptide bundles may even be favored.

Interpretation of the experiment with **F** and **H** peptides was complicated by the fact that the **F** peptide was found, by analytical ultracentrifugation, to form a tetrameric coiled-coil rather than the intended dimeric structure. It was suggested that steric effects, imposed by the larger hFLeu side chain, prevented the **F** peptide forming dimers (4). Thus it could be argued that steric effects, rather than the fluorous nature of the peptide *per se*, may have contributed to the self-segregating behavior. In the present case, one could also argue that steric effects might result in favorable packing of leucine and hFLeu residues within the

hydrophobic core of the protein, which would off-set any tendency for the peptides to self-segregate due to fluororous interactions.

Clearly, the contrast between the self-segregating behavior of the **FF/HH** peptides and that of the $\alpha_4\text{H}/\alpha_4\text{F}_6$ peptides implies that there is still much to learn about modulating protein-protein interactions through fluorinated amino acids. On the other hand, the resistance exhibited by $\alpha_4\text{F}_6$ to solvent denaturation and proteolytic degradation are certainly useful properties that may find biotechnological applications; for example, we have recently show that hFLeu can be used to modulate the properties of the potent antimicrobial peptide MSI-78 as discussed in Chapter 3.

2.5 – References

1. Cesareni, G., Muesing, M. A. and Polisky, B., *Proc. Natl. Acad. Sci.*, **79**, 6313-6317 (1982).
2. Lee, K-H., Lee, H-Y., Slutsky, M. M., Anderson, J. T., Marsh, E. N. G., *Biochemistry*, **43**, 16277-16284 (2004).
3. Lee, H-Y., Lee, K-H., Al-Hashimi, H. M., Marsh, E. N. G., *J. Amer. Chem. Soc.*, **128**, 337-343 (2006).
4. Bilgiçer, B., Xing, X., Kumar, K., *J. Amer. Chem. Soc.*, **123**, 11815-11816 (2001).
5. Meng, H. and Kumar, K., *J. Amer. Chem. Soc.*, **129**, 15615-15622 (2007).
6. Anderson, J. T., Toogood, P. L., Marsh, E. N. G., *Org. Lett.* **4**, 4281-4283 (2002).
7. Rekker, R. F. (1977) The Hydrophobic Fragmental Constant, Elsevier, New York.
8. Laane, C., Boeren, S., Vos, K., and Veeger, C., *Biotechnol. Bioeng.* **30**, 81-87 (1987).
9. Harding, S. E., Rowe, A. J., and Horton, H. C. (1992) Analytical Ultracentrifugation in Biochemistry and Polymer Science, The Royal Society of Chemistry, Cambridge, UK.
10. Cohn, E. J., and Edsall, J. T. (1943) Proteins, Amino Acids and Peptides as Ions and Dipolar Ions, Reinhold, New York.
11. Marsh, E. N. G., *Chem. Bio.*, **7**, R153-R157 (2000).
12. Chatterjee, C. And Gerig, J. T., *Biochemistry*, **45**, 14665-14674 (2006).
13. Roccatano, D., Fioroni, M., Zacharias, M., Colombo, G., *Protein Sci.*, **14**, 2582-2589 (2005).
14. Dwyer, D. S., *Biopolymers*, **49**, 635-645 (1999).
15. Horvath, I. T. and Rabai, J., *Science*, **266**, 72-75 (1994).
16. Studer, A., Hadida, S., Ferritto, R., Kim, S. Y., Jeger, P., Wipf, P. Curran, D. P., *Science*, **275**, 823-826 (1997).
17. Gerig, J. T., *Prog. NMR Spectrosc.*, **26**, 293-370 (1994).
18. Chambers, S. E., Lau, E. Y., Gerig, J. T., *J. Amer. Chem. Soc.*, **116**, 3603-3604 (1994).
19. Griebenow, K. And Klibanov, A. M., *J. Amer. Chem. Soc.*, **118**, 11695-11700 (1996).
20. Laane, C., Boeren, S., Vos, K., Veeger, C., *Biotechnol. Bioeng.*, **30**, 81-87 (1987).
21. Arroyo, M., Torres-Guzman, T. de la Mata, I., Castillon, M. P., Acebal, C., *Enzyme and Microbial Technology*, **27** 122-126 (2000).
22. Khelnitsky, Y. L., Mozhaev, V. V., Belova, A. B., Sergeeva, M. V., Martinek, K., *Eur. J. Biochem.*, **198**, 31-41 (1991).

Chapter 3

Fluorinated α -Helical Antimicrobial Peptides

3.1 – Introduction

3.1.1 – AMPs Mediate the Innate Immunity of Multicellular Organisms

The emergence of bacterial strains resistant to most of the clinically useful antibiotics has provided the impetus to develop new classes of antibiotics that may combat bacterial resistance more effectively. Antimicrobial peptides (AMPs) are small peptides that show promise as therapeutic agents against bacteria, fungi and viruses (1-3). Widely distributed in multicellular organisms, they form part of the initial line of defense in the innate immune system and are also implicated in the activation of the adaptive immune response against microbes (4). The innate and adaptive immune effects of mammalian AMPs, such as defensins, include antimicrobial activity (2), antiviral activity (5), degranulation of mast cells (6, 7), and promotion or enhancement of antigen, cytokine and chemokine response (8, 9).

3.1.2 – Natural AMPs; Variety/Commonality

Although highly diverse in sequence and structure, almost all AMPs share the property of being highly amphipathic, with one face of the peptide being hydrophobic and the other face presenting a cluster of positively charged residues (10, 11). AMPs are often classified based on the structural characteristics of the peptides. These classifications include α -helical, linear, or disulfide bonded (2). The number of disulfide bonds range from 1-4 and result in β -hairpin-like structures.

AMPs with α -helical structures include cecropins from insects (12) and mammals (13), magainins from frogs (3) and cathelicidins from mammals (14, 15). Linear AMPs include indolicidin, a tryptophan rich peptide from cows and PR-39, a proline/arginine rich peptide from pigs (16, 17). The disulfide bond containing AMPs include tachyplesin from horseshoe crab, protegrin-1 from pig and α -defensin (HNP3) from humans (18-20).

The length of AMPs ranges from ~12-50 amino acids making them reasonably easy to synthesize. This has led to a vast number of studies that systematically investigate the importance of amino acid composition, peptide length, net charge, and hydrophobicity on the antibacterial activity of AMPs (21, 22). These investigations and mechanistic studies on gene-encoded AMPs have provided much insight into the mechanisms of AMPs.

3.1.3 – Mechanisms and Selectivity

Whereas some AMPs have been determined to act intracellularly (23), most appear to function primarily by disrupting bacterial cell membranes (24, 25). Bacterial cell membranes contain predominantly negatively charged phospholipids that gives rise to an electrostatic attraction to the highly cationic AMPs. Eukaryotic membranes, which contain predominantly neutral phospholipids, are usually less susceptible to disruption by AMPs. Upon association with the membrane, unstructured peptides become structured and begin thinning the bacterial membrane and proceed to disrupt the membrane through one of three methods (Figure 3.1). The barrel stave method involves peptide insertion into the membrane parallel to the phospholipids (Figure 3.1E), the toroidal method induces bending of the lipid bilayer resulting in pores in the membrane (Figure 3.1F), and the micellization model results in the degradation of membranes through the formation of lipid encompassed peptides (Figure 3.1G) (24, 25).

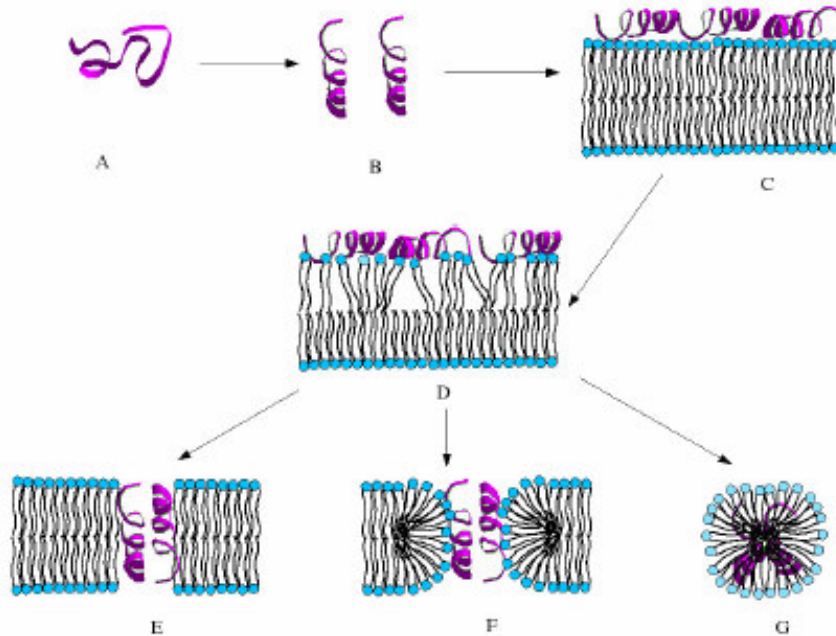


Figure 3.1. Shai-Matsuzaki-Huang Model of membrane disruption (24, 25). Disordered peptides (A) become structured (B) and associate with membranes (C). Disruption of the membrane begins (D) and continues through the barrel-stave method (E) the toroidal method (F) or the micellization method (G). The end results in AMP induced disruption of membranes, regardless of the mechanism, are the loss of transmembrane potential, pH gradients, and osmotic regulation. These factors give rise to cell death (26).

3.1.4 – Origin and Characteristics of MSI-78

Among the hundreds of gene-encoded and designed AMPs, magainin-2 and its analogs have been very well studied. Magainin-2 was co-discovered in 1987 after scientists found that *Xenopus laevis* were able to remain infection-free upon making incisions in the frogs' skin and placing the frog in water containing high levels of microbes (27, 28). Two peptides were isolated from *Xenopus laevis*, magainin-1 and 2. The 23 amino acid magainin-2 was soon found to have

broad-spectrum antibacterial and antifungal activity (29). Many synthetic analogs of magainin-2 have been studied with the most promise arising from MSI-78. Studies have shown that MSI-78 is α -helical and has potent antibacterial activity (29, 30). The peptide is unstructured in free solution but forms a dimeric antiparallel α -helical coiled-coil on association with lipid bilayers (31). The interface of the dimer is a phenylalanine zipper composed of three phenylalanine side chains in each helix (Figure 3.2). The leucine and isoleucine residues near the termini of the helices pack together in the dimer conformation. MSI-78 is believed to exert its antibacterial effect by forming toroidal pores in the bacterial membrane (32).

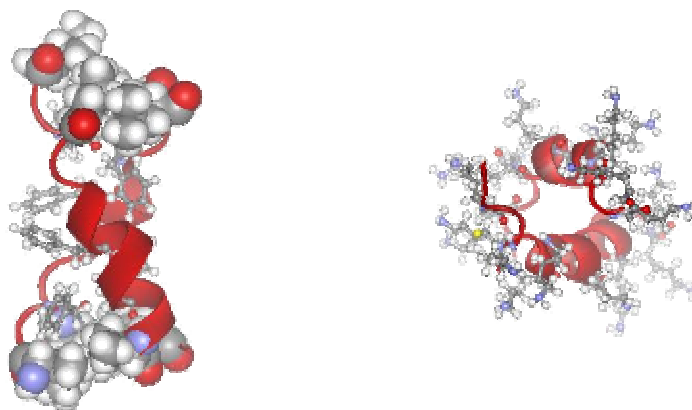


Figure 3.2. MSI-78 model based on NMR structural information of Magainin-2 with Leu depicted in CPK form, Phe and Lys depicted in ball and stick form.

3.1.5 – Fluorogainin Peptides

Although promising as a broad-spectrum antibiotics, MSI-78 and other AMPs are susceptible to proteolysis *in vivo* by endogenous or bacterial proteases, which may considerably diminish their effectiveness. Attempts to overcome this problem by increasing the dose of AMP often leads to toxic side effects, most notably lysis of red blood cells, which has been attributed to non-specific hydrophobic interactions between the peptide and the eukaryotic cell membrane (33, 34). Here a strategy is described to overcome these limitations, by exploiting the unusual physicochemical properties exhibited by fluorocarbons.

Fluorocarbons are noted for their chemical inertness and their extreme hydrophobicity. Work in our laboratory and others has shown that extensively fluorinated analogs of leucine and valine can significantly stabilize small proteins against thermal and chemical denaturation (35-41), an effect that may be attributed to the extremely hydrophobic nature of fluorocarbons. Recently fluorinated amino acids have been incorporated into AMPs (42, 43), and since these studies began, extensively fluorinated or fluorous amino acids have been used to modify the biological properties of AMPs. It was reasoned that if the properties of fluorocarbons could be designed into AMPs, then the expected increased structural stability might provide resistance to proteolysis, without abolishing their biological activity or increasing their toxicity to eukaryotic cells.

To test this concept two fluorous analogs of the potent and well-characterized AMP, MSI-78 (also called pexiganan) were synthesized. Two

leucine and isoleucine residues in MSI-78 were replaced with the fluorinated amino acid L-5,5,5,5',5',5'-hexafluoroleucine (hFLeu) to produce a molecule called fluorogainin-1 and the three phenylalanine residues replaced with L-pentafluorophenylalanine to produce fluorogainin-2 (Figure 3.3).

MSI-78 GIGKFLKKAKKFGKAFVKILKK
Fluorogainin-1 G**X**GKF**X**KKAKKFGKAFVK**X**XKK (**X** = hFLeu)
Fluorogainin-2 GIGK**X**LKKAKK**X**GK**X**VKILKK (**X** = pFPhe)

Figure 3.3. Sequences of MSI-78, Fluorogainin-1 and Fluorogainin-2.

3.2 – Experimental Procedures

3.2.1 - Materials

Rink Amide resin, *t*-Boc-protected amino acids, and 2-(1*H*-benzotriazol-1-yl)-1,1,3,3-tetramethyluronium hexafluorophosphate (HBTU) were purchased from NovaBiochem. L-5,5,5,5',5',5'-Hexafluoroleucine (hFLeu) was synthesized as described previously (44) and converted to the *t*-Boc protected derivative by standard procedures. 1-palmitoyl-2-oleoyl-*sn*-glycero-3-phosphatidylcholine (POPC) and 1-Palmitoyl-2-Oleoyl-*sn*-Glycero-3-[Phospho-*rac*-(1-glycerol)] (POPG) were purchased from Avanti Polar Lipids. Chymotrypsin and trypsin

were purchased from Boeringer Manheim GmbH. All other chemicals were purchased from Fisher and used without any further purification.

3.2.2 - Peptide Synthesis and Purification

Fluorogainin-1 and fluorogainin-2 were synthesized using *t*-Boc-protected amino acids for Merrifield manual solid-phase synthesis on MBHA resin; couplings were performed using *in situ* neutralization/HBTU protocol described by Schnolzer *et al.* on a 0.25 mM scale (45). The peptide was cleaved from the resin under “high”-HF conditions.

The peptides were redissolved at ~10 mg/mL in Milli-Q water and purified by reverse-phase HPLC on a Waters semipreparative C₁₈ column equilibrated in 0.1% formic acid and eluted with a linear gradient from 5 to 50% acetonitrile containing 0.1% formic acid. The peptide was determined to be pure by analytical HPLC and Maldi-TOF MS ES+ mass spectrometry: expected mass for fluorogainin-1 of 2909.9, detected mass of 2909; expected mass for fluorogainin-2 of 2748.0, detected mass of 2748. The concentrations of MSI-78 and fluorogainin-1 were determined by the absorbance at 257 nm due to three phenylalanine residues, using an extinction coefficient of 585 cm⁻¹ M⁻¹. The concentration of fluorogainin-2 was determined by weight.

3.2.3 - Circular Dichroism (C.D.)

CD spectra of peptides were recorded with an Aviv 62DS spectropolarimeter at 25°C in triplicate and averaged. Mean residue ellipticities, Θ_M , were calculated using eq 1 where Θ_{obs} is the measured ellipticity, l is the path length in cm, c is the molar concentration of the sample, and n is the number of residues in the peptide. To examine the secondary structure of MSI-78, fluorogainin-1 and fluorogainin-2 20 μ L of peptide at 684 μ M were diluted 10-fold in Buffer A (100 mM Tris-HCl, 10 mM CaCl₂, pH 7.8). No secondary structure was observed prior to addition of liposomes. POPC liposomes were prepared fresh in Buffer A to make a 13.6 mM solution of unilamellar liposomes by sonication (microtip, 10sec intervals, level 3) with Fisher Scientific 550 Sonic Dismembrator until clarification of the solution. 20 μ L of the liposome solution was added to the diluted peptide to make a solution containing 1 : 200 peptide to lipid. The CD spectrum for each peptide/liposome solution was recorded from 200 – 250 nm in triplicate.

$$\Theta_M = \Theta_{obs}/10/cn \quad (1)$$

3.2.4 – Proteolysis

Stock solutions of peptides at a concentration of 680 μ M in Milli-Q water were prepared and stored at -20°C. 2x Buffer A and a 0.5 mg/mL solution of tryptophan were prepared and stored at -4°C. Protease solutions were prepared

at a concentration of 1 mg/mL in 1 mM HCl just prior to use. Liposome solutions were prepared as described in the C.D. section just prior to use. Proteolysis reactions were performed by mixing 10 μ L of peptide stock, 20 μ L 2x Buffer A, and 0.5 μ L Trp solution. Liposome solution was added when specified and reactions were initiated by the addition of protease, 0.5 μ L of stock or 0.5 μ L of a 10x dilution to give a 1 : 80 or 1 : 800 ratio of peptide to enzyme, respectively. Reaction aliquots (5 – 10 μ L) were removed at different times and quenched using an equal volume of 1 M HCl. Samples were stored at -20°C until analysis by HPLC. Reactions were performed at 0°C or 25°C. All reactions were repeated 3 times. Control reactions containing all reagents except enzyme were performed and no degradation of the parent peptide was observed for MSI-78, fluorogainin-1 or fluorogainin-2 over a 10 hour period. Reaction samples were diluted to ~40 μ L with 5% acetonitrile, 0.15% acetic acid for injection onto an analytical C₁₈ column. Samples were eluted with a linear gradient from 5 to 90% acetonitrile, 0.15% acetic acid. Parent peak heights (peak heights corresponding to the original peptide) were standardized based on the tryptophan peak height. Plots of the parent peak height vs. time were generated to obtain a linear fit of the data. Time zero was extrapolated from the linear fits and % peptide remaining was calculated from eq 2

$$(\text{peak height at } t_n / \text{peak height at } t_0) \times 100 \quad (2)$$

3.2.5 – Isothermal Calorimetry

Peptide solutions (200 μM) in PBS, pH 7.4 were titrated into POPC/POPG (3 : 1 mol/mol) SUVs prepared as described for C.D. experiments. The liposomes were prepared in PBS, pH 7.4 at a concentration of 15 mM. 4 μL injections of peptide into liposome solution or PBS (as a control experiment to determine heat of dilution) were made for a total of 4 injections. It is assumed, for the experiment, that all peptide is bound upon addition to the liposome solution.

3.2.6 – Glutaraldehyde Crosslinking

Peptide solutions (200 μM) in PBS, pH 7.4 were prepared. Crosslinking reactions containing (A) peptide (final concentration of 50 μM) with 0.0015% (w/v) glutaraldehyde, (B) peptide with POPC/POPG in a 3 : 1 ratio (1 mM final concentration) and (C) peptide with 0.001% glutaraldehyde and POPC/POPG in a 3 : 1 ratio were prepared. The final reaction volumes were made to 10 μL with PBS buffer. Reactions were incubated at room temperature and quenched after 30 min with NaBH_4 (final concentration of 1 mM). Reaction aliquots (5 μL) were diluted 2x with gel loading buffer and heated to 95 $^\circ\text{C}$ for 2 min prior to analysis by Tris-Tricine (16%) gel electrophoresis. Gels were silver stained to visualize protein bands.

3.2.7 – Bacterial Strains and Growth

(performed by Dr. Charles Shelburne)

E. coli D5α was obtained from Invitrogen (Invitrogen, Carlsbad, CA). *Enterococcus faecalis* cultures were a gift from Dr. Donald B. Clewell, University of Michigan. *Bacillus subtilis* (ATCC 663), *Kocheria rhizophila* (ATCC 9341), *Errobacter aerogenese* (ATCC 13408), *Klebsiella pneumoniae* ATCC 4352, *Proteus mirabilis* (ATCC 25933), *Salmonella enteritis* Typhimerium ATCC 14028, *Streptococcus pyogenes* (ATCC 19615), *Staphylococcus aureus* (ATCC 6538) and *Shigella sonnei* (ATCC 25931) were obtained from MicroBiologics, St. Cloud, Minnesota. All species were maintained by weekly transfer on Trypticase Soy Agar and broth cultures grown directly from individual colonies in Trypticase Soy Broth.

3.2.8 - MIC Determination

(performed by Dr. Charles Shelburne)

A sterile, 96- well micro-titer plate (NUNC) was used as the platform for the assay. An overnight culture of each bacterium was diluted to 10^6 /mL in sterile phosphate buffered saline and seeded into each well (100 μ l) of the plate. Doubling dilutions (500 μ g/mL - 7.8 μ g/mL) of MSI-78, fluorogainin-1, or fluorogainin-2 (100 μ L) in replicates of 8 were then added and the cultures covered with a sterile adhesive plastic film. After centrifugation for 1 minute at

800 x g to collect the entire inoculum to the bottom of the plate it was incubated at 37 °C overnight in air. Growth was determined by measuring the OD₅₉₅ of each well using a microwell plate reader (GENious, Tecan, Manendorff, Switzerland). The MIC for each organism was determined as the lowest dilution of each peptide without significant growth above the inoculum ($p \leq 0.01$, T-test). The differences between peptides for each bacterial strain were evaluated using a t-test.

3.2.9 – Hemolytic Activity

(performed by Dr. Charles Shelburne)

A sterile, 96- well round bottom micro-titer plate (Costar) was used as the platform for the assay. 2.5% bovine red blood cells in 100 μ L of PBS were added to the wells of the plate. Doubling dilutions (500 μ g/mL - 7.8 μ g/mL) of MSI-78, fluorogainin-1, or fluorogainin-2 (100 μ L) in replicates of 8 were then added and the cultures covered with a sterile adhesive plastic film. The plate was incubated for 2 hours at room temperature and examined by eye. The highest dilution of peptides without an intact cell pellet was noted.

3.3 – Results

3.3.1 – Secondary Structure of Peptides

The secondary structure of the peptides was examined by C.D. spectroscopy. Peptide samples were prepared at 70 μM concentration in 100 mM Tris-Cl buffer, 10mM CaCl_2 , pH 7.8, at 25 $^\circ\text{C}$. In the absence of liposomes all peptides were unstructured, consistent with their being highly positively charged (Figures 3.4, 3.5, and 3.6; solid lines). However, in the presence of small uni-lamellar vesicles (SUVs) prepared from POPC the peptides exhibited C.D. spectra characteristic of an α -helical structure (Figures 3.4, 3.5, and 3.6; dotted lines). Interestingly, fluorogainin-1 appeared significantly less helical than MSI-78 as judged by C.D. with a mean residue ellipticity at 222 nm of only about 2/3 that of the non-fluorinated peptide. This is in accord with recent studies that show hFLeu to have a poor helix propensity (46), despite the fact that it has been found to stabilize α -helical proteins against unfolding. In addition, fluorogainin-2 is much less helical than MSI-78, showing only a slight minimum at 222 nm. This suggests that fluorogainin-2 is predominantly unstructured.

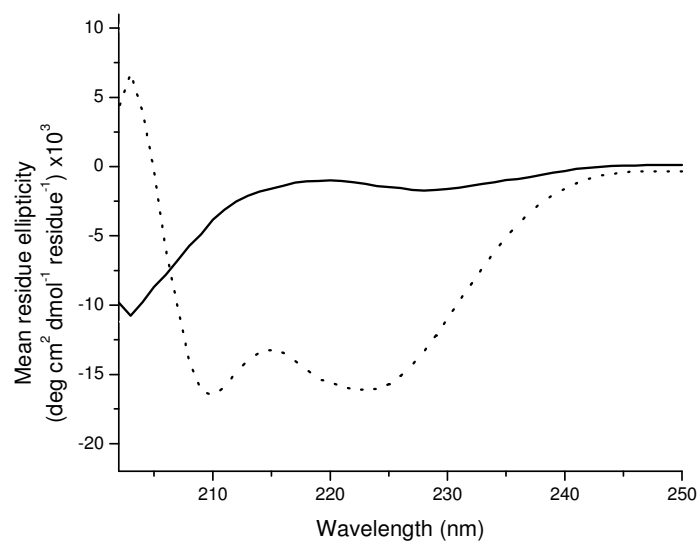


Figure 3.4. C.D. spectra of MSI-78 with POPC vesicles (dotted line) and without vesicles present (solid line).

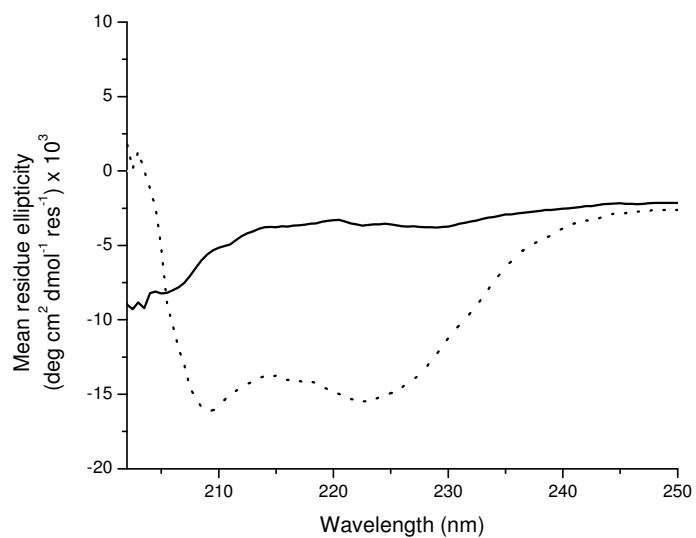


Figure 3.5. C.D. spectra of Fluorogainin-1 with POPC vesicles (dotted line) and without vesicles present (solid line).

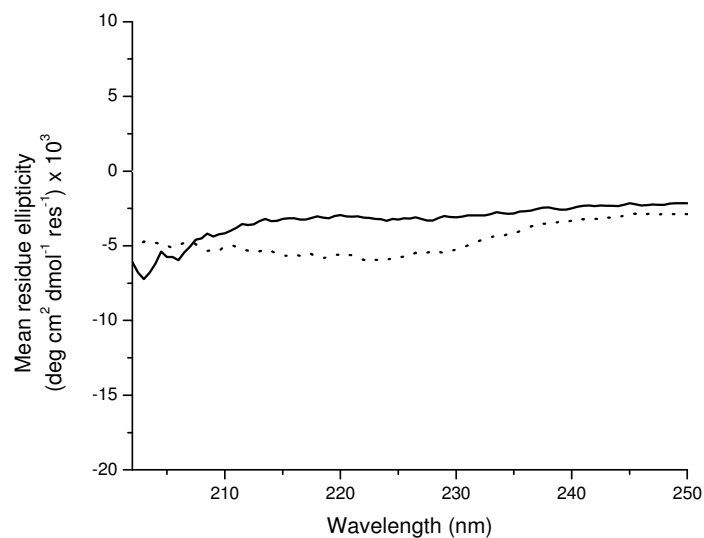


Figure 3.6. C.D. spectra of Fluorogainin-2 with POPC vesicles (dotted line) and without vesicles present (solid line).

3.3.2 – Biological Stability of Peptides

We next examined the stability of MSI-78, fluorogainin-1 and fluorogainin-2 towards proteolysis by two common proteases, trypsin and chymotrypsin. These proteases provide a stringent test for structural stability as both peptides have multiple potential cleavage sites for both enzymes. Peptides (340 μM) were dissolved in 100 mM Tris-Cl buffer, 10 mM CaCl_2 , pH 7.8 and were incubated in the presence of 15 mM POPC liposomes and 1.25 % (w/w) protease at 25 $^\circ\text{C}$ for various times and the extent of proteolysis determined by reverse phase HPLC. Under these conditions MSI-78 was almost completely degraded by either

protease within 30 min, however fluorogainin-2 showed significantly less degradation and fluorogainin-1 showed no signs of degradation even after 10 hours (Figure 3.8). In the absence of liposomes, where the peptides are unstructured, all peptides were equally rapidly degraded by both trypsin and chymotrypsin (Figure 3.7). Therefore, it appears that the resistance of fluorogainin-1 and fluorogainin-2 to proteolysis is due to its interaction with liposomes and not because the incorporation of hFLeu or pFPhe *per se* prevents the peptide from being digested by proteases.

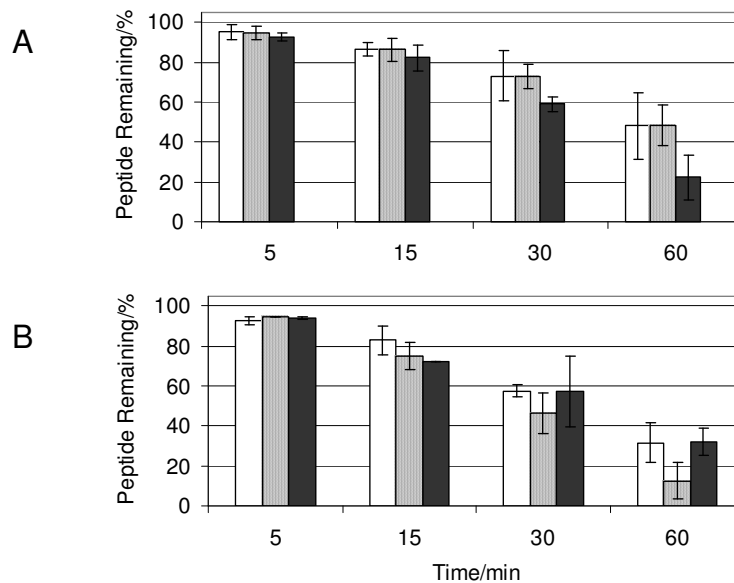


Figure 3.7. Proteolysis of MSI-78 (white), fluorogainin-1 (gray), and fluorogainin-2 (black) by chymotrypsin (A) and trypsin (B).

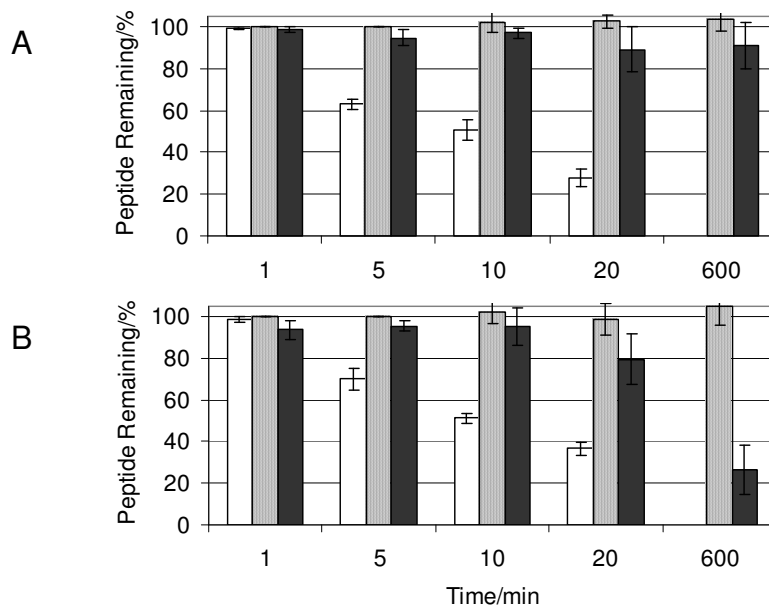


Figure 3.8. Proteolysis of MSI-78 (white), fluorogainin-1 (gray), and fluorogainin-2 (black) by chymotrypsin (A) and trypsin (B) in the presence of POPC vesicles.

3.3.3 – Binding Enthalpy

The interactions between liposomes and the AMPs, were studied by isothermal titration calorimetry. Measurements were made under conditions similar to those used to study the binding of the parent peptide magainin-2 to SUVs (46). SUVs were freshly prepared from a 3 : 1 (mol/mol) mixture of POPC/POPG, final concentration 15 mM in 10 mM potassium phosphate buffer, pH 7.4, containing 100 mM NaCl, thoroughly degassed, and introduced into the calorimeter cell. A 200 μ M solution of peptide (dissolved in the same buffer) was injected in 4 μ L increments into the liposome solution. Fluorogainin-2 was not

included due to inaccuracy of determining the peptide concentrations by weight. MSI-78 and Fluorogainin-1 concentrations were determined by mass and absorbance at 258 nm ($\epsilon = 585 \text{ M}^{-1}\text{cm}^{-1}$). Measurements were made at 25 °C using a Microcal VP calorimeter. Heats of dilution were determined by injecting peptide solutions into buffer lacking SUVs and subtracted from the raw data.

The thermograms for each peptide binding to liposomes are shown in Figure 3.9. The enthalpies (calculated from the peak areas of each injection of peptide) for each peptide binding to the lipids are similar: ΔH for MSI-78 is $-14.4 \pm 0.2 \text{ kcal/mol}$, whereas ΔH for fluorogainin-1 is slightly less exothermic at $-12.5 \pm 0.3 \text{ kcal/mol}$. These enthalpies are similar to those measured previously for magainin-2 peptide binding to SUVs (47). The titration of fluorogainin-1 appears to show a slight increase in heat released with increasing injection number indicating some dependence on peptide concentration, although the significance of this is unclear. The enthalpic contribution to liposome binding has been determined to arise primarily from electrostatic interactions between the positively charged peptide and negatively charged lipid head groups (47). Since MSI-78 and fluorogainin-1 contain identical cationic residues, the electrostatic interactions are expected to be very similar. This result strongly suggests that the increase in hydrophobicity imparted by the fluorous residues is primarily responsible for modifying the biological properties of fluorogainin-1.

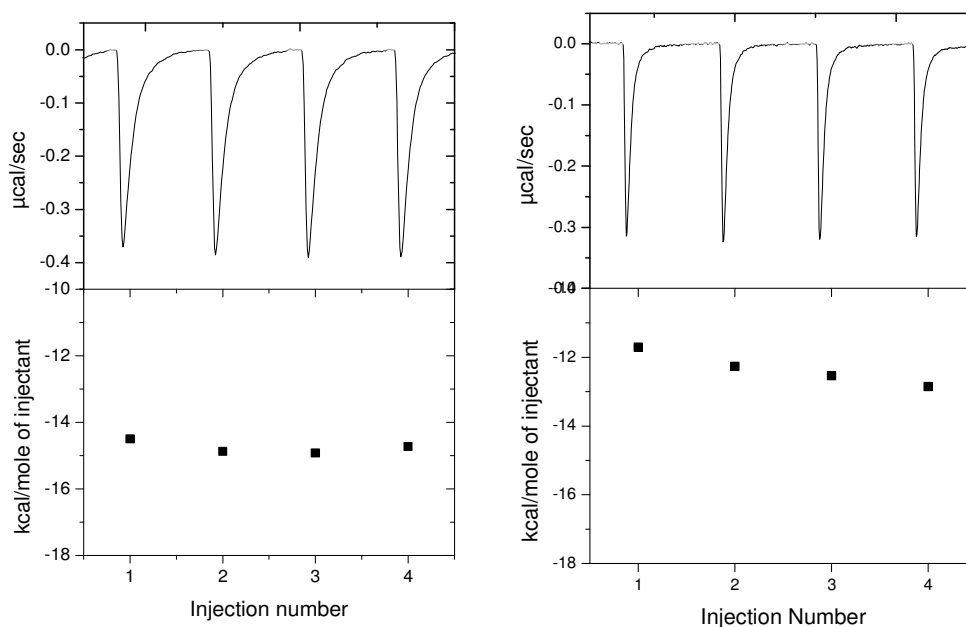


Figure 3.9. Left panel shows heat of reaction (upper) and integration of the peaks (lower) for the titration calorimetry of MSI-78 into SUVs. Right panel shows heat of reaction (upper) and integration of the peaks (lower) for the titration calorimetry of Fluorogainin-1 into SUVs.

3.3.4 – Oligomerization States

The oligomerization states of MSI-78, fluorogainin-1 and fluorogainin-2 were qualitatively determined in a glutaraldehyde crosslinking experiment. Peptides were incubated with 0.0015% (w/v) glutaraldehyde in either the presence or the absence of lipids and allowed to react for 30 min prior to quenching with NaBH_4 . Peptides showed crosslinking only when glutaraldehyde and lipids were present in the reaction mixtures (Figure 3.10, lane 4). The bands

corresponding to monomeric peptides migrate at a molecular weight of ~2.5 kDa and the bands corresponding to dimeric or crosslinked peptides migrate at a molecular weight of about 4 kDa based on the molecular weight standards (Figure 3.10, lane 1). These results indicate that the oligomerization state is unchanged in fluorogainin-1 and fluorogainin-2, remaining dimeric in the presences of lipids. This suggests that, even though fluorogainin-2 appears unstructured based on C. D. spectroscopy, it is forming some tertiary interactions in the presence of lipids.

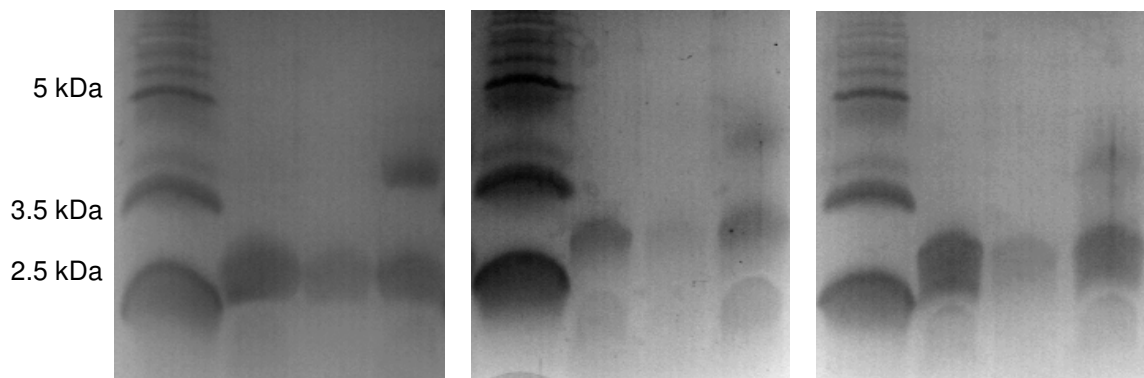


Figure 3.10. Glutaraldehyde crosslinking of peptides. Lane 1 is molecular weight standard, lane 2 is the peptide with lipids, lane 3 is the peptide with glutaraldehyde, lane 4 is the peptide with lipid and glutaraldehyde. Panel A is MSI-78, panel B is Fluorogainin-1, and panel C is Fluorogainin-2.

3.3.5 – Toxicity of Peptides

To determine whether fluorination might result in increased toxicity, the hemolytic activity of all AMPs was tested against bovine erythrocytes, using a standard lysis assay for hemoglobin release from erythrocytes as described

previously (48). Neither MSI-78 nor fluorogainin-1 exhibited any hemolytic activity at concentrations up to 250 $\mu\text{g}/\text{mL}$. To place this result in context, many AMPs exhibit hemolytic activity at concentrations well below 100 $\mu\text{g}/\text{mL}$. It appears, therefore, that even though the hFLeu side-chain is considerably more hydrophobic than Leu or Ile (38) this does not result in the peptide binding to erythrocyte membranes. The incorporation of pFPhe does appear to have considerable effects on the toxicity of the peptide, whereas no hemolysis was observed for MSI-78 or fluorogainin-1 up to 250 $\mu\text{g}/\text{mL}$, fluorogainin-2 showed hemolytic activity at 15.6 $\mu\text{g}/\text{mL}$ (Table 3.1). This is considerable since the activity of AMPs is often in the low $\mu\text{g}/\text{mL}$ range (Table 3.2).

Table 3.1 Hemolytic activity in percent of lysed bovine red blood cells.

| Peptide concentration ($\mu\text{g}/\text{mL}$) | MSI-78 | Fluorogainin-1 | Fluorogainin-2 | Triton-100 (1%)* | HBS |
|---|--------|----------------|----------------|------------------|-----|
| 250 | 0 | 0 | 100 | 100 | 0 |
| 125 | 0 | 0 | 100 | 100 | 0 |
| 62.5 | 0 | 0 | 100 | 100 | 0 |
| 31.25 | 0 | 0 | 100 | 100 | 0 |
| 15.625 | 0 | 0 | 32 | 100 | 0 |
| 7.8125 | 0 | 0 | 0 | 100 | 0 |
| 3.90625 | 0 | 0 | 0 | 0 | 0 |
| 1.953125 | 0 | 0 | 0 | 0 | 0 |

3.3.6 – Activity of Peptides

The effect of fluorination on the antimicrobial activity of the three peptides was compared. The minimum inhibitory concentration (MIC) of MSI-78, fluorogainin-1, and fluorogainin-2 were determined by the microdilution antimicrobial assay procedure, as described previously (49). A panel of bacterial strains were chosen that included both Gram positive and Gram negative strains of common pathogenic bacteria. Two-fold serial dilutions of each AMP were made into cultures of each bacterial strain and the minimum concentration needed to prevent bacterial growth determined. The results are summarized in Table 3.2.

The fluorous AMP's retained the broad-spectrum antibiotic activity of MSI-78, even though the incorporation of 4 hFLeu residues into the fluorogainin-1 and 3 pFPhe residues in fluorogainin-2 might be considered quite an extensive modification of the structure. Although MSI-78 appears slightly more active than fluorogainin-1 against many of the bacteria, differences of two-fold or less in MIC cannot be considered statistically significant in this type of dilution assay. However, fluorogainin-1 and fluorogainin-2 were significantly more potent ($p < 0.05$) against two important pathogenic bacteria: the MIC of fluorogainin-1 against *Klebsiella pneumoniae* was 16 $\mu\text{g/mL}$ and 25 $\mu\text{g/mL}$ for fluorogainin-2 whereas MSI-78 showed no activity. The MIC of fluorogainin-1 was \sim four times lower than MSI-78 against *Staphylococcus aureus*. Fluorogainin-2 showed very good activity against *Enterococcus faecalis* with a MIC of 6.25 $\mu\text{g/mL}$ while no

activity was observed for MSI-78 or fluorogainin-1. In addition fluorogainin-2 was found to have significant activity against *Candida albicans*, a fungus, and no activity was observed for MSI-78. The only bacterium tested for which fluorogainin-1 was significantly ($p < 0.05$) less effective than MSI-78 was *Streptococcus pyogenes*.

Table 3.2. Minimum inhibitory concentrations of MSI-78, Fluorogainin-1, and Fluorogainin-2 for a variety of bacterial strains.

| | | | MSI-78 | Fluorogainin-1 | Fluorogainin-2 |
|------------------|--------|--------|---------------------|----------------|----------------|
| Strain Name | ATCC # | type | MIC values in ug/mL | | |
| B. subtilis | 6633 | gram+ | 6.25 | 7.81 | 6.25 |
| K. rhizophila | 9341 | gram + | 6.25 | 7.81 | 25 |
| E. aerogenes | 13048 | gram - | 3.13 | > 250.00 | 12.5 |
| K. pneumoniae | 4352 | gram - | >200 | 15.6 | 25 |
| P. mirabilis | 25933 | gram - | >200 | >250.00 | >200 |
| S. enterica | 14028 | gram - | 6.25 | 31.3 | 6.25 |
| S. pyogenes | 19515 | gram + | 7.81 | 62.5 | |
| E. coli | DH5a | gram - | <3.91 | 7.81 | |
| S. aureus | UH11 | gram+ | 62 | 15.6 | 35 |
| S. enterica | | gram - | 6.25 | 31.3 | 6.25 |
| E. fecaelis | OG1 X | gram + | >200 | >250.00 | 6.25 |
| Y. enterocolitca | | gram - | 6.25 | | 25 |
| S. sonnei | | gram - | 6.25 | | 25 |
| C. albicans | | fungi | >200 | | 12.5 |

3.4 – Discussion

In conclusion, introducing fluorous amino acid residues into an AMP has conferred almost complete resistance to proteolysis of the fluorous AMP fluorogainin-1 and significant protection from proteolysis of fluorogainin-2 under

conditions where the non-fluorinated AMP is rapidly degraded, while retaining the broad spectrum of antimicrobial activity. Protection against proteolysis is only observed in the presence of liposomes, suggesting that lipid-peptide interactions are important. MSI-78 has been shown to dimerize to form a coiled-coil in a membrane environment (31), this is confirmed by the crosslinking experiments performed and suggests that the fluorinated AMPs also dimerize in a membrane environment, although fluorogainin-2 appears to have no significant helicity. Based on this observation, one plausible explanation of the protease resistance exhibited by fluorogainin-1 and fluorogainin-2 is that incorporation of the more hydrophobic hFLeu or pFPhe side-chains strengthen the hydrophobic interactions between AMP dimers, just as was demonstrated for α_4H and α_4F_6 in Chapter 2 (38, 39). This would, in turn, promote the formation of structured dimers that are resistant to proteolysis.

It is also noteworthy that fluorogainin-1 and fluorogainin-2 show a selectivity towards bacterial strains that are slightly different from that of MSI-78. Fluorogainin-1 exhibits significantly improved potency against *K. pneumoniae* and *S. aureus*, with MICs of 16 $\mu\text{g}/\text{mL}$ against both bacteria. Fluorogainin-2 shows improved activity against *K. pneumoniae* and *E. faecalis* with MICs of 25 $\mu\text{g}/\text{mL}$ and 6.25 $\mu\text{g}/\text{mL}$, respectively. In addition, fluorogainin-2 was found to have significant activity against *Candida albicans*, a fungus, and no activity was observed for MSI-78. In addition, fluorogainin-2 has significant hemolytic activity which could be attributed to a greater ability to insert into sterol containing membranes such as fungi and erythrocytes. The lack of secondary structure of

fluorogainin-2 may be decreasing the selectivity of the peptide. Since the overall hydrophobicity of the peptide is less than that of fluorogainin-1 the decrease in selectivity is not likely to be due to increase in hydrophobicity. Although the selectivity of AMPs for some bacteria and not others is poorly understood (33), it is known that the resistance of *S. aureus* to AMPs is due, at least in part, to secretion of proteases (50). The resistance of fluorogainin-1 to proteolysis may explain its improved potency against this important bacterial pathogen.

More generally, these results suggest the strategy of incorporating fluororous residues into biologically active membrane-associated peptides could be used to enhance the efficacy or modulate the activity of other biologically important peptides. For example, membrane-active peptides are known to be important in membrane fusion and ion-channel formation, and have also been found to have anti-cancer and anti-viral activities (51-54).

3.5 – References

1. Shai, Y., *Curr. Pharmaceutical Design*, **8**, 715-725 (2002).
2. Zasloff, M., *Nature*, **415**, 389-395 (2002).
3. Boman, H. G., *Ann. Rev. Immunol.*, **13**, 61-92 (1995).
4. Oppenheim, J. J., Biragyn, A., Kwak, L. W., Yang, D., *Ann. Rheum. Dis.*, **62**, 17-21 (2003).
5. Rugeles, M. T., Trubey, C. M., Bedoya, V. I., Pinto, L. A., Oppenheim, J. J., Rybak, S. M., *AIDS*, **17**, 481-486 (2003).
6. Niyonsaba, F., Someya, A., Hirata, M., Ogawa, H., Nagaoka, I., *Eur. J. Immunol.*, **31**, 1066-1075 (2001).
7. Huang, H. J., Ross, C. R., Blecha, F., *J. Leukoc. Biol.*, **61**, 624-629 (1997).
8. Lillard, J. W. Jr., Boyaka, P. N., Chertov, O., Oppenheim, J. J., McGhee, J. R., *Proc. Natl. Acad. Sci.*, **96**, 651-656 (1999).
9. Tani, K., Murphy, W. J., Chertov, O., Salcedo, R., Koh, C. Y., Utsunomiya, I., *Int. Immunol.*, **12**, 691-700 (2000).
10. Shai, Y., *Biochim. Biophys. Acta-Biomembranes*, **1462**, 55-70 (1999).
11. Wu, M. H., Maier, E., Benz, R., Hancock, R. E. W., *Biochemistry*, **38**, 7235-7242 (1999).
12. Bals, R., Wang, X., Zasloff, M., Wilson, J., *Proc. Natl. Acad. Sci.*, **95**, 9541-9546 (1998).
13. Lee, J.-Y., Boman, A., Sun, C., Andersson, M., Jornvall, H., Mutt, V., Boman, H. G., *Proc. Natl. Acad. Sci.*, **86**, 9159-9162 (1989).
14. Bevins, C. L., Zasloff, M., *Ann Rev. Biochem.*, **59**, 395-414 (1990).
15. Barra, D., Simmaco, M., *TIBTECH*, **13**, 205-209 (1998).
16. Selsted, M. E., Novotny, M. J., Morris, W. L., Tang, Y. Q., Smith, W., Cullor, J. S., *J. Biol. Chem.*, **267**, 4292-4295 (1992).
17. Agerberth, B., Lee, J.-Y., Bergman, T., Carlquist, M., Boman, H. G., Mutt, V., Jornvall, H., *Eur. J. Biochem.*, **202**, 849-854 (1991).
18. Nakamura, T., Furunaka, H. T. T. M., Tokunaga, F., Muta, T., Iwanaga, S., Niwa, M., Takao, T., Shimonishi, Y., *J. Biol. Chem.*, **263**, 16709-16713 (1988).
19. Harwig, S. S., Waring, A., Yang, H. J., Cho, Y., Tan, L., Lehrer, R. I., *Eur. J. Biochem.*, **240**, 352-357 (1996).
20. Ganz, T., Selsted, M.E., Szklarek, D., Harwig, S.S., Daher, K., Bainton, D.F., Lehrer, R.I., *J. Clin. Invest.* **76**, 1427–1435 (1985).
21. Tossi, A., Sandri, L., Giangaspero, A., *Biopolymers*, **44**, 4-30 (2000).
22. Dennison, S. R., Wallace, J., Harris, F., Phoenix, D. A., *Protein Pep. Lett.*, **12**, 31-39 (2005).
23. Brogen, K. A., *Nature*, **3**, 238-250 (2005).
24. Oren, Z. and Shai, *Biopolymers*, **47**, 451-463 (1998).
25. Huang, H. W., *Phys. Rev. Lett.*, **92**, 198304-1—198304-4 (2004).
26. Westerhoff, H. V., Juretic, D., Hendler, R. W., Zasloff, M., *Proc. Natl. Acad. Sci.*, **86**, 6597-6601 (1989).

27. Zasloff, M. *Proc. Natl. Acad. Sci.* **84**, 5449-5453 (1987).
28. Giovannini, M. G., Poulter, L., Gibson, B. W., Williams, D. H., *Biochem. J.*, **243**, 113-120 (1987).
29. Zasloff, M., Martin, B., Chen, H.-C., *Proc. Natl. Acad. Sci.*, **85**, 910-913 (1988).
30. Matsuzaki, K., *Biochim. Biophys. Acta-Rev. Biomembranes*, **1376**, 391-400 (1988).
31. Porcelli, F., Buck-Koehntop, B. A., Thennarasu, S., Ramamoorthy, A., Veglia, G., *Biochemistry*, **45**, 5793-5799 (2006).
32. Hallock, K. J., Lee, D. K., Ramamoorthy, A., *Biophys. J.*, **84**, 3052-3060 (2003).
33. Zelezetsky, I., Tossi, A. *Biochim. Biophys. Acta-Biomembranes*, **1758**, 1436-1449 (2006).
34. Maloy, W. L., Kari, U. P., *Biopolymers*, **37**, 105-122 (1995).
35. Yoder, N. C. and Kumar, K., *Chem. Soc. Rev.*, **31**, 335-341 (2002).
36. Marsh, E. N. G., *Chem. Biol.*, **7**, R153-R157 (2002).
37. Bilgicer, B., Kumar, K., *Proc. Natl. Acad. Sci. (USA)*, **101**, 15324-15329 (2004).
38. Lee, K.-H., Lee, H.-Y., Slutsky, M. S., Anderson, J. T., Marsh, E. N. G., *Biochemistry*, **43**, 16277-16284 (2004).
39. Lee, H.-Y., Lee, K.-H., Al-Hashimi, H. M., Marsh, E. N. G., *J. Am. Chem. Soc.*, **128**, 337-343 (2006).
40. Tang, Y., Ghirlanda, G., Vaidehi, N., Kua, J., Mainz, D. T., Goddard, W. A., DeGrado, W. F., Tirrell, D. A., *Biochemistry*, **40**, 2790-2796 (2001).
41. a) Niemz, A., Tirrell, D. A., *J. Am. Chem. Soc.*, **123**, 7407-7413 (2001); b) Bilgicer, B., Fichera, A., Kumar, K., *J. Am. Chem. Soc.*, **123**, 4393-4399 (2001).
42. Gimenez, D., Andreu, C., del Olmo, M., Varea, T., Diaz, D., Asensio, G., *Bioorg. Med. Chem.*, **14**, 6971-6978 (2006).
43. Meng, H. and Kumar, K., *J. Amer. Chem. Soc.*, **129**, 15615-15622 (2007).
44. Anderson, J. T., Toogood, P. L., Marsh, E. N. G., *Org. Lett.* **4**, 4281-4283 (2002).
45. Schnolzer, M., Alewood, P., Jones, A., Alewood, D., and Kent, S. B. H., *Int. J. Pept. Protein Res.*, **40**, 180-193 (1992).
46. Chiu, H. P., Suzuki, Y., Gullickson, D., Ahmad, R., Kokona, B., Fairman, R., Cheng, R. P., *J. Am. Chem. Soc.*, **128**, 15556-15557 (2006).
47. Wenk, M. R., Seelig, J., *Biochemistry*, **37**, 3909-3916 (1998).
48. Ramamoorthy, A., Thennarasu, S., Tan, A. M., Gottipati, K., Sreekumar, S., Hey, D. L., An, F. Y. P., Shelburne, C. E., *Biochemistry*, **45**, 6529-6540 (2006).
49. Shelburne, C. E., An, F. Y. P., Dholpe, V., Ramamoorthy, A., Lopatin, D. E., Lantz, M. S., *J.f Antimicrob. Chemotherapy*, **59**, 297-300 (2007).
50. Sieprawska-Lupa, M., Mydel, P., Krawczyk, K., Wojcik, K., Puklo, M., Lupa, B., Suder, P., Silberring, J., Reed, M., Pohl, J., Shafer, W., McAleese, F., Foster, T., Travis, J., Potempa, J., *Antimicrob. Agents and Chemotherapy*, **48**, 4673-4679 (2004).

51. Hartmann, R., Wal, J. M., Bernard, H., Pentzien, A. K., *Curr. Pharmaceutical Design*, **13**, 897-920 (2007).
52. Dennison, S. R., Whittaker, M., Harris, F., Phoenix, D. A., *Curr. Protein & Peptide Sci.*, **7**, 487-499 (2006).
53. Ouellet, M., Otis, F., Voyer, N., Auger, M., *Biochim. Biophys. Acta-Biomembranes*, **1758**, 1235-1244 (2006)..
54. Martin, I., Ruyschaert, J. M., Epand, R. M., *Adv. Drug Delivery Rev.*, **38**, 233-255 (1999).

Chapter 4

Fluorinated β -hairpin Antimicrobial Peptides

4.1 – Introduction

4.1.1 – Basis for Selectivity of AMPs

As discussed in Chapter 3, the selectivity of AMPs for bacterial membranes arises primarily from electrostatic interactions between the positively charged peptide and the negatively charged lipids. However, some AMPs are cytotoxic at low concentrations; for example Mellitin (1), indolicidins (2), and protegrin-1 (3) have significant hemolytic activity. The molecular basis of membrane selectivity is, therefore, influenced by more than electrostatic interactions. To understand the basis of selectivity of AMPs for prokaryotic cells over eukaryotic cells more thoroughly it is important to understand the composition of the cell membranes. Eukaryotic and prokaryotic cell membranes differ significantly in phospholipids that make up the membrane bilayer, the absence or presence of sterols, and the underlying cytoskeleton.

The outer membrane of prokaryotic cells contain a high percentage of poly-anionic lipopolysaccharides (Gram-negative bacteria) and anionic phospholipids such as phosphatidylglycerol and cardiolipin (4). Eukaryotic outer

membranes, in contrast, are composed of zwitterionic phospholipids such as phosphatidylcholine, sphingomyelin, and phosphatidylethanolamine (5, 6). The structures of common cell membrane components are illustrated in Figure 4.1. Generally, cationic AMPs have a higher affinity for anionic bacterial cell membrane as opposed to neutral eukaryotic cell membranes, but selectivity is not based simply on “negative attracts positive”. Glukhov, et al. studied 12 natural and *de novo* AMPs and concluded that the placement of positively charged residues within the sequence was very important in the selectivity of AMPs. Peptides that were designed with cationic side chains grouped together were observed to be more selective for bacterial cells than those peptides that had cationic residues more dispersed within the sequence (7).

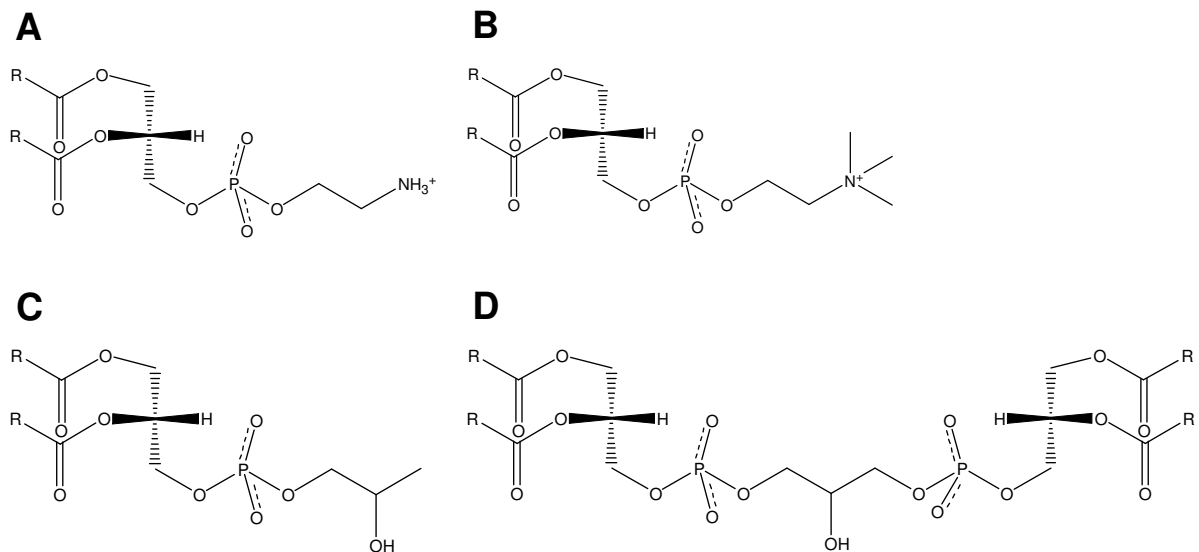


Figure 4.1 Phospholipid head groups of common eukaryotic; phosphatidylethanolamine (A) and phosphatidylcholine (B), and prokaryotic; phosphatidylglycerol (C) and cardiolipin (D), cell components.

Another important difference between eukaryotic and prokaryotic cell membranes is that eukaryotic cell membranes contain an abundance of sterols (Figure 1.2) (8), that are not present in prokaryotic cell membranes (4). Cholesterol's ability to increase acyl chain order in lipid membranes was found to protect cells from AMP insertion into the membrane and, therefore, disruption of the cell membrane (9). The sterol found in fungi, ergosterol, induces less order than cholesterol providing less protection from AMP-induced membrane disruption (9).

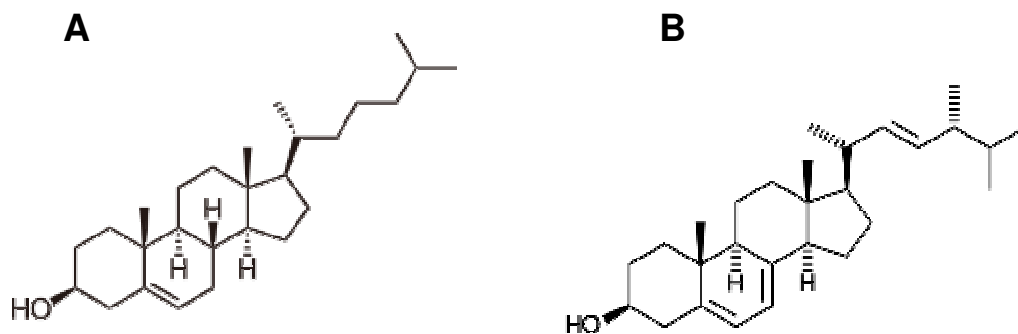


Figure 4.2 Structures of the eukaryotic sterol, cholesterol (A), and the fungi sterol, ergosterol (B).

The overall neutral environment of the eukaryotic cell membrane and the ordering of acyl chains due to the presence of sterols results in a more hydrophobic environment. Increasing hydrophobicity of AMPs, therefore, often correlates with increases in eurythrocyte toxicity of AMPs. Magainin-2 analogs with conserved charge and α -helical secondary structure based on C.D. analysis

were observed to have increased hemolytic activity as they were made more hydrophobic (10, 11). This is due to favorable hydrophobic interactions with eukaryotic cell membranes.

4.1.2 – Protegrin-1

Protegrin-1 (PG-1) is a broad spectrum antimicrobial peptide and, as mentioned previously, has significant hemolytic activity. PG-1 was originally isolated from porcine leukocytes (12) and is an 18 amino acid, amidated peptide (Figure 1.3A). The four cysteine residues form two disulfide bonds and stabilize the β -hairpin structure of the peptide (Figure 1.3B) (13, 14). PG-1 is believed to form pores in lipid membranes upon oligomerization of the peptide at a critical concentration (15, 16).

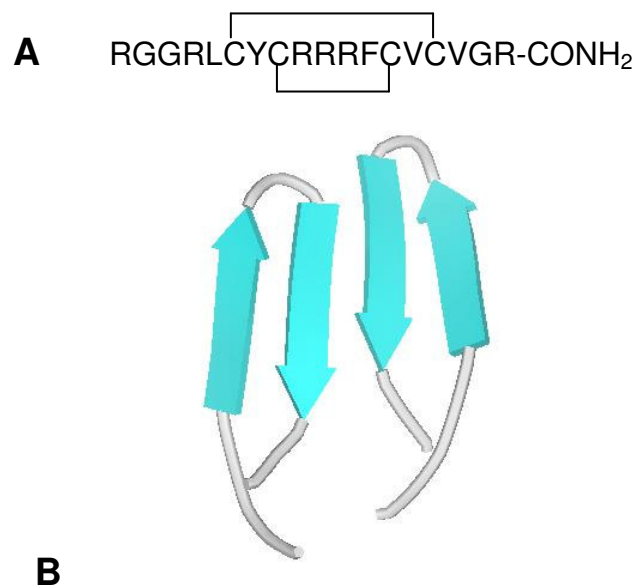


Figure 4.3 Protegrin-1 sequence (A) and solution structure (B) shown as a dimer (13).

The intramolecular disulfide bonds in PG-1 are important in the formation of the β -hairpin structure and also the activity of the peptide (17). Upon removal of one or both disulfide bonds PG-1 activity is decreased and further decreases at physiological salt concentrations (17, 18). The presence of high salt concentration does not affect the peptide activity when the disulfide bonds are present.

The selectivity of PG-1 is very dependant on membrane composition. Differences in hemolytic activity have been observed between porcine, bovine, and human red blood cells (19). This has been attributed to the differences in phosphatidylcholine and phosphatidylethanolamine composition across species (20). Studies on the effects of phospholipid head groups and tail packing on PG-1 association and insertion into lipid films show that peptide concentration is very important suggesting a highly cooperative oligomerization of PG-1 molecules is necessary for pore formation (21). Anionic head groups are important for initial association and insertion into membranes (21). The insertion of PG-1 into membranes was also found to be inversely proportional to the packing density of the lipids were the more densely packed lipids, those that contain sterols, are less likely to be inserted into (21).

4.1.3 – Fluorinated β -hairpin Antimicrobial Peptides

Structure-activity studies of PG-1 have shown that the peptide is very tolerant to substitution of amino acids, with regard to its secondary structure (22).

However, systematic studies on the importance of the hydrophobic residues on the activity and toxicity of PG-1 have yet to be conducted. In order to further our understanding of differences in selectivity observed among AMPs, PG-1 and two PG-1 analogs with increasing overall hydrophobicity were synthesized and characterized. The first analog, PG-1 LL, is a double mutant of the wildtype PG-1 peptide with leucine residues in place of valines at positions 14 and 16 (Figure 4.4 A and B). The second analog, PG-1 FF, contains two 5,5,5,5',5',5'-hexafluoroleucine (hFLeu) residues in place of valines at positions 14 and 16 of PG-1 (Figure 4.4 A and C). Substitution of leucine or hFLeu for valine in PG-1 increases the hydrophobicity of the peptide. It also tests the tolerance of the peptide to withstand non-isosteric amino acid substitutions and incorporation of amino acids, specifically leucine, with low β -sheet propensities, as discussed in Chapter 1.

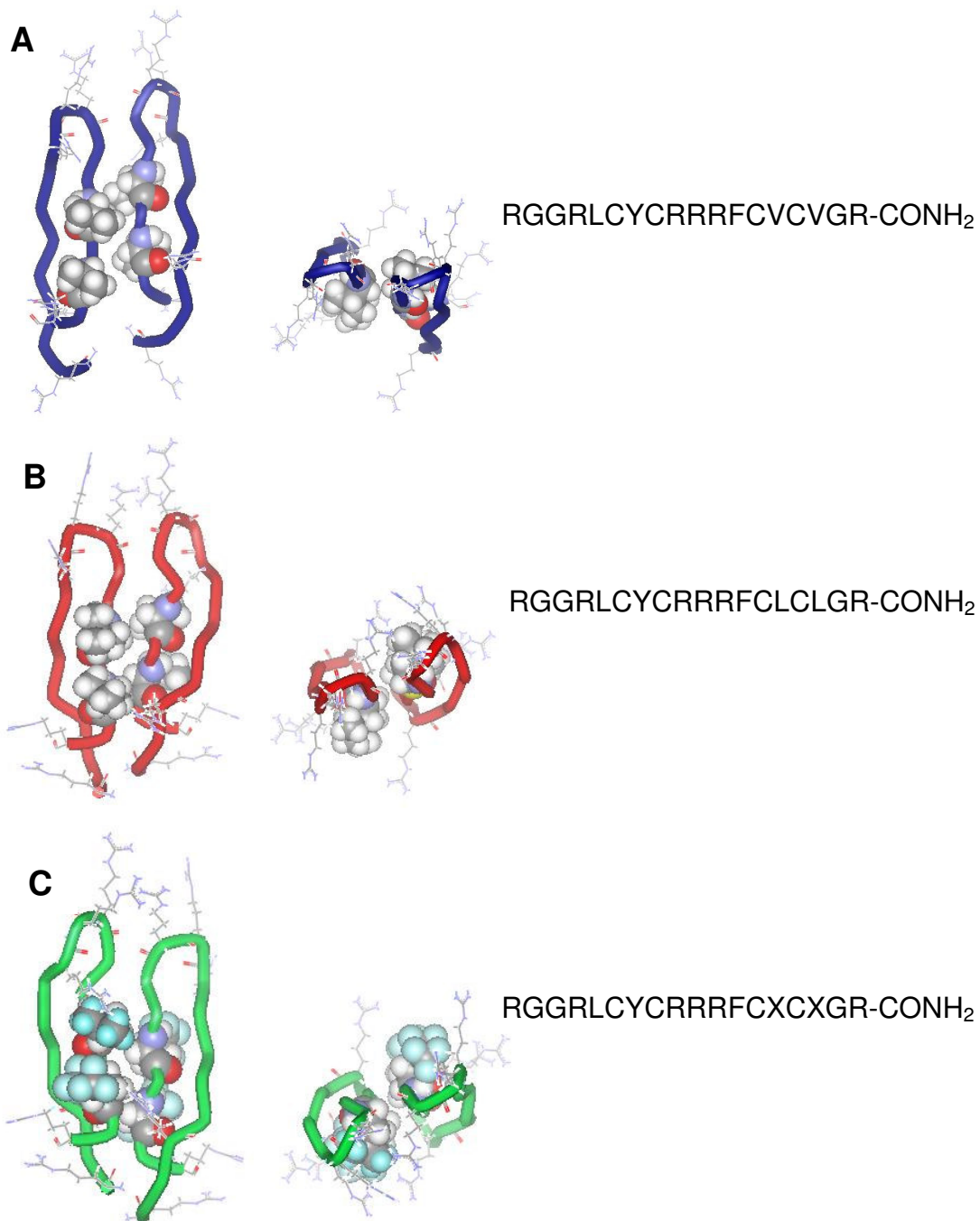


Figure 4.4 PG-1 (A), PG-1 LL (B), and PG-1 FF (C) structures at left and primary sequence at right. Hydrophobic residues at positions 14 and 16 in CPK and arginine residues depicted in line. Structures generated by Insight II based on energy minimizations of PG-1 structure (13) with double mutations. The single letter amino acid code X is hFLeu.

4.2 – Experimental Procedures

4.2.1 – Materials

Rink Amide resin, *t*-Boc-protected amino acids, and 2-(1*H*-benzotriazol-1-yl)-1,1,3,3-tetramethyluronium hexafluorophosphate (HBTU) were purchased from NovaBiochem. L-5,5,5,5',5',5'-Hexafluoroleucine (hFLeu) was synthesized as described previously (23) and converted to the *t*-Boc protected derivative by standard procedures. 1-palmitoyl-2-oleoyl-*sn*-glycero-3-phosphotidylcholine (POPC) and 1-Palmitoyl-2-Oleoyl-*sn*-Glycero-3-[Phospho-*rac*-(1-glycerol)] (POPG) were purchased from Avanti Polar Lipids. Chymotrypsin and trypsin were purchased from Boeringer Manheim GmbH. All other chemicals were purchased from Fisher and used without any further purification.

4.2.2 - Peptide Synthesis and Purification.

Peptides PG-1, PG-1 V14L V16L, and PG-1 V14hFLeu V16hFLeu were synthesized using *t*-Boc-protected amino acids for Merrifield manual solid-phase synthesis on MBHA resin; couplings were performed using *in situ* neutralization/HBTU protocol described by Schnolzer *et al* (24). on a 0.25mM scale. The peptide was cleaved from the resin using “high”-HF conditions.

The peptides were redissolved at ~10 mg/mL in 8 M Urea and 10 mM DTT and purified by reverse-phase HPLC on a Waters semipreparative C₁₈ column

equilibrated in 0.1% formic acid and eluted with a linear gradient from 5 to 50% acetonitrile containing 0.1% formic acid. Acetonitrile was removed under a stream of nitrogen and the solution adjusted to pH 7.0 with 10x PBS buffer and pH adjustment with 1 M HCl. DMSO was added to a final concentration of 20% (v/v). The peptide solutions were stirred for 48 hours at 4°C open to the atmosphere for oxidation to occur. The peptide solutions were lyophilized to concentrate the peptides and remove DMSO. Peptides were redissolved in 5% acetonitrile, 0.1% formic acid and purified by reverse-phase HPLC on a Waters semi-preparative C₁₈ column equilibrated in 0.1% formic acid and eluted with a linear gradient from 5 to 50% acetonitrile containing 0.1% formic acid. The peptides were determined to be pure by analytical HPLC and mass spectrometry. Concentration of the peptides was determined by the absorbance at 278 nm using an extinction coefficient of 1520 cm⁻¹ M⁻¹.

4.2.3 – Mass Spectral Analysis

Peptide samples at ~0.01 mg/mL were diluted in half with matrix solution (10 mg/mL α -cyano-4-hydroxycinnamic acid in 50% acetonitrile and 50% ethanol). Samples were loaded on the sample plate (2 μ L) and solvents were evaporated on the bench top. Samples were then subjected to Maldi-TOF mass spectrometry in refractive mode. Spectra were collected for ~30 sec then combined to obtain good signal to noise combined spectra for each peptide.

4.2.4 – Hydrophobicity Analysis.

Peptide samples were analyzed by RP-HPLC using a C₁₈ column to compare the hydrophobicity of the non-fluorinated and fluorinated samples. A linear gradient of a two buffer system from 0 - 30% buffer B from 0 - 5 min and 30 - 70% buffer B from 5 - 35 min was used. Buffer B is 90% acetonitrile with 0.1% formic acid and buffer A is 5% acetonitrile with 0.1% formic acid.

4.2.5 - Circular Dichroism (C.D.)

To examine the secondary structure of PG-1, PG-1 LL, and PG-1 FF 20 μ L of peptide at 680 μ M were diluted 10-fold in PBS buffer pH 7.4. POPC liposomes were prepared fresh in PBS buffer pH 7.4 to make a 13.6 mM solution of unilamellar liposomes by sonication (microtip, 10 sec intervals, level 3) with a Fisher Scientific 550 Sonic Dismembrator until the solution was clear. 20 μ L of the liposome solution was added to the diluted peptide to make a solution containing 1 : 200 (mole/mole) peptide to lipid. The CD spectra for each peptide and peptide/liposome solution were recorded from 200 - 250 nm with an Aviv 62DS spectropolarimeter at 25 °C. Mean residue ellipticities, Θ_M , were calculated using equation 1 where Θ_{obs} is the ellipticity measured in millidegrees, c is the molar concentration, l is the cell path length in centimeters, and n is the number of residues in the protein.

$$\Theta_M = \Theta_{\text{obs}}/10/cn \quad (1)$$

4.2.6 – Isothermal Titration Calorimetry

POPC/POPG (3:1 mol/mol) SUVs (10 mM), prepared as described for C.D. experiments, were titrated into peptide solutions (~55 μM) in PBS, pH 7.4. The liposomes were freshly prepared in PBS, pH 7.4. 3 μL injections of liposomes into peptide solution or PBS (as a control experiment to determine heat of dilution) were made for a total of 15 injections. Fitting was performed using the Microcal/Origin software.

4.2.7 – Bacterial Strains and Growth

(performed by Dr. Charles Shelburne)

E. coli D5 α was obtained from Invitrogen (Invitrogen, Carlsbad, CA). *Enterococcus faecalis* cultures were a gift from Dr. Donald B. Clewell, University of Michigan. *Bacillus subtilis* (ATCC 663), *Kocheria rhizophila* (ATCC 9341), *Earobacter aerogenese* (ATCC 13408), *Klebsiella pneumoniae* ATCC 4352, *Proteus mirabilis* (ATCC 25933), *Salmonella enteritis* Typhimerium ATCC 14028, *Streptococcus pyogenes* (ATCC 19615), *Staphylococcus aureus* (ATCC 6538) and *Shigella sonnei* (ATCC 25931) were obtained from MicroBiologics, St. Cloud, Minnesota. All species were maintained by weekly transfer on Trypticase Soy

Agar and broth cultures grown directly from individual colonies in Trypticase Soy Broth.

4.2.8 - MIC Determination

(performed by Dr. Charles Shelburne)

A sterile, 96- well micro-titer plate (NUNC) was used as the platform for the assay. An overnight culture of each bacterium was diluted to 10^6 /mL in sterile phosphate buffered saline and seeded into each well (100 μ L) of the plate. Doubling dilutions (200 μ g/mL - 3.13 μ g/mL) of PG-1, PG-1 LL, or PG-1 FF (100 μ L) in replicates of 8 were then added and the cultures covered with a sterile adhesive plastic film. After centrifugation for 1 minute at 800 x g to collect the entire inoculum to the bottom of the plate it was incubated at 37 °C overnight in air. Growth was determined by measuring the OD₅₉₅ of each well using a microwell plate reader (GENious, Tecan, Manendorf, Switzerland). The MIC for each organism was determined as the lowest dilution of each peptide without significant growth above the inoculum ($p \leq 0.01$, T-test). The differences between peptides for each bacterial strain were evaluated using a t-test.

4.2.9 – Hemolytic Activity

(performed by Dr. Charles Shelburne)

A sterile, 96- well round bottom micro-titer plate (Costar) was used as the platform for the assay. 2.5% bovine red blood cells in 100 μ L of PBS were added to the wells of the plate. Doubling dilutions (200 μ g/mL - 3.13 μ g/mL) of PG-1, PG-1 LL, or PG-1 FF (100 μ L) in replicates of 8 were then added and the cultures covered with a sterile adhesive plastic film. The plate was incubated for 2 hours at room temperature and examined by eye. The highest dilution of peptides without an intact cell pellet was noted.

4.3 – Results

4.3.1 – Disulfide Oxidation of Peptides

The PG-1 peptides were synthesized with cysteine in the reduced form. To assume their biologically active conformations it was necessary to oxidize the cysteines and form two disulfide bridges. This was achieved by stirring peptide solutions at pH 7.0 in PBS buffer with 10% DMSO open to the atmosphere for 2 days at 4°C. Disulfide bond formation was determined by Maldi-TOF ES+. The masses obtained for PG-1, PG-1LL and PG-1 FF indicate that the peptides contain two disulfide bonds after oxidation in the presence of DMSO (Table 4.1).

Table 4.1. Maldi-TOF results for β -hairpin peptides confirming the desired peptide and oxidation state.

| Peptide | Calculated MW (oxidized) | Experimental MW |
|---------|-----------------------------|--------------------|
| PG-1 | 2156.58 | 2156.15 |
| PG-1 LL | 2184.64 | 2184.32 |
| PG-1 FF | 2400.52 | 2400.96 |

4.3.2 Secondary Structure of Peptides

To verify that the peptides were forming the intended β -hairpin-like secondary structures necessary for activity the secondary structures of PG-1, PG-1 LL, and PG-1 FF were investigated by C. D. spectroscopy. Peptide spectra were recorded in PBS buffer and in PBS with small uni-lamellar vesicles (SUVs) prepared from POPC. The lipid to peptide ratio in the samples was 200 : 1. The spectra of PG-1 (Figure 4.5) exhibited a minimum at ~ 210 nm is indicative of the β -hairpin structure. The C.D. spectra are very similar for peptide in buffer and peptide in buffer containing SUVs. The C. D. spectra of PG-1 LL (Figure 4.6) indicates the peptide is less structured than PG-1 and the minimum at ~ 203 nm indicates the peptide is primarily random coil. However, in the presence of SUVs, the spectrum of PG-1 LL has a minimum at ~ 210 nm, suggesting some β -hairpin structure is induced by lipids. The spectrum of PG-1 FF (Figure 4.7) in the absence of lipids is characteristic of random coil with a minimum at ~ 204 nm. The spectrum exhibits a shift in the minimum mean residue ellipticity upon addition of

SUVs to 210 nm and the minimum Θ_M of $-12,000 \text{ deg cm}^2 \text{ dmol}^{-1} \text{ res}^{-1}$ is approximately twice that of PG-1, $\Theta_M = -6,000 \text{ deg cm}^2 \text{ dmol}^{-1} \text{ res}^{-1}$, and 4x that of PG-1 LL, $\Theta_M = -3,000 \text{ deg cm}^2 \text{ dmol}^{-1} \text{ res}^{-1}$.

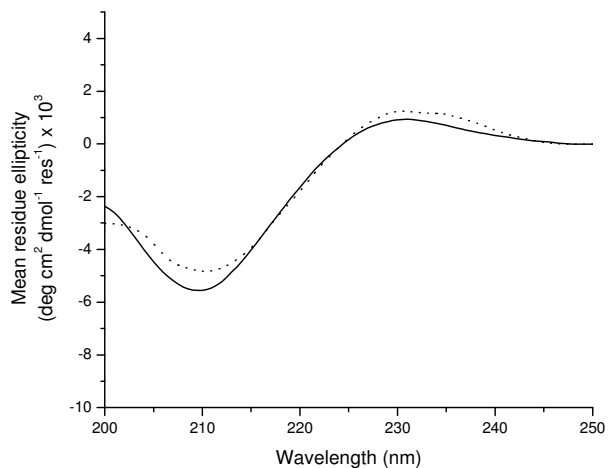


Figure 4.5 CD spectrum of PG-1 (solid line) and PG-1 with SUVs (dotted line).

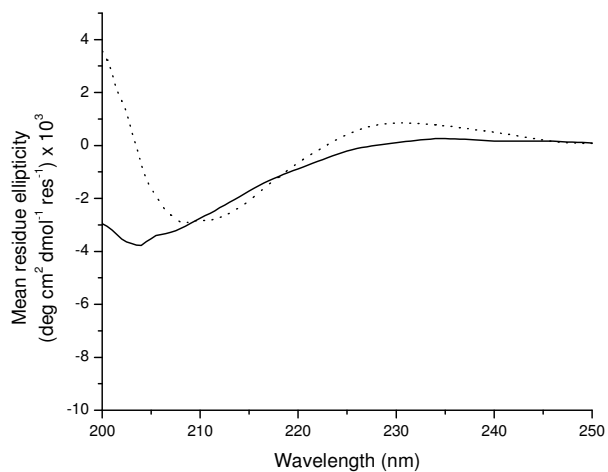


Figure 4.6 CD spectrum of PG-1 LL (solid line) and PG-1 LL with SUVs (dotted line).

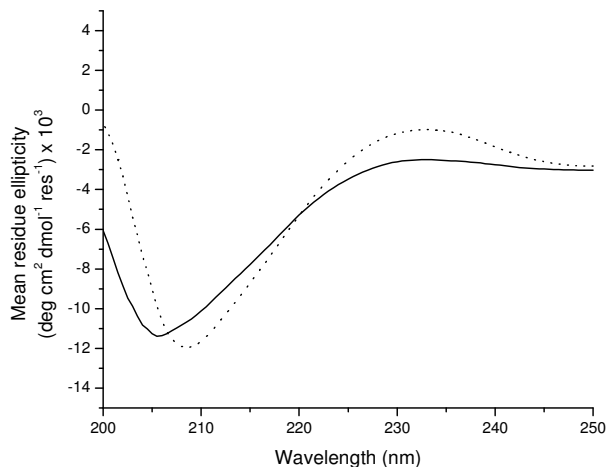


Figure 4.7 CD spectrum of PG-1 FF (solid line) and PG-1 FF with SUVs (dotted line).

4.3.3 – Hydrophobicity of Peptides

The hydrophobicity of peptides was compared by reversed phase HPLC using an analytical C₁₈ column. The chromatograms of each peptide are overlaid in Figure 4.8. PG-1 elutes at the earliest time of ~16.8 min followed by PG-1 LL at ~ 18.2 min, then PG-1 FF at ~20.2 min. The gradual and systematic increase in hydrophobicity of the peptides is evident in the increase in elution times of the peptides.

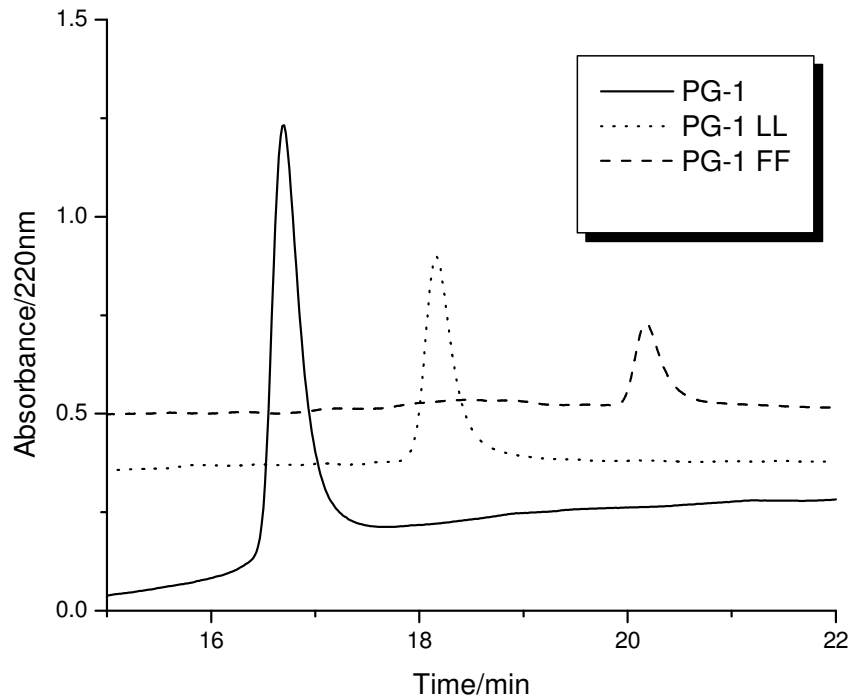


Figure 4.8. HPLC traces of protegrin based peptides with the elution time in minutes on the x-axis and relative absorbance at 220 nm on the y-axis. A linear gradient from 30 to 70% buffer B from 5 to 35 min was used. Buffer B is 90% acetonitrile with 0.1% formic acid and buffer A is 5% acetonitrile with 0.1% formic acid.

4.3.4 – Thermodynamic Parameters

The thermodynamic parameters of the peptides interacting with lipid bilayers were obtained by isothermal titration calorimetry (ITC). SUVs composed of 7.5 mM POPC and 2.5 mM POPG were titrated in 3 μ L increments into 55 μ M peptide solutions. The binding of peptides to SUVs was exothermic for all peptides (Figures 4.9 – 4.11, top panels). Integration of the binding energy peaks and subsequent fitting of the data points to a single binding site model

(Figure 4.9 – 4.11, lower panels) gives the thermodynamic parameters listed in Table 4.2.

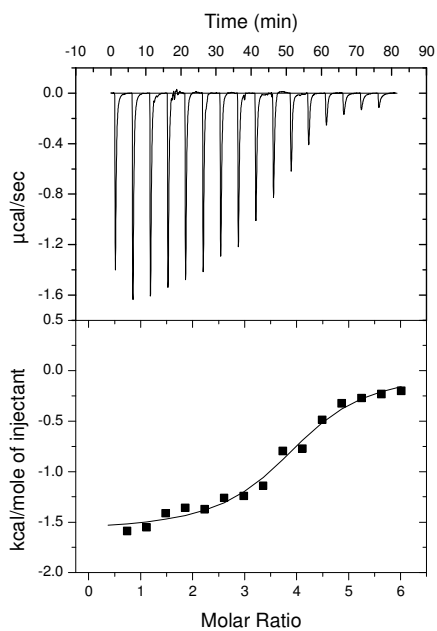


Figure 4.9 ITC titration at 30°C in PBS, pH 7.4. SUVs of POPC/POPG (3:1) 10mM were titrated into 55 μM PG-1 in 3 μL injection volumes. The top panel shows the actual titration as a function of time and the bottom panel shows kcal/mol injectant as a function of molar ratio of SUVs.

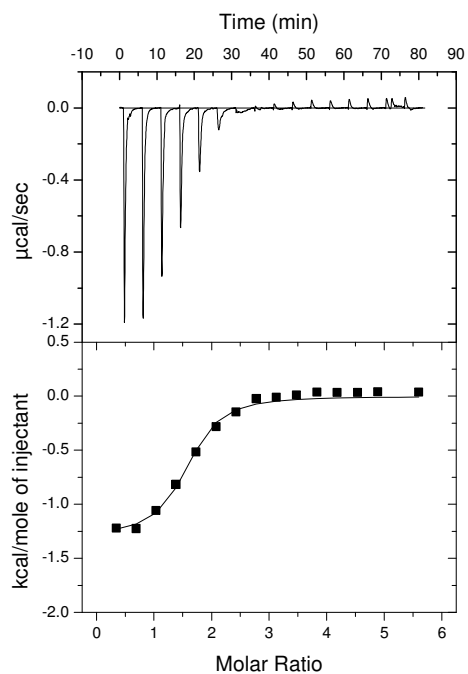


Figure 4.10 ITC titration at 30°C in PBS, pH 7.4. SUVs of POPC/POPG (3:1) 10mM were titrated into 55 µM PG-1 LL in 3 µL injection volumes. The top panel shows the actual titration as a function of time and the bottom panel shows kcal/mol injectant as a function of molar ratio of SUVs.

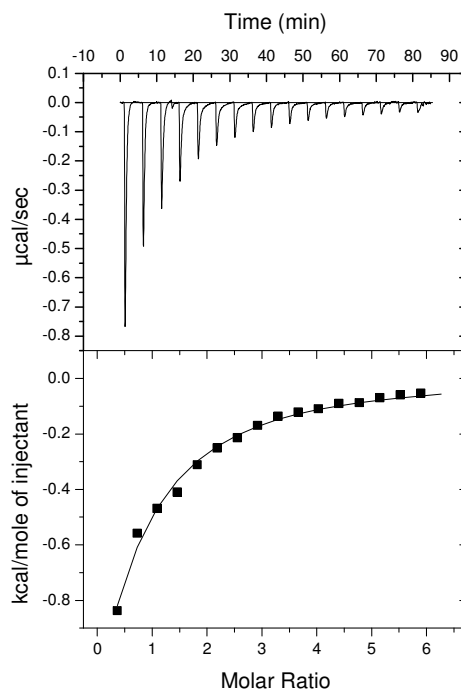


Figure 4.11 ITC titration at 30°C in PBS, pH 7.4. SUVs of POPC/POPG (3:1) 10mM were titrated into 55 μM PG-1 FF in 3 μL injection volumes. The top panel shows the actual titration as a function of time and the bottom panel shows kcal/mol injectant as a function of molar ratio of SUVs.

The association constants (K) of PG-1 and PG-1 LL are similar at $1.2 \times 10^5 \text{ M}$ and $2.7 \times 10^5 \text{ M}$. The association constant of PG-1 FF is an order of magnitude lower at $1.7 \times 10^4 \text{ M}$. The binding stoichiometry of PG-1 is 3.9 lipid to peptide while the molar ratios for PG-1 LL and PG-1 FF are significantly lower at 1.5 and 1.3 lipid to peptide, respectively. The binding enthalpies of PG-1 LL and PG-1 FF are similar (-1.3 kcal/mol) and lower than that of PG-1 (-1.6 kcal/mol). The peptides all vary from one another in terms of the entropy contribution of binding. PG-1 LL has the largest entropy contribution of 21 cal/mole/deg , PG-1 FF has the smallest entropy contribution of 15 cal/mole/deg , and PG-1 has a moderate

entropy contribution of 19 cal/mole/deg. The free energies of binding are -7, -8 and -6 kcal/mole for PG-1, PG-1 LL and PG-1 FF, respectively.

Table 4.2 Thermodynamic parameters of PG-1, PG-1 LL, and PG-1 FF. K (association constant), N (stoichiometry), and ΔH (enthalpy of binding) were fitted to the data in Figures 4.9 – 4.11. ΔS (entropy of binding) and ΔG (free energy of binding) were calculated from previous parameters.

| Peptide | K | N | ΔH (kcal/mol) | ΔS (cal/mol/deg) | ΔG (kcal/mol) |
|---------|--|----------------|--------------------------|-----------------------------|--------------------------|
| PG-1 | 1.2×10^5 $\pm 2.5 \times 10^4$ | 3.9 ± 0.07 | $-1.6 \pm .05$ | 18 | -7 |
| PG-1 LL | 2.7×10^5 $\pm 6.9 \times 10^4$ | 1.5 ± 0.04 | $-1.3 \pm .05$ | 21 | -8 |
| PG-1 FF | 1.7×10^4 $\pm 1.9 \times 10^3$ | 1.3 ± 0.1 | $-1.3 \pm .16$ | 15 | -6 |

4.3.5 – Toxicity

The hemolytic activity of the peptides was determined for bovine red blood cells. The hemolytic activity of the three peptides is very similar showing lysis at minimum concentrations between 3.9 – 7.8 $\mu\text{g/mL}$ (Table 4.3). The fluorinated peptide, PG-1 FF, is slightly more hemolytic than the non-fluorous peptides; PG-1 and PG-1 LL. PG-1 LL is the least hemolytic, however, is still significantly cytotoxic.

Table 4.3. Hemolytic activity as a percentage of lysed bovine red blood cells.

| Peptide concentration (µg/mL) | PG-1 | PG-1LL | PG-1 FF | Triton-100 (1%) | HBS |
|-------------------------------|------|--------|---------|-----------------|-----|
| 250 | 100 | 100 | 100 | 100 | 0 |
| 125 | 100 | 100 | 100 | 100 | 0 |
| 62.5 | 100 | 100 | 100 | 100 | 0 |
| 31.25 | 100 | 100 | 100 | 100 | 0 |
| 15.625 | 100 | 100 | 100 | 100 | 0 |
| 7.8125 | 44 | 26 | 100 | 100 | 0 |
| 3.90625 | 16 | 0 | 51 | 0 | 0 |
| 1.953125 | 0 | 0 | 0 | 0 | 0 |

4.3.6 – Antimicrobial Activity

The antimicrobial activities of PG-1, PG-1 LL and PG-1 FF vary from peptide to peptide (Table 4.4). The most significant results are the loss of activity for PG-1 FF for *B. subtilis* and *K. rhizophila*, two gram positive bacteria. The hydrophobic peptides, PG-1 LL and PG-1 FF have increased activity for *S. aureus*, also a gram positive bacterium. PG-1 LL has excellent activity against *Y. enterocolitca*, *E. facealis*, and *S. sonnei* with minimum inhibitory concentrations of 1.56, 3.13, and 3.13 µg/mL, respectively. PG-1 LL and PG-1 FF were also very active against *C. albicans*, a fungi, however the activity of PG-1 was not determined against this organism.

Table 4.4. Minimum inhibitory concentrations of PG-1, PG-1 LL, and PG-1 FF for a variety of bacterial strains.

| | | | PG-1 | PG-1 LL | PG-1 FF |
|-------------------------|--------|--------|--------------------|---------|---------|
| Strain Name | ATCC # | Type | MIC values (ug/mL) | | |
| <i>B. subtilis</i> | 6633 | Gram+ | 25 | 6.25 | >200 |
| <i>K. rhizophila</i> | 9341 | Gram + | 25 | 12.5 | >200 |
| <i>E. aerogenes</i> | 13048 | Gram - | 6.25 | 6.25 | 12.5 |
| <i>K. pneumoniae</i> | 4352 | Gram - | ND | 6.25 | 50 |
| <i>P. mirabilis</i> | 25933 | Gram - | >200 | >200 | >200 |
| <i>S. enterica</i> | 14028 | Gram - | 6.25 | 6.25 | 6.25 |
| <i>S. aureus</i> | UH11 | Gram+ | 25 | 6.25 | 6.25 |
| <i>S. enterica</i> | | Gram - | 6.25 | 6.25 | 6.25 |
| <i>E. fecaelis</i> | OG1 X | Gram + | ND | 3.13 | 12.5 |
| <i>Y. enterocolitca</i> | | Gram - | 25 | 1.56 | 12.5 |
| <i>S. Sonnei</i> | | Gram - | 12.5 | 3.13 | 12.5 |
| <i>C. albicans</i> | | Fungi | ND | 3.13 | 6.25 |

4.4 – Discussion

Overall, the most active and least hemolytic peptide among the three peptides studied is PG-1 LL. The leucine analog of PG-1 is the least well structured peptide as determined by C.D. spectroscopy, however, the thermodynamic parameters for the peptide binding to SUVs reveals a favorable increase in entropy. The leucine-containing peptide has a free energy of binding 1 kcal/mol more favorable than the wild type, PG-1 peptide and 2 kcal/mol more favorable than the fluorinated peptide, PG-1 FF.

The significant decrease in the mole ratio of SUV binding to peptide from ~4 for PG-1 to 1.5 and 1.3 for PG-1 LL and PG-1 FF, respectively, could be attributed to a higher oligomerization state of these peptides in SUVs or in solution. Both PG-1 LL and PG-1 FF appeared to aggregate in solution at concentrations of approximately 0.5 - 1 mM. The solubility of the peptides was noticed to decrease with increasing hydrophobicity.

The results presented suggest that the hydrophobicity of the peptide can be used to modulate the activity and toxicity of PG-1. The broad spectrum antimicrobial activity of PG-1 LL is improved or retained in comparison to PG-1 for all bacterial strains tested and significant activity is observed against the fungus *C. albicans*. The incorporation of fluorine into PG-1 is less promising. The lipophilicity of fluorous amino acids may contribute to higher hemolytic activity and the antimicrobial activity of PG-1 FF is improved for fewer bacterial strains and is lost for some strains that are susceptible to PG-1.

Finally, although the secondary structure of PG-1 is effected by the non-isosteric amino acid substitutions of val14 and val16 to leucine in PG-1 LL, it does not appear to hinder the oxidation of the two stabilizing disulfide bonds, nor diminish the antimicrobial activity of the peptide, nor increase the toxicity of the peptide. These results suggest that the hydrophobicity of PG-1 can be used to modulate activity and toxicity, however, fluorous amino acids do not show promise for improving PG-1 as previously observed for the α -helical AMP, MSI-78 discussed in Chapter 3.

4.5 – References

1. Oren, Z. and Shai, Y., *Biochemistry*, **36**, 1826-1835 (1997).
2. Selsted, M. E., Novotny, M. J., Morris, W. L., Tang, Y. Q., Smith, W., Cullor, J. S., *J. Biol. Chem.*, **267**, 4292-4295 (1992).
3. Storici, P., Zanetti, M., *Biochem. Biophys. Res. Commun.*, **196**, 1363-1368 (1993).
4. Ratledge, C. and Wilkinson, S. G., Microbial Lipids, Academic Press, London (1988)
5. Verkleij, A. J., Zwaal, R. F. A., Roelofsen, B., Comfurius, P., Kastelij, D., Van Deenen, L. L. M., *Biochim. Biophys. Acta*, **323**, 178-193 (1973).
6. Keller, S. L., Pitcher III, W. H., Huestis, W. H., McConnell, H. M., *Phys. Rev. Lett.*, **81**, 5019-5022 (1998).
7. Glukhov, E., Stark, M., Burrows, L. L., Deber, C. M., *J. Bio. Chem.*, **280**, 33960-33967 (2007).
8. Turner, J. D. and Rouser, G., *Anal. Biochem.*, **38**, 423-436 (1970).
9. Mason, A. J., Marquette, A., Bechinger, B., *Biophys. J.*, **93**, 4289-4299 (2007).
10. Dathe, M., Wieprecht, T., Nikolenko, H., Handel, L., Maloy, W. L., MacDonald, D. L., Beyermann, M., Bienert, M., *FEBS Lett.*, **403**, 208-212 (1997).
11. Wieprecht, T., Dathe, M., Krause, E., Beyermann, M., Maloy, W. L., MacDonald, D. L., Bienert, M., *FEBS Lett.*, **417**, 135-140 (1997).
12. Kokryakov, V. N., Harwig, S. S., Panyutich, E. A., Shevchenko, A. A., Aleshina, G. M., Shamova, O. V., Korneva, H. A., Lehrer, R. I., *FEBS Lett.*, **327**, 231-236 (1993).
13. Aumelas, A., Mangoni, M., Roumestand, C., Chiche, L., Despaux, E., Grassy, G., Calas, B., Chavanieu, A., *Eur. J. Biochem.*, **237**, 575-583 (1996).
14. Fahrner, R. L., Dieckman, T., Harwig, S. S., Lehrer, R. I., Eisenberg, J., Feigon, J., *Chem. Biol.*, **3**, 543-550 (1996).
15. Heller, W. T., Waring, A. J., Lehrer, R. I., Huang, H. W., *Biochemistry*, **37**, 17331-17338 (1998).
16. Mani, R., Waring, A. J., Lehrer, R. I., Hong, M., *Biochim. Biophys. Acta*, **1716**, 11-18 (2005).
17. Harwig, S. S., Waring, A., Yang, H. J., Cho, Y., Tan, L., Lehrer, R. I., *Eur. J. Biochem.*, **240**, 352-357 (1996).
18. Lai, J. R., Epand, R. F., Weisblum, B., Epand, R. M., Gellman, S. H., *Biochemistry*, **45**, 15718-15730 (2006).
19. Bellm, L., Lehrer, R. I., Ganz, T., *Expert Opin, Investig. Drugs*, **9**, 1731-1742 (2000).
20. Nouri-Sorkhabi, M. H., Wright, L. C., Sullivan, D. R., Gallagher, C., Kuchel, P. W., *Lipids*, **31**, 765-770 (1996).

21. Ishitsuka, Y., Pham, D. S., Waring, A. J., Lehrer, R. I., Lee, K. Y. C., *Biochim. Biophys. Acta*, **1758**, 1450-1460 (2006).
22. Chen, J., Falla, T. J., Liu, H., Hurst, M.A., Fujii, C.A., Mosca, D.A., Embree, J.R., Lory, D.J., Radcl, P.A., Chang, C.C., Gu, L., Fiddes, J.C., *Biopolymers*, **55**, 88-98 (2000).
23. Anderson, J. T., Toogood, P. L., Marsh, E. N. G., *Org. Lett.* **4**, 4281-4283 (2002).
24. Schnolzer, M., Alewood, P., Jones, A., Alewood, D., and Kent, S. B. H., *Int. J. Pept. Protein Res.*, **40**, 180-193 (1992).

Chapter 5

Symmetry Assembled Protein Superstructures

5.1 – Introduction

5.1.1 – Natural Superassemblies

There are a variety of highly ordered, protein based superassemblies in living systems. Superassemblies are assemblies of protein subunits into higher order quaternary structures often forming biological large structures on the nanometer scale. Forms of protein superassemblies vary from one dimensional filaments to three dimensional nanohedra. Actin is a well studied example of a filamentous protein assembly (1). It is composed of 42 kDa subunits that assemble into helical superassemblies upon ATP hydrolysis (2, 3). Viral capsids are natural polyhedra that encapsulate viral DNA or RNA. The crystal structure of the hepatitis B viral capsid (Figure 5.1) reveals the isosahedral assembly of 240 protein subunits (4). Naturally occurring protein superstructures have inspired scientists to employ proteins in designing self-assembling nanostructures for potential use as biomimetics, *in vitro* delivery vehicles, nanoscale filters, sensors and other biomaterial based products. Current challenges in this new field include designing protein-protein interactions to divert

the assembly of proteins into the desired structures, and controlling the assembly or disassembly of the superstructures in response to changes in conditions or specific signaling molecules.

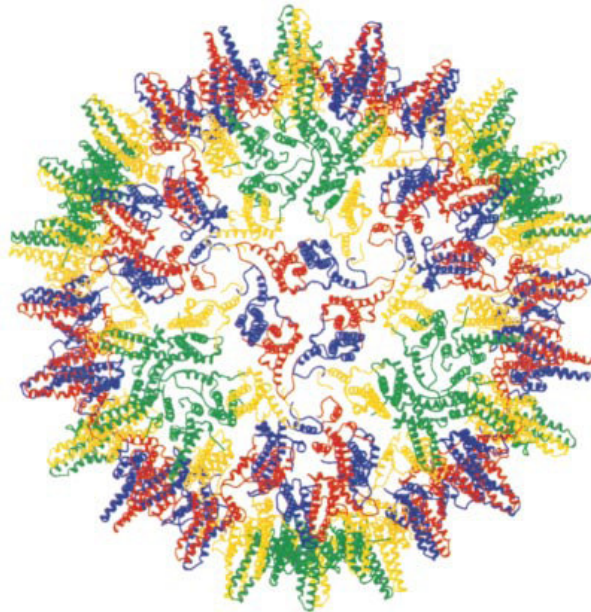


Figure 5.1 Hepatitis B viral capsid structure at 3.3 Å resolution (4). Protein data bank identification number 1QGT.

5.1.2 – Designed Superassemblies

Filamentous or linear protein superassemblies are an alternate design target due to potential applications as nanowires, biomimetics, and for further understanding of protein aggregation diseases such as Alzheimer's. One dimensional assemblies are also potentially more simple to design than two and

three-dimensional structures. Designs based on the assembly of β -sheet peptides (5, 6), α -helical peptides (7-10) and fusion of two natural dimerization domains (Figure 5.2) (11) have been used to produce linear protein assemblies. The assembly of β -sheets to form de novo amyloid proteins has been accomplished by West, et al (5). The ability to design such proteins gives insight into amyloidogenic proteins and diseases that result in this type of aggregation (12, 13). Assembly of α -helical peptides into filamentous superassemblies include an example from Pandya, et al (Figure 5.2A) (7). A heterodimeric parallel coiled-coil was designed with 'sticky' ends which allows for 2-dimensional extension upon interaction of dimers at the 'sticky' ends (Figure 5.2C) (11). This concept has been developed further to control extension in two-dimensions by including 'kinking' peptide subunits for controlling protein fiber morphology (14).

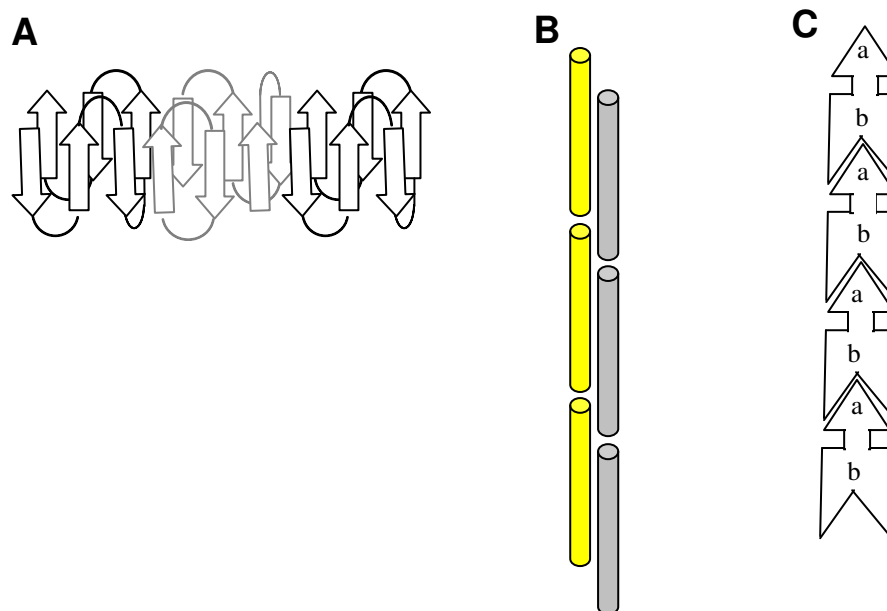


Figure 5.2 Schematic representations of designed linear protein superassemblies from; (A) hexameric β -sheets proteins with individual subunits shown in alternating black or grey for clarification, (B) heterodimeric parallel α -helices, and (C) fusion of two dimerization domains with domains labeled (*a*) and (*b*).

Lattices or arrays are desired assembly orientations for development of nanoscale sensors and catalysts. Polyvalent design is required for assembly in two or more dimensions. Lectin, a tetrameric protein was assembled into a protein lattice through the binding of a bivalent carbohydrate ligand (15) (Figure 5.3 a). Ligand binding is a desirable means of assembly provided they have high affinity and specificity for the proteins they bind to; for example the high affinity of biotin for streptavidin was used to direct assembly of proteins into lattice networks by Ringer and Schultz (16).

Encapsulated finite assemblies also require polyvalent design and the success in such designs is limited to a tetrahedral cage structure made upon assembly of fusion proteins composed of a dimerization domain to a trimerization domain (11) (Figure 5.3 b).

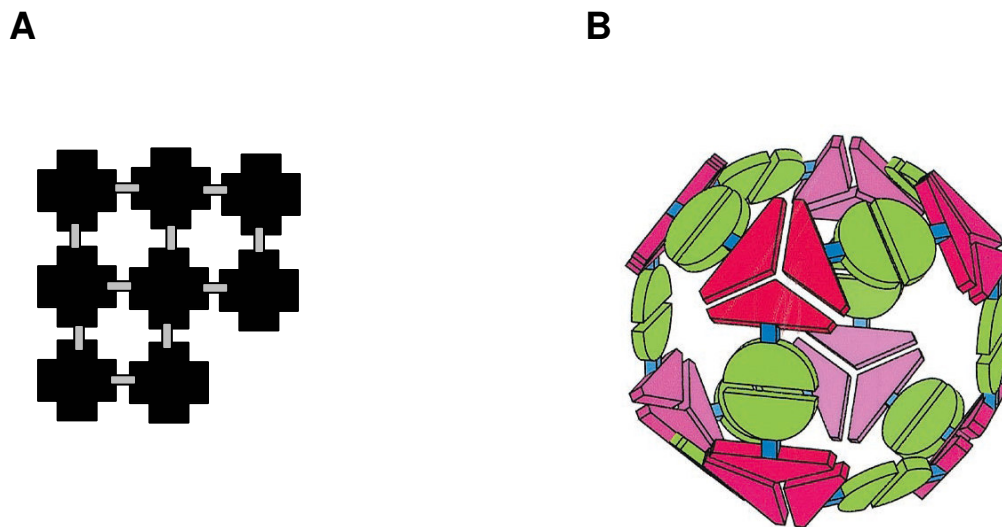


Figure 5.3 (A) Lattice assembly of proteins (black crosses) through small molecule binding (grey rectangles) (15) and (B) protein polyhedra assembled through protein-protein interactions of a fused (blue is fusion region) dimerization domain (green) and trimerization domain (red and pink) (11).

5.1.3 – Symmetry Based Directed Assembly

Homo-oligomeric proteins are ideal building blocks for symmetry based assembly. The symmetry implicit in proteins with dimer, trimer, and tetramer structures was exploited to assemble proteins in the examples described in the previous section. Higher order oligomers provide the polyvalency required for

multidimensional assembly. The structure of the assembly is very dependent on the method used to direct the assembly. Ligand binding has been shown to direct assembly into lattices or two-dimensional arrays (15, 16) while protein-protein interactions leading to dimerization gives rise to linear, two-dimensional or three-dimensional structures (5-11).

Symmetry of protein building blocks that arises from homo-oligomerization provides a basis for predicting potential assembled structures. If the polyvalency of homo-oligomeric proteins (greater than dimers) is simplified to common geometric shapes that have the same number of sides as the protein valency, the simplest possible outcomes of assembly are more easily visualized as shown in Figures 5.4 for two-dimensional and Figure 5.5 for three-dimensional Archimedean solids. Another possible assembled structure not presented in Figures 5.4 or 5.5 is the face-to-face assembly of any simple geometric shape.

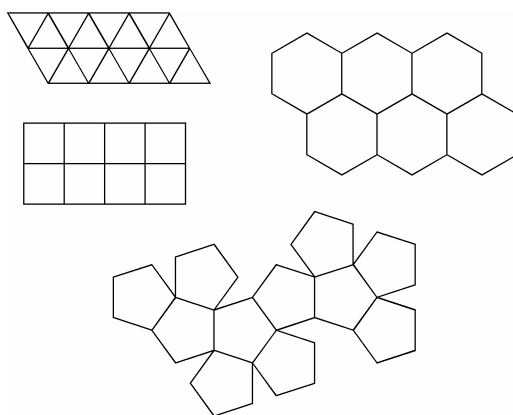


Figure 5.4 Two-dimensional arrays made up of various simple geometric shapes with the highest number of side-to-side interactions.

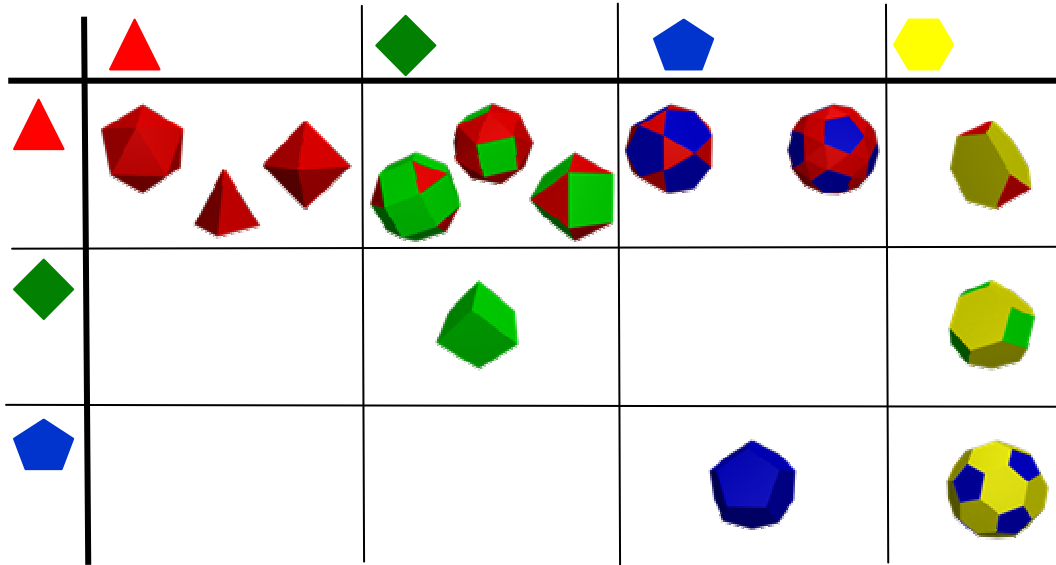


Figure 5.5 Three-dimensional polyhedra based on assembly of triangles, squares, pentagons, and hexagons.

5.1.4 – CTXB as a Building Block

In the research described in this chapter a homopentameric protein, cholera toxin B, was chosen as the building block. This building block provides a highly symmetric and stable structure for protein assembly into higher order structures. Cholera toxin B (CTXB) is a subunit of cholera toxin (CT) from *Vibrio cholerae* (Figure 5.6) which is primarily responsible for the symptoms of cholera (17). CTXB binds to GM1 gangliosides on the surface of intestinal cells while CTXA activates adenylate cyclase and cAMP accumulates to cause severe diarrhea. CTXB alone is not toxic and has been employed as a useful

assembly outcomes upon association at all points of attachment to dodecahedral, or face-to-face assemblies.

5.1.5 – Assembly Methods

Assembling proteins into higher order superstructures can be achieved by covalent crosslinking or non-covalent protein-protein interactions. Covalent crosslinking reagents are well known and often used for studying natural protein-protein interactions. In such situations the protein-protein interactions increase the effective concentrations of the two reactive amino acid side chains or protein termini. When no protein-protein interaction is present, crosslinking does not occur with many of the small molecule crosslinkers at μM concentrations.

Non-covalent methods of assembly include the use of protein-protein interactions such as fusion of dimerization domains to the terminus of the major protein building block, as exemplified by the assemblies in Figures 5.2 and 5.3. In the research presented here, protein-protein interactions and 'click' chemistry are employed for assembly of CTXB into higher order protein superstructures. A series of GCN-4-like domains were fused to the N-terminus of the CTXB subunit to mediate protein assembly by non-covalent interaction. 'Click' chemistry was employed to study the ability to covalently assemble proteins into higher order superstructures.

5.2 – Experimental Procedures

5.2.1 – Protein Expression and Purification

A cholera toxin B construct was obtained from the laboratory of Paulo Lee Ho (24). The DNA was transformed into chemically competent *E. coli* BL21 (DE3). Cells were grown in 1 L 2YT media to an OD₆₀₀ of 0.6 - 0.8 at 30°C in conical flasks then induced by addition of IPTG. After 4 - 16 hrs cells were harvested by centrifugation for 15 min at 6,000x g and 4°C. The cell pellets collected (3 - 5 g/L) were resuspended in 5 mL of lysis buffer (100 mM Tris, 500 mM NaCl, 0.1% Triton X-100, pH 8.0) per gram of cells. The suspension was placed on ice and sonicated to lyse cells (mictotip, level 5, 3 min (30 sec pulse, 2 min rest)). Sonication was repeated if solution did not become homogenous. Lysate was centrifuged (16,500x g, 4°C, 10 min) to retain the pellet. The pellet was washed with 50 mM Tris, 100 mM NaCl, 1 M Gu-HCl, pH 7.0 (2 x 20 mL) and centrifuged (16,500x g, 4°C, 15 min) to remove supernatant. The pellet was resuspended in 50 mM Tris, 6 M Gu-HCl, pH 9 (~10 mL) by placing a stir bar (~1 cm long) in the centrifuge tube and stirring gently at 4°C, 2 - 4 hrs. Resuspended protein was clarified by centrifugation at ~25,000x g, 4°C, 30 - 60 min. Protein was refolded and purified by Ni-NTA as described in the results section. Eluted protein was concentrated to ~25 mL using an amicon ultrafiltration cell. Protein was dialyzed at 4°C against PBS pH 7.4 and 5 mM EDTA (2 L) then without EDTA (2 L).

5.2.2 – Mutagenesis and Cloning

Single site mutations were performed using the QuikChange site directed mutagenesis kit from Stratagene. Fusion proteins were constructed by PCR using commercially synthesized oligomers with terminal BamHI and KpnI, or BssHII and KpnI restriction sites designed into the PCR products for easy digest and insertion into the N-terminus of the CTXB gene. DNA sequence analysis confirmed all constructs.

5.2.3 – Thiol Estimation Assay using Ellman's Reagent

A calibration curve was prepared by measuring free thiol content in a freshly prepared cysteine solution of known concentration. The solutions were prepared by adding Cys or protein solution (0 - 160 μ L), followed by 40 μ L of 1 M Tris, pH 8.5 and 200 μ L of Dithio-bis(2-nitrobenzoic acid) (DTNB) (2 mM in 50 mM NaOAc). The reaction solutions were made to 400 μ L final volume with Milli-Q H₂O. Reaction solutions were incubated at room temperature for 15 min followed by measurement of the absorbance at 412nm.

5.2.4 – Reagent Synthesis and Protein Derivatization

3-azido-propylamine: 3-bromo-propylamine (5 g) and sodium azide (4.5 g) were dissolved in water (25 mL) and heated to 80°C for 16 hrs. Water was

removed by rotary evaporator until ~10 mL remained. Potassium hydroxide (1 g) and diethyl ether (10 mL) were added and product was extracted with diethylether (3 x 10 mL) and dried over magnesium sulfate. Extracted product dried by rotary evaporation and its identity confirmed by 300 MHz H^1 NMR ($CDCl_3$); m 1.75 ppm (2H), tt 2.71 ppm (2H), tt 3.32 ppm (2H), t 4.85 (2H). Product yield was 70% (25).

N-(3-azido-propyl)-2-bromoacetamide: 3-azido-propylamine (0.1 g) was dissolved in dry toluene (1 mL) and 0.13 g of sodium bicarbonate was added. The mixture was cooled in an ice bath and bromoacetyl bromide (87 μ L, 0.2 g) was added dropwise. The reaction was slowly warmed to room temperature over 1 hr. then diluted with water (3 mL). The product was extracted with diethylether (3 x 10 mL) and dried over magnesium sulfate. The product was concentrated to an orange oil and its identity confirmed by 300 MHz H^1 NMR ($CDCl_3$); m 1.79 ppm (2H), m 3.36 ppm (4H), s 3.83 ppm (2H), s 7.22 ppm (1H). Product yield was 86% (26).

3-azido propyl CTXB Q3C; Freshly reduced then dialyzed CTXB Q3C in 25 mM, Tris pH 8.0 at 100 μ M (800 μ L) was mixed with *N*-(3-azido-propyl)-2-bromo-acetamide at 10 mM in DMSO (200 μ L). The reaction was stirred in the dark at 4°C, overnight. The reaction extent of protein modification was determined by ESI MS+; calculated mass 14005 Da, experimental mass 14006 Da. Excess *N*-(3-azido-propyl)-2-bromo-acetamide and DMSO were removed by dialysis against 25 mM HEPES, 10mM NaCl, pH 8.4 (2 x 2 L).

Dansylalkyne; Dansylchloride (0.5 g) was dissolved in dichloromethane (5 mL) followed by the addition of triethylamine (0.275 mL) and propargylamine (0.138 mL). The reaction was continued under a nitrogen atmosphere and was complete after 30 min by TLC. The reaction was quenched by addition of 100 mM phosphate buffer, pH 7.0 (5 mL) and the product was extracted with dichloromethane (3 x 5 mL). The product was concentrated to a yellow oil and purified by silica gel chromatography using diethylether/hexanes (1:1). The product identity was confirmed by 300 MHz ^1H NMR (CDCl_3); t 1.95 ppm (1H), s 2.97 ppm (6H), dd 3.79 ppm (2H), broad 4.96 (1H), d 7.25 ppm (1H), m 7.58 ppm (2H), d 8.41 ppm (2H), m 8.63 ppm (1H). The yield was quantitative (27).

N,N'-diethynylpentanediamide. Glutaryl dichloride (57 μL , 1 eq.) was dissolved in acetonitrile (8 mL) and cooled to 0 °C. Propargyl amine was added to the solution dropwise and the solution was warmed slowly to room temperature. Solvent was removed by rotary evaporator and the remaining residue was dissolved in methanol and crystallized at 4 °C to yield a clear crystalline solid. The product identity was confirmed by 300 MHz ^1H NMR (MeOD); quintet 2.89 ppm (2H), t 2.23 ppm (4H), t 2.58 ppm (2H), d 3.98 (4H), s 4.89 ppm (2H). The yield was quantitative.

5.2.5 – Analytical Ultracentrifugation

Sedimentation equilibrium experiments were performed using a Beckman XLA analytical ultracentrifugation equipped with scanning u.v.-visible optics (28).

Initial protein concentrations were 60 μM or 30 μM in PBS buffer, pH 7.4 containing either no SDS or 0.3% (w/v) SDS. The temperature was 293 K. The samples were centrifuged at 10,000, 20,000 and 25,000 rpm and were judged to have obtained equilibrium when successive radial scans were indistinguishable. The data were fitted to either a single species, monomer – pentamer equilibrium or, monomer – pentamer – decamer using the Ultrascan software package (B. Demeler, University of Texas Health Science Center at San Antonio; www.ultrascan.uthscsa.edu). Partial specific volumes were calculated using the method of Cohn and Edsall (29): the partial specific volume of CTXB was calculated as $0.72 \text{ cm}^3\text{g}^{-1}$.

5.2.6 – Transmission Electron Microscopy

Holey carbon grids were glow discharged prior to addition of protein samples (0.1 - 1 μM in Milli-Q water). Excess liquid was removed by wicking with filter paper after 30 sec and 2% uranyl acetate solution was placed on the grid for 30 sec prior to wicking excess solution away with filter paper. Grids were rinsed to remove excess stain by gently dipping in Milli-Q water. Images were collected in bright field mode at 50,000x and 100,000x magnification on a Joel-3011 by Dr. Kai Sun of the University of Michigan Electron Microbeam Analysis Laboratory.

5.3 – Results

5.3.1 – Cysteine Mutants of CTXB

CTXB was mutated to add cysteine residues to the protein surface to facilitate conjugation with protein crosslinking reagents. Three single cysteine mutants were made; CTXB Q3C, CTXB H13C, and CTXB N44C. The three mutations are located along the outer edges of the protein (Figure 5.7). All mutations were confirmed by DNA sequence analysis and plasmids were then transformed and expressed in *E. coli*, strain BL21 (DE3). The mutant proteins, like the wild type, were expressed as inclusion bodies. However, refolding the mutant proteins was problematic due to the presence of the third cysteine. CTXB H13C and CTXB N44C required the use of redox conditions for disulfide bond shuffling and proper refolding. CTXB Q3C was able to be refolded without disulfide bond shuffling, but the yield of purified, properly folded protein remained low at 2 – 3 mg/L of cell culture

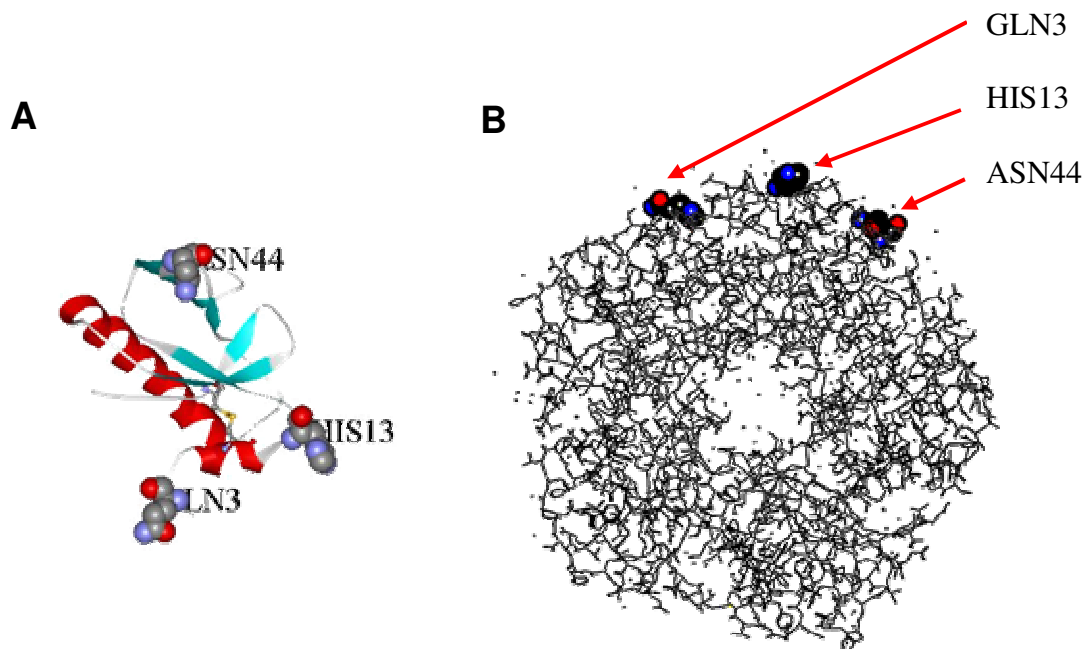


Figure 5.7 Monomeric subunit of CTXB depicting locations of Q3, H13, and N44 with secondary structure shown in ribbon view (A). Pentameric CTXB shown in stick view with Q3, H13 and N44 shown in CPK view (B).

5.3.2 – Inclusion Body Refolding and Ellman's Analysis

Denatured CTXB or CTXB Q3C were refolded by slow removal of chaotropic agents on an affinity column. Protein was loaded onto a Ni-NTA column pre-equilibrated in Buffer A (10mM Tris, 2.5mM imidazole, 0.5M NaCl, 10% glycerol, pH 8) containing 3M Gu-HCl. A linear gradient of Buffer A + 3M Gu-HCl to Buffer A with no Gu-HCl was applied over 30 column volumes and was sufficient for protein refolding of CTXB and CTXB Q3C on the column. Buffer A was continued for 6 column volumes followed by protein elution with 5 column volumes of 10mM Tris, 0.5M imidazole, 10% glycerol, pH 7.4. CTXB

H13C required refolding under redox reshuffling conditions. Denatured and reduced CTXB H13C was purified under denaturing conditions (6M Gu-HCl) by Ni-NTA. Purified and denatured protein samples at approximately 8 mg/mL were desalted on a sephadex G-25 column equilibrated in 10 mM HCl. Protein samples in 10 mM HCl at approximately 1 mg/mL were diluted two-fold into 100 mM Tris, pH 9.5, and 1 M arginine. The solution was degassed under argon followed by addition of solid oxidized and reduced glutathione (final concentrations of 0.5 mM and 5 mM, respectively). Refolding was allowed to continue under in a sealed container overnight at room temperature. CTXB N44C was expressed at very low levels could not be refolded to obtain pentameric protein based on SDS-PAGE analysis.

CTXB was obtained in high purity as seen in Figure 5.8 at a yield of 5-10 mg/L of cell culture. The cysteine mutant CTXB Q3C was obtained at a yield of 2-3 mg/L of cell culture and was found to co-purify with a contaminating protein of approximately 31 kDa (Figure 5.9). The ratio of pentameric to monomeric protein also appears to be less than that observed for the wild type CTXB (Figure 5.8). The mutant, CTXB H13C, was also co-purified with a contaminating protein of ~31 kDa and was expressed at low levels (Figure 5.10). After redox refolding the protein formed high molecular weight aggregates (>200 kDa). After desalting and reduction of the refolded protein the high molecular weight aggregates were reduced to a molecular weight indicative of pentameric and monomeric protein assembly (Figure 5.10).

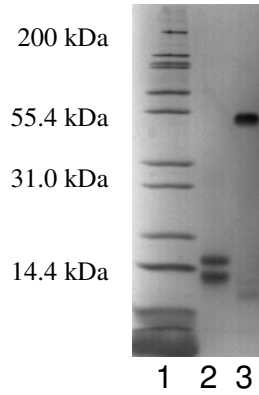


Figure 5.8 CTXB after refolding by dilution. Lane 1 is a molecular weight standard, lane 2 is CTXB reduced with DTT and boiled, and lane 3 is CTXB not reduced or boiled.

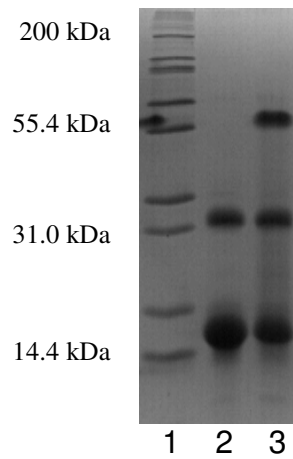


Figure 5.9 CTXB Q3C after refolding on Ni-NTA column. Lane 1 is a molecular weight standard, lane 2 is CTXB Q3C reduced with DTT and boiled, and lane 3 is CTXB Q3C not reduced or boiled.

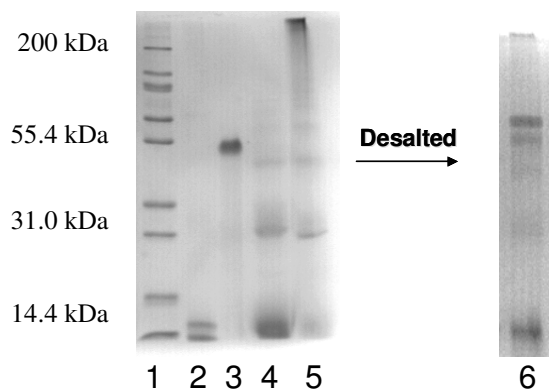


Figure 5.10 CTXB H13C (lane 4) after redox refolding (lane 5) and desalting (lane 6, sample reduced with DTT and boiled). Lanes 1-3 are molecular weight standard (lane 1), CTXB that has been reduced with DTT and boiled prior to loading on the gel (lane 2) and CTXB not reduced or boiled (lane 3).

Ellman's test was used to determine the accessibility and oxidation states of the cysteines residues in CTXB mutants Q3C and H13C. The results for CTXB H13C suggests that the surface cysteine is primarily in the oxidized form (Table 5.1). This result and the observation of high molecular weight protein aggregates by SDS-PAGE (Figure 5.10) suggest that the H13C mutant is highly susceptible to oxidation and could be forming intermolecular disulfide bonds.

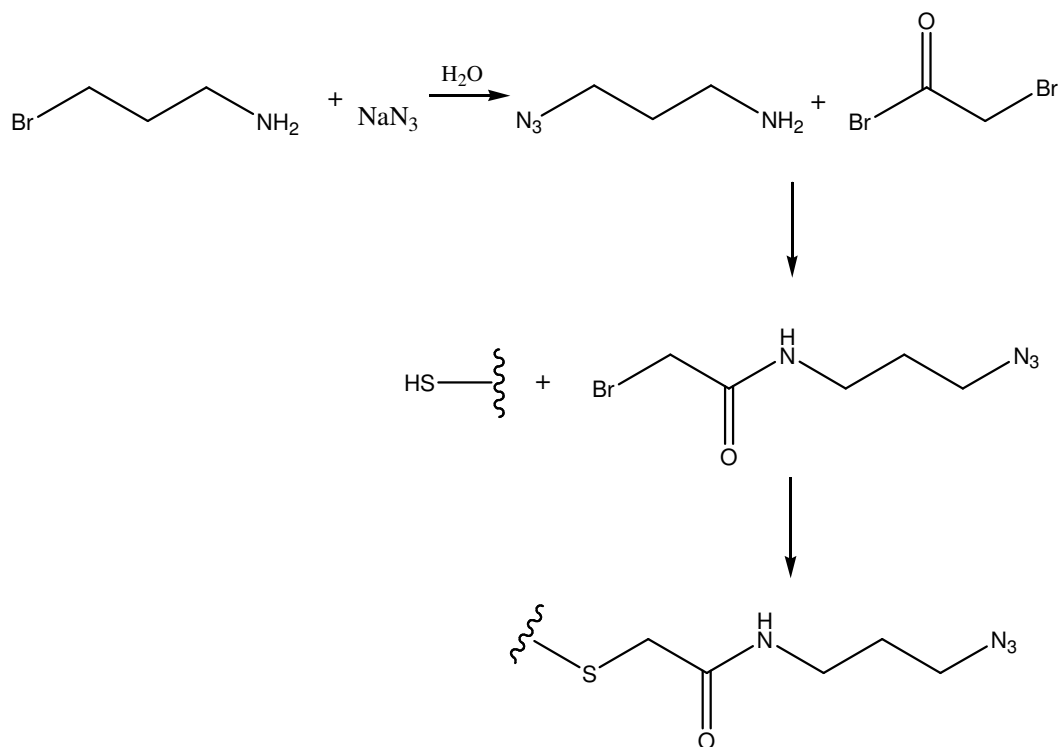
The oxidation state of CTXB Q3C is pH dependant as seen in Table 5.1. More than 80% of the cysteines are reduced at pH 7.7 making this mutant ideal for derivatization without having to keep the protein under highly reducing conditions or low pH, which is not conducive to thiol reactivity.

Table 5.1 Ellman's test results for CTXB Q3C and CTXB H13C at pH 7.0 to pH 8.5.

| Mutant | pH | Free thiol/monomer |
|--------|-----|--------------------|
| Q3C | 8.5 | 0.28 |
| Q3C | 7.7 | 0.82 |
| Q3C | 7.0 | 1.11 |
| H13C | 8.5 | 0.24 |
| H13C | 7.7 | 0.30 |

5.3.3 – CTXB Derivatization of Surface Cysteines

Synthesis of 3-azido-propylamine and N-(3-azido-propyl)-2-bromo-acetamide (Scheme 5.1) were achieved in good yield and high purity. N-(3-azido-propyl)-2-bromo-acetamide could be conjugated to CTXB Q3C under mild reaction conditions to give the azide derivatized protein at quantitative yields as detected by ESI-MS⁺ (Figure 5.11). The derivatized protein was stable at 4 °C and room temperature over days and the oligomerization state of the protein was not changed upon conjugation based on SDS-PAGE (Figure 5.12).



Scheme 5.1 Synthesis of N-(3-azido-propyl)-2-bromoacetamide and subsequent derivatization of cysteine to incorporate azide functional group on protein surface.

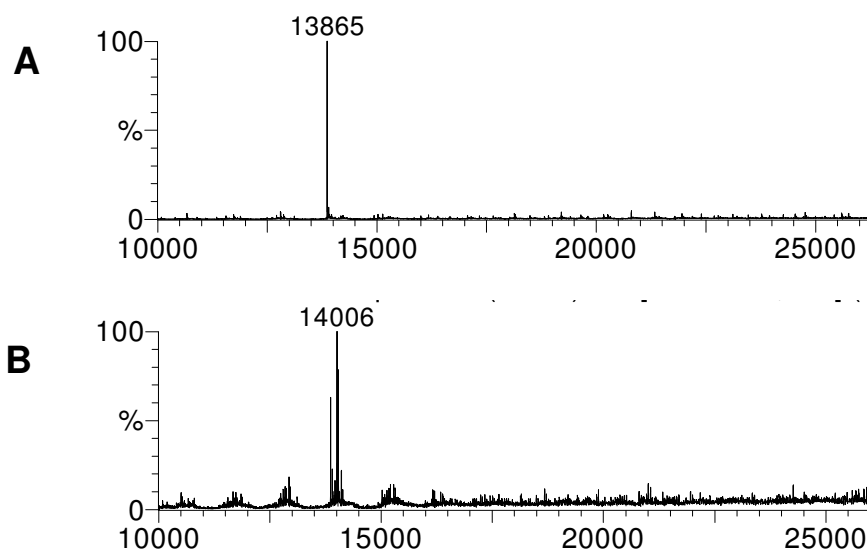


Figure 5.11 ESI-MS⁺ spectra of CTXB Q3C (A) and 3-azido propyl CTXB Q3C (B).

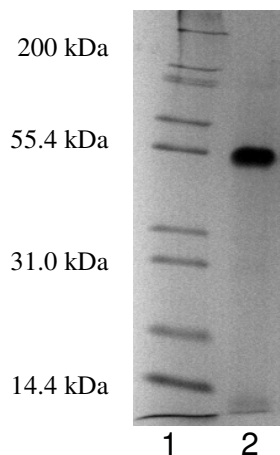
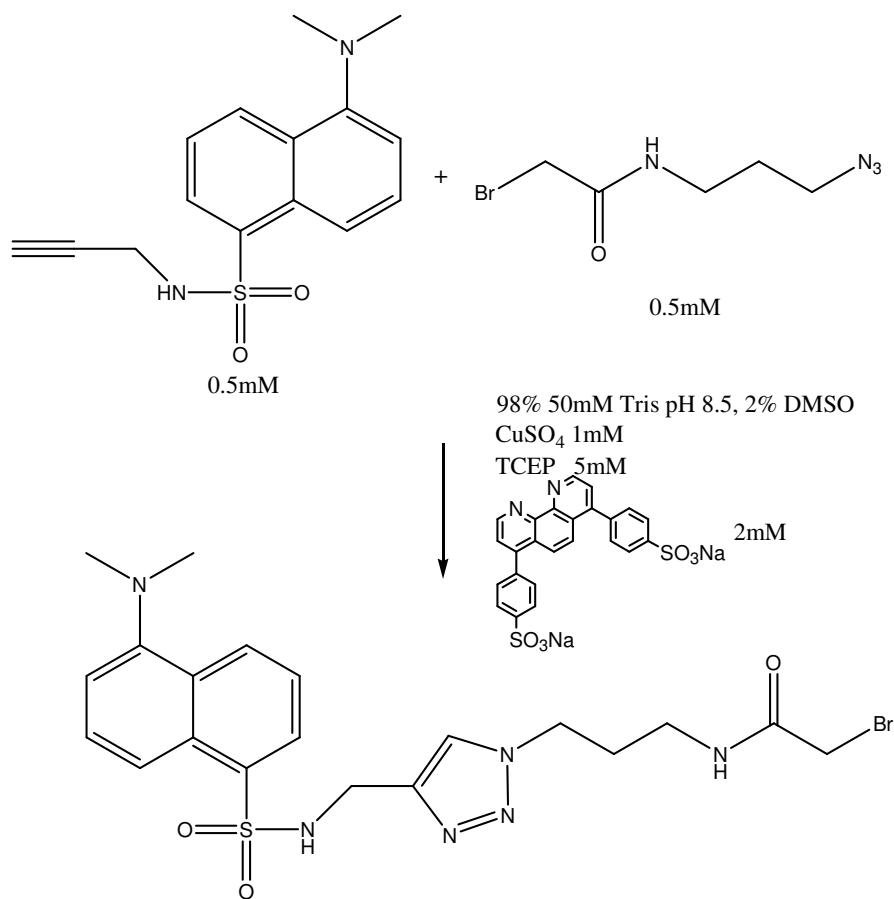


Figure 5.12 Tris-glycine SDS-PAGE (20% acrylamide) of molecular weight standard (lane 1) and 3-azido propyl CTXB Q3C.

5.3.4 – ‘Click’ Crosslinking Conditions

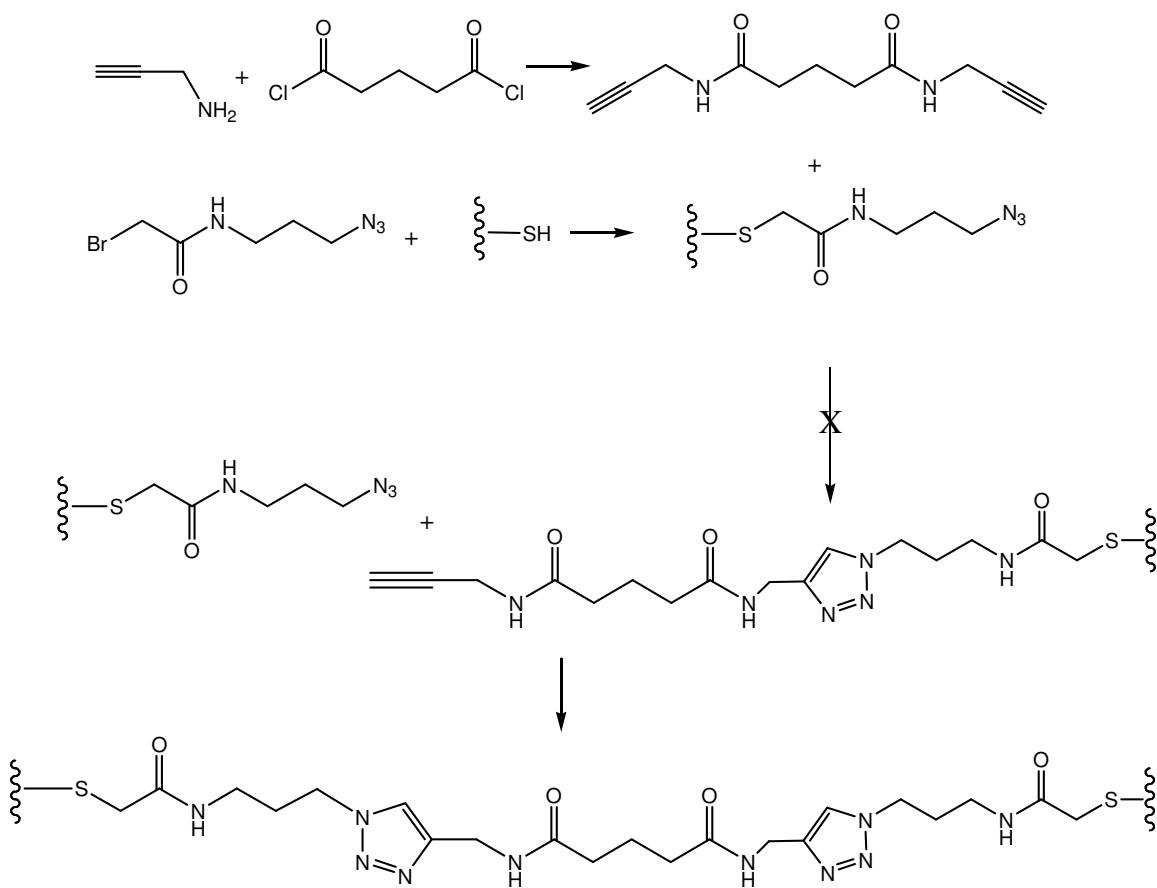
Dansyl alkyne was synthesized and purified easily by silica gel chromatography. The fluorescent alkyne and N-(3-azido-propyl)-2-bomo-acetamide were employed to test the ‘click’ reaction conditions (Scheme 5.2). The final concentrations of reagents used were; dansyl alkyne 5 mM, N-(3-azido-propyl)-2-bomo-acetamide 5 mM, copper chelator 10 mM, copper (II) sulfate 10 mM, and TCEP 10 mM. The reaction was complete after 3 hrs. at room temperature and pH 8.5 indicating the conditions were sufficient for the reaction to occur at a reasonable rate.



Scheme 5.2 'Click' test reaction performed at room temperature. The reaction was complete by TLC after 3 hrs.

Azide-derivatized CTXB Q3C was subjected to 'click' chemistry conditions in attempts to assemble the protein into higher order superassemblies. Scheme 5.3 illustrates the synthesis of the N,N'-diethynylpentanediamide and azide derivatized CTXB Q3C. The subsequent 'click' reaction was performed under a variety of conditions as seen in Table 5.2. The reactions were performed in 10 mM HEPES buffer at a pH between 8.0-8.3. In addition, reactions 8-10 in Table 5.2 were repeated with 20% DMSO to increase the solubility of the diyne. No crosslinking was observed by SDS-PAGE analysis under the conditions attempted. Conjugation of the azide-derivatized CTXB Q3C with the N,N'-

diethynylpentanediamide crosslinker could not be detected by ESI-MS+ because the spectra had low signal to noise ratios due to metal ions present in the reaction mixtures. Conjugation was attempted using the dansyl alkyne and azide labeled CTXB Q3C for ease of detecting the reaction, however, fluorescently labeled protein was not detected by SDS-PAGE.



Scheme 5.3 Reaction scheme for the synthesis of N,N'-diethynylpentanediamide, derivatized CTXB Q3C, and subsequent 'click' reactions.

Table 5.2 'Click' reaction conditions used for the crosslinking of 3-azido-propyl CTXB Q3C and N,N'-diethynylpentanediamide.

| | Protein Conc. (μM) | Reducing Agent | Chelator | Cu Conc. (μM) | Alkyne Conc. (μM) | Reducing Agent Conc. (μM) | Chelator Conc. (μM) |
|----|---------------------------------|----------------|----------|----------------------------|--------------------------------|--|----------------------------------|
| 1 | 300 | Cu wire | BPDS | 300 | 161 | | 600 |
| 2 | 300 | Cu wire | BPDS | 300 | 150 | | 300 |
| 3 | 53 | Cu wire | BPDS | 530 | 270 | | 1600 |
| 4 | 67 | Cu wire | Bipy | 550 | 270 | | 1600 |
| 5 | 83 | Cu wire | Bipy | 680 | 3300 | | 2000 |
| 6 | 83 | Ascorbate | Bipy | 680 | 3300 | 2200 | 2000 |
| 7 | 83 | TCEP | Bipy | 680 | 3300 | 2200 | 2000 |
| 8 | 83 | Cu wire | BPDS | 680 | 3300 | | 2000 |
| 9 | 83 | Ascorbate | BPDS | 680 | 3300 | 2200 | 2000 |
| 10 | 83 | TCEP | BPDS | 680 | 3300 | 2200 | 2000 |

5.3.5 – Fusion Constructs

Three fusion protein constructs were prepared that contain a GCN4-like dimerization domain at the N-terminus and a CTXB pentamerization domain at the C-terminus. The linker region between the two protein domains consists of 3, 4, or 6 glycine residues. The nomenclature used for the fusion constructs is FUS_n, where n is indicative of the glycine linker length. The constructs are, therefore, FUS₃, FUS₄, and FUS₆. FUS₃ contains an additional 7 amino acid residues at the C-terminus of the dimerization domain, while FUS₄ and FUS₆ do not contain these residues which shortens the dimerization domain by approximately two turns of the α -helix. DNA and protein sequences of the fusion proteins are shown in Figure 5.13 – 5.15.

| | | | | |
|-----|-----------------------------|-------------------------------------|-----------------|-----|
| 1 | atg cat cac cat cac cat cac | ctc gag gga tcc | cgt atg aaa cag | 45 |
| 1 | Met His His His His His His | Leu Glu Gly Ser | Arg Met Lys Gln | 15 |
| 46 | ctg gaa gat aaa gtg gaa gaa | ctg ctt tcg aaa aac tat cat ctg | | 90 |
| 16 | Leu Glu Asp Lys Val Glu Glu | Leu Leu Ser Lys Asn Tyr His Leu | | 30 |
| 91 | gag aat gaa gta gcg cgc ctg | aaa aaa cta gtg ggt ggt ggt acc | | 135 |
| 31 | Glu Asn Glu Val Ala Arg Leu | Lys Lys Leu Val Gly Gly Gly | Thr | 45 |
| 136 | ccg cag aac atc acc gac ctg | tgc gcc gag agc cac aac acc cag | | 180 |
| 46 | Pro Gln Asn Ile Thr Asp Leu | Cys Ala Glu Ser His Asn Thr Gln | | 60 |
| 181 | atc tac acc ctg aac gac aag | atc ttc tcg tac acc gag agc ctg | | 225 |
| 61 | Ile Tyr Thr Leu Asn Asp Lys | Ile Phe Ser Tyr Thr Glu Ser Leu | | 75 |
| 226 | gcc ggt aag cgt gaa atg gcc | atc atc acc ttc aag aac ggt gcg | | 270 |
| 76 | Ala Gly Lys Arg Glu Met Ala | Ile Ile Thr Phe Lys Asn Gly Ala | | 90 |
| 271 | atc ttc cag gtg gag gtc ccg | agc agc cag cac atc gat tcg cag | | 315 |
| 91 | Ile Phe Gln Val Glu Val Pro | Ser Ser Gln His Ile Asp Ser Gln | | 105 |
| 316 | aag aag gcc atc gag cgt aTG | AAG GAC ACC CTG CGT ATC GCC TAC | | 360 |
| 106 | Lys Lys Ala Ile Glu Arg Met | Lys Asp Thr Leu Arg Ile Ala Tyr | | 120 |
| 361 | CTG ACC GAA GCC AAG GTG | GAA AAG CTG TGC GTC TGG AAC AAC AAG | | 405 |
| 121 | Leu Thr Glu Ala Lys Val Glu | Lys Leu Cys Val Trp Asn Asn Lys | | 135 |
| 406 | ACG CCG CAC GCC ATC GCC | GCC ATC AGC ATG GCC AAC ACG CGT GAA | | 450 |
| 136 | Thr Pro His Ala Ile Ala Ala | Ile Ser Met Ala Asn Thr Arg Glu | | 150 |
| 451 | TCC TAA | 456 | | |
| 151 | Ser End | | | |

Figure 5.13 DNA and amino acid sequences for fusion protein FUS3. Green shaded areas represent the 6X-His tag for protein purification, pink shaded areas are thrombin cleavage sites, blue shaded areas are the GCN4-like dimerization domain, and yellow shaded areas are the poly-glycine linker regions. The CTXB domain is the remaining, unshaded sequence following the linker regions.

```

1   atg cat cac cat cac cat cac ctc gag gga tcc cgt atg aaa cag   45
1   Met His His His His His His Leu Glu Gly Ser Arg Met Lys Gln   15

46  ctg gaa gat aaa gtg gaa gaa ctg ctt tcg aaa aac tat cat ctg   90
16  Leu Glu Asp Lys Val Glu Glu Leu Leu Ser Lys Asn Tyr His Leu   30

91  gag aat gaa gta ggt ggt ggt ggt acc ccg cag aac atc acc gac   135
31  Glu Asn Glu Val Gly Gly Gly Gly Thr Pro Gln Asn Ile Thr Asp   45

136 ctg tgc gcc gag agc cac aac acc cag atc tac acc ctg aac gac   180
46  Leu Cys Ala Glu Ser His Asn Thr Gln Ile Tyr Thr Leu Asn Asp   60

181 aag atc ttc tcg tac acc gag agc ctg gcc ggt aag cgt gaa atg   225
61  Lys Ile Phe Ser Tyr Thr Glu Ser Leu Ala Gly Lys Arg Glu Met   75

226 gcc atc atc acc ttc aag aac ggt gcg atc ttc cag gtg gag gtc   270
76  Ala Ile Ile Thr Phe Lys Asn Gly Ala Ile Phe Gln Val Glu Val   90

271 ccg agc agc cag cac atc gat tcg cag aag aag gcc atc gag cgt   315
91  Pro Ser Ser Gln His Ile Asp Ser Gln Lys Lys Ala Ile Glu Arg   105

316 atg aag gac acc ctg cgt atc gcc tac ctg acc gaa gcc aag gtg   360
106 Met Lys Asp Thr Leu Arg Ile Ala Tyr Leu Thr Glu Ala Lys Val   120

361 gaa aag ctg tgc gtc tgg aac aac aag acg ccg cac gcc atc gcc   405
121 Glu Lys Leu Cys Val Trp Asn Asn Lys Thr Pro His Ala Ile Ala   135

406 gcc atc agc atg gcc aac acg cgt gaa tcc taa   438
136 Ala Ile Ser Met Ala Asn Thr Arg Glu Ser End

```

Figure 5.14 DNA and amino acid sequences for fusion protein FUS4. Green shaded areas represent the 6X-His tag for protein purification, pink shaded areas are thrombin cleavage sites, blue shaded areas are the GCN4-like dimerization domain, and yellow shaded areas are the poly-glycine linker regions. The CTXB domain is the remaining, unshaded sequence following the linker regions.

| | | | | |
|-----|-----------------------------|---------------------------------|-----------------|-----|
| 1 | atg cat cac cat cac cat cac | ctc gag gga tcc | cgt atg aaa cag | 45 |
| 1 | Met His His His His His His | Leu Glu Gly Ser | Arg Met Lys Gln | 15 |
| 46 | ctg gaa gat aaa gtg gaa gaa | ctg ctt tcg aaa aac tat cat ctg | | 90 |
| 16 | Leu Glu Asp Lys Val Glu Glu | Leu Leu Ser Lys Asn Tyr His Leu | | 30 |
| 91 | gag aat gaa gta ggt ggt ggt | ggt ggt ggt acc ccg cag aac atc | | 135 |
| 31 | Glu Asn Glu Val Gly Gly Gly | Gly Gly Gly Thr Pro Gln Asn Ile | | 45 |
| 136 | acc gac ctg tgc gcc gag agc | cac aac acc cag atc tac acc ctg | | 180 |
| 46 | Thr Asp Leu Cys Ala Glu Ser | His Asn Thr Gln Ile Tyr Thr Leu | | 60 |
| 181 | aac gac aag atc ttc tcg tac | acc gag agc ctg gcc ggt aag cgt | | 225 |
| 61 | Asn Asp Lys Ile Phe Ser Tyr | Thr Glu Ser Leu Ala Gly Lys Arg | | 75 |
| 226 | gaa atg gcc atc atc acc ttc | aag aac ggt gcg atc ttc cag gtg | | 270 |
| 76 | Glu Met Ala Ile Ile Thr Phe | Lys Asn Gly Ala Ile Phe Gln Val | | 90 |
| 271 | gag gtc ccg agc agc cag cac | atc gat tcg cag aag aag gcc atc | | 315 |
| 91 | Glu Val Pro Ser Ser Gln His | Ile Asp Ser Gln Lys Lys Ala Ile | | 105 |
| 316 | gag cgt atg aag gac acc ctg | cgt atc gcc tac ctg acc gaa gcc | | 360 |
| 106 | Glu Arg Met Lys Asp Thr Leu | Arg Ile Ala Tyr Leu Thr Glu Ala | | 120 |
| 361 | aag gtg gaa aag ctg tgc gtc | tgg aac aac aag acg ccg cac gcc | | 405 |
| 121 | Lys Val Glu Lys Leu Cys Val | Trp Asn Asn Lys Thr Pro His Ala | | 135 |
| 406 | atc gcc gcc atc agc atg gcc | aac acg cgt gaa tcc taa | 444 | |
| 136 | Ile Ala Ala Ile Ser Met Ala | Asn Thr Arg Glu Ser End | | |

Figure 5.15 DNA and amino acid sequences for fusion protein FUS6. Green shaded areas represent the 6X-His tag for protein purification, pink shaded areas are thrombin cleavage sites, blue shaded areas are the GCN4-like dimerization domain, and yellow shaded areas are the poly-glycine linker regions. The CTXB domain is the remaining, unshaded sequence following the linker regions.

Expression and purification of the fusion proteins was performed as described for CTXB and SDS-PAGE analysis (Figure 5.14) was used to determine the oligomerization state of the CTXB domains. FUS3 did not retain its pentameric state whereas FUS4 and FUS6 were pentameric under non-reducing condition by SDS-PAGE. In addition, FUS4 and FUS6 eluted from a Superose 6 gel filtration column at volumes that indicate pentamer formation or higher oligomerization state (Figure 5.15). The broad peaks of FUS4 and FUS6

indicate that higher order assembly of the fusion proteins may be occurring and that the assembled proteins may not be significantly larger than pentamers of fusion domains.

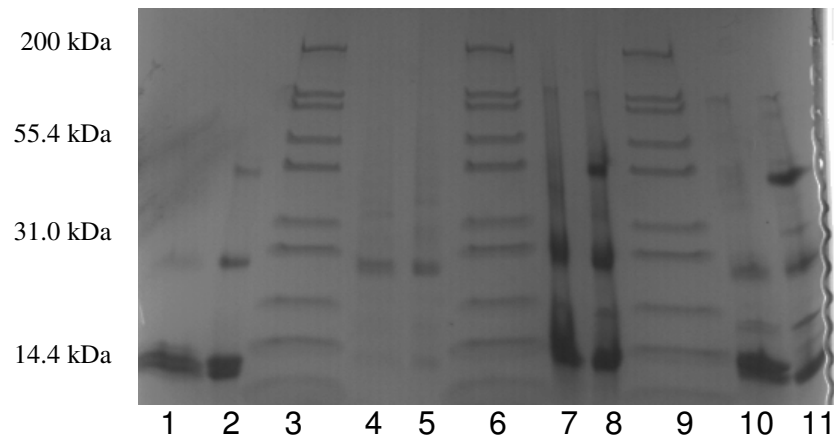


Figure 5.16 Tris-glycine SDS-PAGE (20% acrylamide) of CTXB reduced (lane 1) and oxidized (lane 2), molecular weight standard (lane 3, 6, 9), FUS3 reduced (lane 4) and oxidized (lane 5), FUS4 reduced (lane 7) and oxidized (lane 8), and FUS6 reduced (lane 10) and oxidized (lane 11).

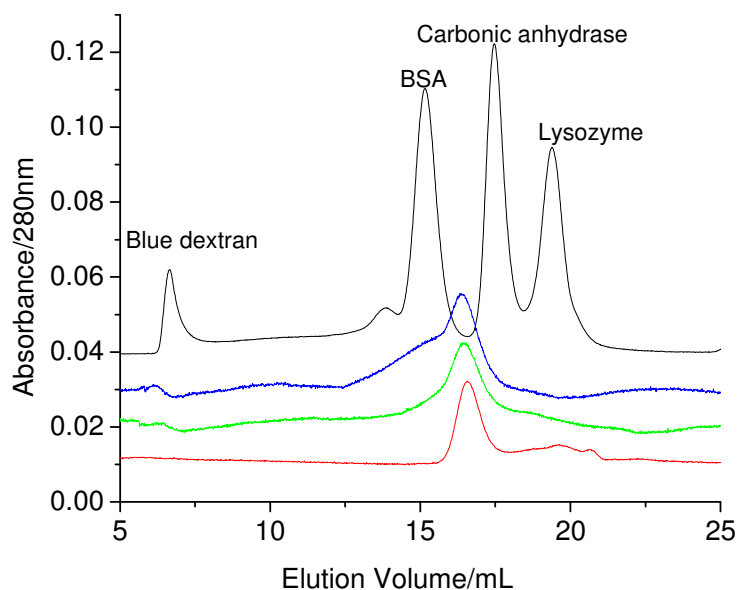


Figure 5.17 Gel filtration chromatograms of standard proteins (black), CTXB (red), FUS4 (green), and FUS6 (blue). Proteins were eluted from a Superose 6 column at 0.3 mL/min in PBS buffer, pH 7.4 with 0.1% SDS.

5.3.6 – Analytical Ultracentrifugaion

To determine the homogeneity and molecular weights of assembled fusion proteins FUS4 and FUS6 were analyzed by sedimentation equilibrium analytical ultracentrifugation. Protein samples at 30 or 60 μM were analyzed in either the presence or absence of 0.3% SDS (w/v). SDS has been shown to disrupt the helicity and oligomerization of GCN4, sequence shown in Figure 5.16, at 0.3 mM (30) while CTXB remains pentameric at 0.35 mM SDS (1% w/v)) (Figure 5.8).

STHMKQLEDKVEELLSKNYHLENEVARLKKLVGER

Figure 5.18 GCN4 leucine zipper sequence (30) with the shaded region indicating the sequence of the GCN4 domain of FUS4 and FUS6 were residue 3 is Arg instead of His.

Fitting of scans obtained at 15,000, 20,000 and 25,000 RPMs to monomer-pentamer or monomer-pentamer-decamer models for CTXB, FUS4, and FUS6 indicate that in the presence of 0.3% SDS all proteins fit to a monomer-pentamer model with fitted molecular weights of $18,700 \pm 1500$ (theoretical Mr of 14,400, Figure 5.17), $20,000 \pm 1500$ (theoretical Mr of 16,500, Figure 5.18) and $16,300 \pm 1000$ (theoretical Mr of 16,700, Figure 5.19) for CTXB, FUS4 and FUS6, respectively. These molecular weights indicate that all proteins formed pentamers and that interaction of the coiled-coil dimerization domain was not occurring. Samples containing no SDS were fitted to monomer-pentamer and monomer-pentamer-decamer models. Scans of CTXB sedimenting could be fitted to a monomer-pentamer model with a molecular weight of $16,300 \pm 1000$ (Figure 5.20), FUS6 could be fitted to a monomer-pentamer-decamer model with a fitted molecular weight of $23,700 \pm 1500$ (Figure 5.21). Scans for FUS4 in the absence of SDS were unable to be fit to any models suggesting heterogeneity in assembly of the fusion protein.

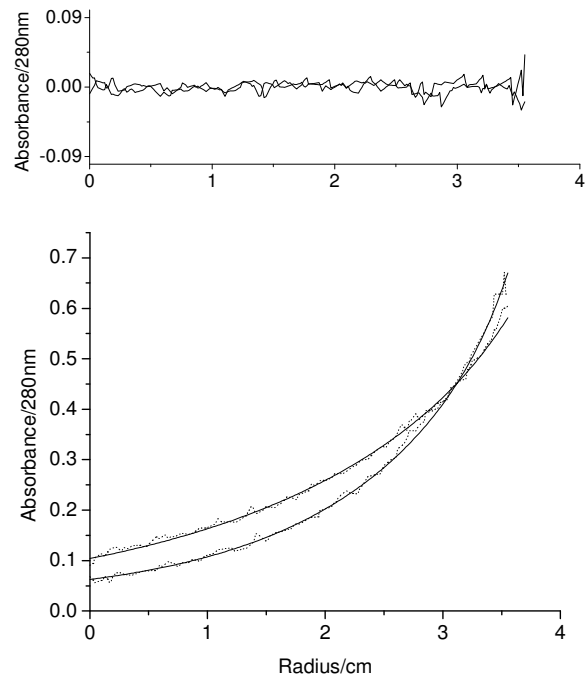


Figure 5.19 Sedimentation equilibrium scans (dotted lines) and monomer-pentamer model fits (solid lines) for CTXB in 0.3% SDS (lower panel) and residuals (upper panel).

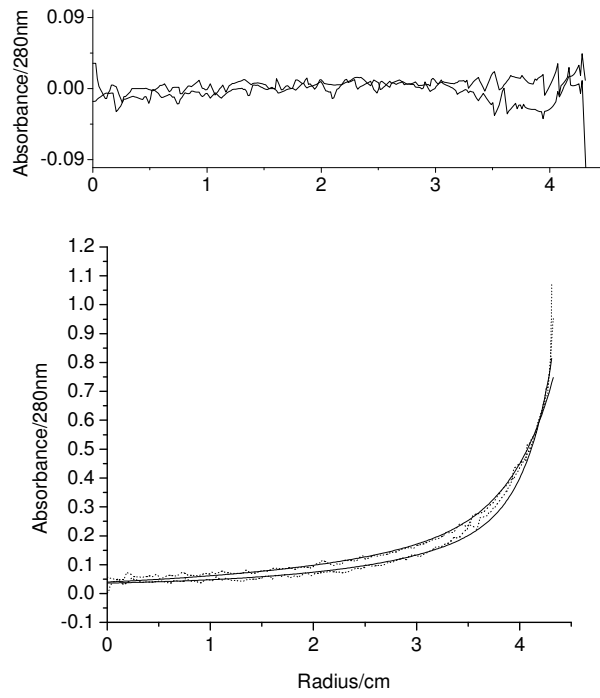


Figure 5.20 Sedimentation equilibrium scans (dotted lines) and monomer-pentamer model fits (solid lines) for FUS4 in 0.3% SDS (lower panel) and residuals (upper panel).

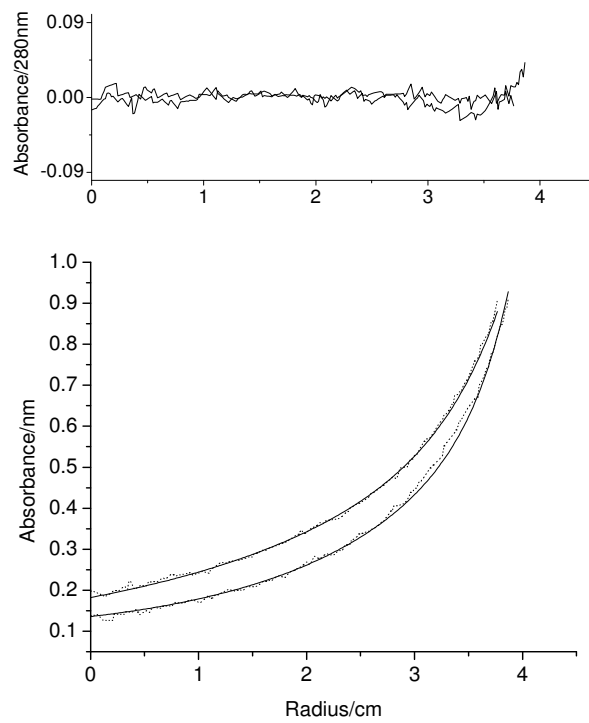


Figure 5.21 Sedimentation equilibrium scans (dotted lines) and monomer-pentamer model fits (solid lines) for FUS6 in 0.3% SDS (lower panel) and residuals (upper panel).

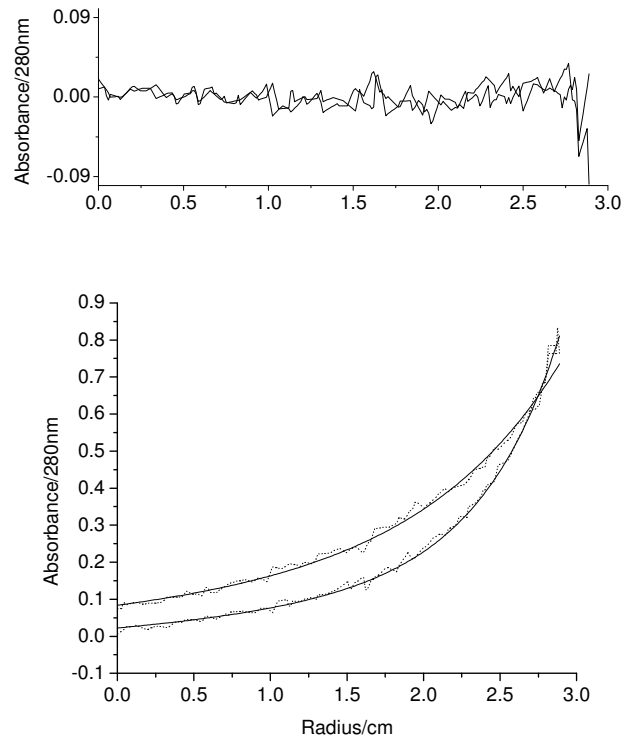


Figure 5.22 Sedimentation equilibrium scans (dotted lines) and monomer-pentamer model fits (solid lines) for CTXB (lower panel) and residuals (upper panel).

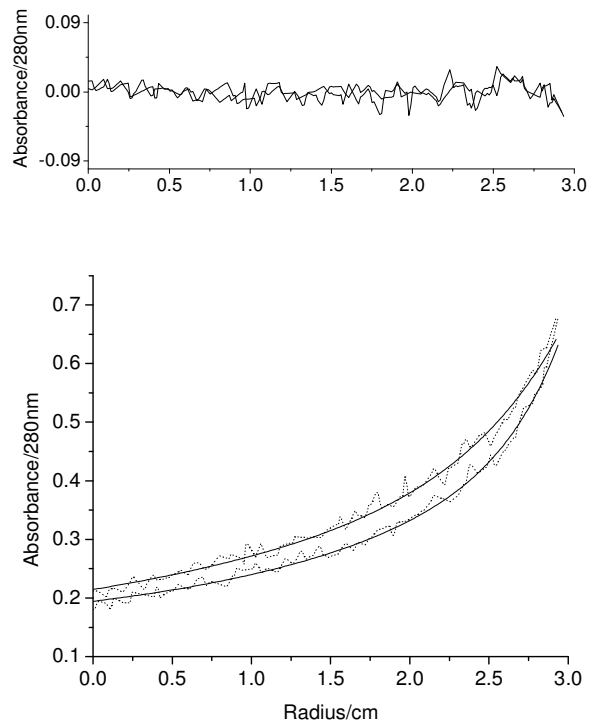


Figure 5.23 Sedimentation equilibrium scans (dotted lines) and monomer-pentamer-decamer model fits (solid lines) for FUS6 (lower panel) and residuals (upper panel).

5.3.7 – TEM

Transmission electron microscopy was used to observe the homogeneity and size of FUS6 at 50,000x and 100,000x magnification (Figure 5.22). Protein samples appear homogenous in the images and have a diameter of approximately 15 nm (Figure 5.22, indicated by yellow circle). Some smaller proteins are also observed with a diameter of approximately 10 nm (Figure 5.22, indicated by blue circle). The estimated diameter of CTXB based on atomic force microscopy measurements is 6 nm (31) therefore; we may be observing FUS6

pentamer (~10 nm) and FUS6 that has assembled into decamers through the interaction of the five GCN4-like dimerization domains (~15 nm).

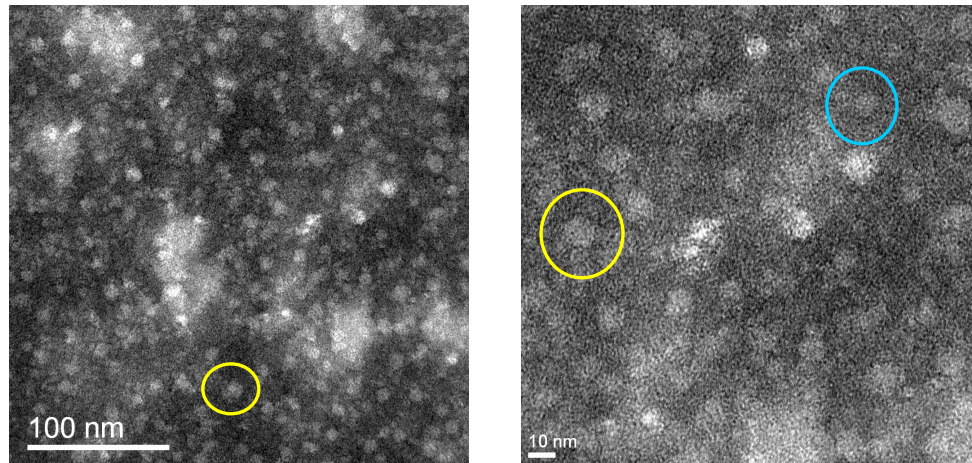


Figure 5.24 TEM images in bright field mode of FUS6 at 50,000x magnification with a 100 nm scale bar (A) and 100,000x magnification with a 10 nm scale bar (B).

5.4 – Discussion

Analytical ultracentrifugation and TEM evidence suggest the homogenous assembly of FUS6 in a face-to-face manner. Assembly is easily reversed by the addition of SDS at low concentrations which disrupts the GCN4-like domain of the fusion protein while not affecting the pentamer structure of the CTXB domain. Whereas the formation of inclusion hindered efforts to obtain useful quantities of protein, refolding and purification could be achieved for CTXB and fusion proteins FUS4 and FUS6 at approximately 10, 4, and 4 mg/L of cell culture. The ability to refold the insoluble proteins on a Ni-NTA column combines the refolding and

purification steps and allows easier scale-up of protein expression and purification than the previously reported dilution method for refolding (24).

The CTXB building block, tolerates the fusion of a protein domain to its N-terminus when the linker region is sufficiently long to allow the protein subunits to fold independently. FUS3 does not fold properly most probably because the linker region is too short. FUS4 is able to refold into pentamers, however, the assembly of FUS4 appears to be non-homogenous based on the inability to obtain fits for the sedimentation equilibrium data using all models. This suggests that the protein solution contains more than three components and is, therefore, non-homogenous. These results are supported by the observation that natural linker domains are usually at least five amino acids long (32). Subtle differences in the linker region of the fusion proteins are very important in the proper folding and assembly of CTXB. Incorporation of different amino acids into the linker region may be useful in directing the assembly of CTXB fusion proteins into different three-dimensional structures. The length of the dimerization domain may also be altered to adjust the stability of the protein assembly.

Covalent crosslinking of CTXB could not be achieved because the addition of a third cysteine to the CTXB subunit to provide a reactive moiety on the protein surface hindered the refolding of the protein. The strategy of introducing cysteine residues as a point of attachment may be more suited to a protein that is expressed solubly and without disulfide bonds. This would avoid the need for redox refolding of the protein. Derivatization of the CTXB cysteine mutant Q3C was very successful; however, subsequent steps in the reaction

were not. High protein concentrations are desired for chemical crosslinking of non-interacting protein subunits. At the low levels of protein obtained for CTXB Q3C, chemical crosslinking is difficult particularly when multiple steps are required to achieve crosslinking. Also, the divalent molecule used in the crosslinking reactions, N,N'-diethynylpentanediamide, may be too short to span the distance needed to bring together two protein subunits or its solubility too low to be effective in a primarily aqueous solution. Finally, CTXB was found to precipitate over time even at low concentration of metal ions including copper (II). The low stability of CTXB in the presence of metals makes it a poor candidate for 'click' chemistry.

5.5 – References

1. Remedios, C. G., Thomas, D. D., *Results Probl. Cell Differ.*, **32**, 1-7 (2001).
2. Straub, F.B. and Feuer, G., *Biochim. Biophys. Acta.* **4**, 455-470 (1950).
3. Kabsch, W., Mannherz, E.G., Suck, D., Pai, E.F., and Holmes, K.C. *Nature*, **347**, 37-44 (1990).
4. Wynne, S. A., Crowther, R. A., Leslie, A. G. W., *Mol. Cell*, **3**, 771-780 (1999).
5. West, M. W., Wang, W. X., Patterson, J., Mancias, J. D., Beasley, J. R., Hecht, M. H., *Proc. Natl. Acad. Sci.*, **96**, 11211-11216 (1999).
6. Rapaport, H., Kjaer, K., Jensen, T. R., Leiserowitz, L., Tirrell, D. A., *J. Amer. Chem. Soc.*, **122**, 12523-12529 (2000).
7. Pandya, M. J., Spooner, G. M., Sunde, M., Thorpe, J. R., Rodger, A., Woolfson, D. N., *Biochemistry*, **39**, 8728-8734 (2000).
8. Potekhin, S. A., Melnik, T. N., Popov, V., Lanina, N. F., Vazina, A. A., Rigler, R., Verdini, A. S., Corradin, G., Kajava, A. V., *Chem. Biol.*, **8**, 1025-1032 (2001).
9. Ogihara, N. L., Ghirlanda, G., Bryson, J. W., Gingery, M., DeGrado, W. F., Eisenberg, D., *Proc. Natl. Acad. Sci.*, **98**, 1404-1409 (2001).
10. Bennett, M. J., Schlunegger, M. P., Eisenberg, D., *Protein Sci.*, **4**, 2455-2468 (1995).
11. Padilla, J. E., Colovos, C., Yeates, T. O., *Proc. Natl. Acad. Sci.*, **98**, 2217-2221 (2001).
12. MacPhee, C. E., Dobson, C. M., *J. Am. Chem. Soc.*, **122**, 12707-12713 (2000).
13. Wang, W. X., Hecht, M. H., *Proc. Natl. Acad. Sci.*, **99**, 2760-2765 (2002).
14. Ryadnov, M. G., Woolfson, D. N., *Nat. Mat.*, **5**, 329-332 (2003).
15. Dotan, N., Arad, D., Frolow, G., Freeman, A., *Angew. Chem. Int. Ed.*, **38**, 2362-2366 (1999).
16. Ringler, P., and Schulz, G. E., *Science*, **302**, 106-109 (2003).
17. Holmgren, J., *Nature*, **292**, 413-417 (1981).
18. Bergquist, C., Johansson, E. V., Lagergard, T., Holmgren, J., Rubin, A., *Infect. Immun.*, **65**, 2676-2684 (1997).
19. Rubin, A., Riise, G. C., Holmgren, J., *Infect. Immun.*, **67**, 2884-2890 (1999).
20. Tamura, S., Samegai, Y., Kurata, H., Nagamine, T., Aizawa, C., Kurata, T., *Vaccine*, **6**, 409-413 (1998).
21. Wiedermann, U., Jahn-Schmid, B., Lindblad, M., Rask, C., Holmgren, J., Kraft, D., Ebner, C., *Int. Immunol.*, **11**, 1717-1724 (1999).
22. Bergerot, I., Ploix, C., Peterson, J., Moulin, V., Rask, C., Fabien, N., Lindblad, M., Mayer, A., Czerkinsky, C., Holmgren, J., Thivolet, C., *Proc. Natl. Acad. Sci.*, **94**, 4610-4614 (1997).

23. Merritt, E. A., Kuhn, P., Sarfaty, S., Erbe, J. L., Holmes, R. K., Hol, W, G. J., *J. Mol. Bio.*, **282**, 1043-1059 (1998).
24. Mattos Arêas, A. P., de Oliveira, M. L. S., Ramos, C. R. R., Sbrogio-Almeida, M. E., Raw, I., Ho, P. L., *Protein Exp. And Purification*, **25**, 481-487 (2002).
25. Carboni, B., Benalil, A., Vaultier, M., *J. Org. Chem.* **58**, 3736-3741 (1993).
26. Wang, Q., Chan, T. R., Hilgraf, R., Fokin, V. V., Sharpless, K. B., Finn, M. G., *J. Amer. Chem. Soc.*, **125**, 3192-3193 (2003).
27. Dieter, A., Cropp, T. A., Mukherji, M., Chin, J. W., Anderson, C., Schultz, P. G., *J. Amer. Chem. Soc.*, **125**, 11782-11783 (2003).
28. Harding, S. E., Rowe, A. J., and Horton, H. C. (1992) *Analytical Ultracentrifugation in Biochemistry and Polymer Science*, The Royal Society of Chemistry, Cambridge, UK.
29. Cohn, E. J., and Edsall, J. T. (1943) *Proteins, Amino Acids and Peptides as Ions and Dipolar Ions*, Reinhold, New York.
30. Meng, F-G., Zeng, X., Hong, Y-K., Zhou, H-M., *Biochimie*, **83**, 953-956 (2001).
31. Mou, J., Yang, J., Shao, Z., *J. Mol. Bio.*, **248**, 507-512 (1995).
32. Argos, P., *J. Mol. Bio.*, **211**, 943-958 (1990).

Chapter 6

Conclusions and Future Directions

6.1 – Overview

Proteins are the most diverse class of biomolecules, both structurally and functionally, and have evolved to accomplish many tasks in living systems. The variety of structures and sizes is quite remarkable. The features of proteins and peptides that contribute to their structure, stability and activity have been elucidated through an enormous body of experimental work. Central to this endeavor have been protein engineering and design studies. Knowledge of the basic principles underlying protein folding, stability, and activity provide insight into the fundamental processes *in vivo* and offer the potential of designing protein/peptide based materials and therapeutic agents.

The extensive research on protein design and incorporation of non-natural amino acids into peptides and proteins forms the basis for the research described in the preceding chapters. A *de novo* designed peptide was used to study the increased stability and potential self-segregating properties imparted by use of the highly fluorinated amino acid, L-5,5,5,5'-hexafluoroleucine (hFLeu). Also, a series of antimicrobial peptides was studied to deduce the affects of fluorination on the stability and antimicrobial activity of α -helical and β -hairpin

peptides. Finally, an α -helical peptide was investigated for its use in mediating higher order assembly of the highly symmetric cholera toxin B protein. The long term objectives of this research here to contribute to our basic knowledge of protein design principles and apply this to the development of protein/peptide based therapeutics and bio-materials.

6.2 – Fluorinated Peptides

6.2.1 – *de novo* Designed Peptides

Incorporation of extensively fluorinated side-chains, such as hFleu, into a model protein has been shown to significantly stabilize the protein against proteolysis and unfolding by “conventional” organic solvents. These properties can be attributed to the greater thermodynamic stability of α_4F_6 compared to α_4H , which, as has been discussed previously (1, 2), can be explained by the increase in hydrophobicity of the hFleu side-chains that comprise the hydrophobic core of the protein. Notably, however, my experiments have failed to find any evidence for the “fluorous” behavior predicted for α_4F_6 , i.e. preferential interactions between fluorocarbon groups, either within the protein or between protein and solvent molecules. On the other hand, the resistance exhibited by α_4F_6 to solvent denaturation and proteolytic degradation are certainly useful properties that may find biotechnological applications.

6.2.2 – Fluorinated AMPs

Building on the insights gained from studying the thermodynamic properties of the model α_4F_6 peptides, I was able to design an antimicrobial peptide with improved biological properties that incorporate hFLeu. Introducing fluorinated amino acids into MSI-78 has conferred resistance to proteolysis of the fluorinated AMPs under conditions where the non-fluorinated AMP is rapidly degraded, while retaining the broad spectrum of antimicrobial activity. Protection against proteolysis is only observed in the presence of liposomes, suggesting that lipid-peptide interactions are important. MSI-78 has been shown to dimerize to form a coiled-coil in a membrane environment (3), this is confirmed by the crosslinking experiments performed and suggests that the fluorinated AMPs also dimerize in a membrane environment, although fluorogainin-2 appears to have no significant helicity. Based on this observation, one plausible explanation of the protease resistance exhibited by fluorogainin-1 is that incorporation of the more hydrophobic hFLeu side-chain strengthens the hydrophobic interactions between AMP dimers, just as was demonstrated for α_4H and α_4F_6 . This would, in turn, promote the formation of structured dimers that are resistant to proteolysis.

More generally, these results suggest the strategy of incorporating fluorinated residues into biologically active membrane-associated α -helical peptides could be used to enhance the efficacy or modulate the activity of other biologically important peptides. For example, membrane-active peptides are

known to be important in membrane fusion and ion-channel formation, and have also been found to have anti-cancer and anti-viral activities (4-7).

β -sheet AMPs containing hFLeu show less promise. The results presented here suggest that the hydrophobicity of the peptide can be used to modulate the activity and toxicity of PG-1. The broad spectrum antimicrobial activity of PG-1 LL is improved or retained in comparison to PG-1 for all bacterial strains tested and significant activity is observed against the fungus *C. albicans*. However, the incorporation of fluorine into PG-1 has decreased selectivity. The lipophilicity of fluorous amino acids may contribute to higher hemolytic activity when secondary structure is diminished. The antimicrobial activity of PG-1 FF is improved against only a few bacterial strains and is lost against some strains that are susceptible to PG-1.

Importantly, the secondary structure of PG-1 LL is reduced by the non-isosteric amino acid substitution of val14 and val16 to leucine, but this does not appear to hinder the oxidation of the two stabilizing disulfide bonds, diminish the antimicrobial activity of the peptide, nor increase the toxicity of this AMP. These results suggest that the hydrophobicity of PG-1 can be used to modulate activity and toxicity, however, fluorous amino acids do not show promise for improving the biological activity of PG-1, in contrast to the results obtained for the α -helical AMP, MSI-78.

6.3 – Symmetry Assembled Protein Superstructures

6.3.1 – Peptide Mediated Protein Superstructures

The CTXB-GCN4 fusion construct containing a 6-glycine linker region between the protein subunits is expected to assemble through protein-protein interactions of the CTXB portion to form pentamers and interactions of the GCN4 region to form dimers. Analytical ultracentrifugation and TEM evidence suggest the homogenous assembly of FUS6 in a face-to-face manner. Assembly is easily reversed by the addition of SDS at low concentrations which disrupts the GCN4-like domain of the fusion protein while not affecting the pentamer structure of the CTXB domain. The ability to refold the insoluble proteins on a Ni-NTA column combines the refolding and purification steps and allows easier scale-up of protein expression and purification than the previously reported dilution method for refolding (8).

The major building block, CTXB, tolerates the fusion of a protein domain to its N-terminus when the linker region is sufficiently long enough to allow the protein subunits to fold independently. These results are supported by the observation that natural linker domains are usually at least five amino acids long (9). Subtle differences in the linker region of the fusion proteins are very important in the proper folding and assembly of protein subunits. This was evident with the lack of structure observed for the fusion constructs with a short

linker lengths of 3 glycine residues. In addition, it appears that the construct with the 4 glycine linker region assembled in a non-homogenous manner.

6.3.2 – Covalent Crosslinking of Non-interacting Proteins

Covalent crosslinking of CTXB was hindered by the addition of a third cysteine to the CTXB subunit for a reactive 'handle' on the protein surface. Cysteine residues as a point of attachment may be more suited to a protein that is expressed in solubly with no disulfide bridges. This would avoid the need for redox refolding of proteins. Derivatization of the CTXB cysteine mutant Q3C was very successful, however, subsequent steps in the reaction were not. High protein concentrations are desired for chemical crosslinking of non-interacting protein subunits. At low levels of expression and refolding, chemical crosslinking is difficult, particularly when multiple steps are needed to achieve crosslinking. Also, the divalent molecule used in the crosslinking reactions, N,N'-diethynylpentanediamide, may be too short to span the distance needed to bring together two protein subunits or the solubility too low to be sufficiently reactive in a primarily aqueous solution. Finally, CTXB was found to precipitate over time even at low concentration of metal ions including copper (II). The low stability of CTXB in the presence of metals makes it a poor candidate for 'click' chemistry.

6.4 – Future Directions

The research presented provides valuable information to the field of protein/peptide design. Highly fluorinated peptides are very well characterized and are obviously more stable chemically and biologically than their non-fluorous counterparts. Detailed structural information on such peptides has, however, continued to be elusive. A solution structure of α_4F_6 based on NMR spectroscopic data is underway as well as attempts to crystallize the peptide to obtain an x-ray structure of the peptide. In addition, solid state NMR experiments are being conducted with the fluorinated AMPs to understand the mechanisms of these peptides and compare them with the non-fluorinated AMPs. Structural and mechanistic data on fluorinated peptides should give rise to better designs that incorporate non-natural amino acids like hFLeu and pentafluorophenylalanine (pFPhe).

Research with symmetry assembled protein superstructures is also being continued to finely tune the assembly outcomes based on protein-protein interactions. Incorporation of different amino acids into the linker region may be useful in directing the assembly of CTXB fusion proteins into different three-dimensional structures. The length of the dimerization domain may also be altered to adjust the stability of the protein assembly. Research is currently underway using an antiparallel heterodimer system for assembly of protein subunits, specifically aldolase. Aldolase is a homotrimer that is overexpressed at

very high levels in *E. coli* and the use of a heterodimer system for assembly allows for control of the formation of superassemblies.

6.5 – References

1. Lee, K-H., Lee, H-Y., Slutsky, M. M., Anderson, J. T., Marsh, E. N. G., *Biochemistry*, **43**, 16277-16284 (2004).
2. Lee, H-Y., Lee, K-H., Al-Hashimi, H. M., Marsh, E. N. G., *J. Amer. Chem. Soc.*, **128**, 337-343 (2006).
3. Porcelli, F., Buck-Koehntop, B. A., Thennarasu, S., Ramamoorthy, A., Veglia, G., *Biochemistry*, **45**, 5793-5799 (2006).
4. Hartmann, R., Wal, J. M., Bernard, H., Pentzien, A. K., *Curr. Pharmaceutical Design*, **13**, 897-920 (2007).
5. Dennison, S. R., Whittaker, M., Harris, F., Phoenix, D. A., *Curr. Protein & Peptide Sci.*, **7**, 487-499 (2006).
6. Ouellet, M., Otis, F., Voyer, N., Auger, M., *Biochim. Biophys. Acta-Biomembranes*, **1758**, 1235-1244 (2006)..
7. Martin, I., Ruyschaert, J. M., Epand, R. M., *Adv. Drug Delivery Rev.*, **38**, 233-255 (1999).
8. Mattos Arêas, A. P., de Oliveira, M. L. S., Ramos, C. R. R., Sbrogio-Almeida, M. E., Raw, I., Ho, P. L., *Protein Exp. And Purification*, **25**, 481-487 (2002).
9. Carboni, B., Benalil, A., Vaultier, M., *J. Org. Chem.* **58**, 3736-3741 (1993).